ELECTRON RESONANCE STUDIES IN SILVER CHLORIDE CRYSTALS

Thesis submitted for the Degree of Doctor of Philosophy at the University of Keele.

by

K.A. HAY

Department of Physics

University of Keele

1966

ABSTRACT

Silver chloride crystals containing different transition metal ions have been investigated by electron spin resonance spectroscopy. The properties of iron impurity have been studied in detail. The irradiation of crystals containing divalent iron leads to the formation of a trigonal trivalent complex when the temperature of the crystal is about 170°K. Subsequent warming of the crystal to 200°K converts this complex into the cubic centre which has been identified by Hayes, Pilbrow and Slifkin. A model is proposed for the trigonal spectrum and a mechanism is suggested for the processes which occur in the crystal during and after irradiation. A number of other spectra have been observed, but owing to difficulties in reproducing these, it is only possible to make general comments regarding their classification and origin. The S-state spectra for both the cubic and the trigonal sites exhibit some unusual characteristics which are discussed in some detail.

Single crystal experiments have been carried out on a 100Kc/s field modulation, X-band spectrometer at 20°K, 77°K and at 300°K. The e.s.r. spectrometer is conventional apart from the absorption cell which is a standing wave helix rather than a microwave cavity. The use of a helix in an e.s.r. spectrometer is described, and ideal design criteria are calculated to take account of dielectric loading of the helix by non-lossy samples. The spectrometer sensitivity is comparable with a similar cavity instrument, principally because of the high filling factor which can be obtained.

ACKNOWLEDGMENTS

The author would like to thank:

Professor D.J.E. Ingram for his continued encouragement and supervision of this work.

Professor H.A. Buckmaster for many helpful and useful discussions.

The members (past and present) of the E.S.R. research group for their cooperation and assistance (particularly to Mr. A.S. Woodward for his advice and discussions).

Dr. D.C. Lainé for assistance in the running of this project and for reading the proofs of this thesis.

The University of Keele for personal support and the Physics Department for the provision of apparatus.

The Chemistry Department for the use of an optical spectrophotometer and X-Ray goniometer (particularly to Dr. D.O. Hughes for instruction in the X-Ray crystal orientation).

Miss K. Davies for her care in typing and duplicating this thesis.

My wife for her invaluable encouragement, for typing the first draft of this thesis and for assistance with the preparation of diagrams.

CONTENTS

CHAPTER I

INTRODUCTION

Electron Spin Resonance (E.S.R.) spectroscopy is a technique which detects transitions between unpaired electrons spin states in a magnetic field. In the systems considered in this thesis, the paramagnetic or unpaired electrons are those of transition metal ions dissolved in silver chloride crystals. The energy levels of paramagnetic electrons in a crystal are generally very sensitive to the local environment of the atom; the unpairing of electron spins implies that they are among the least firmly bound electrons in the crystal and hence are associated in some way with the bonding of the crystal. It is for this reason that E.S.R. can be a very useful technique for investigating, often in fine detail, local crystalline symmetries and the bonding around paramagnetic ions. When it is necessary to take into account more than the simple ionic effect of neighbouring ions around a paramagnetic ion, the neighbours are called "ligands" and the molecular system comprising a central ion and its ligands is called a "complex". Some emphasis is placed on the importance of the molecular effects as these appear to be of considerable relevance in the iron complexes which have been studied.

It has been possible to study the hole trapping which follows the irradiation of silver chloride containing divalent iron ions and then to understand the mechanisms of ionic rearrangement which

take place at particular temperatures. Such processes in silver halides are of importance in many of the physical properties of the crystals and the part played by impurities such as iron is of particular interest. The results of this work are presented in Chapter VII and they are discussed in the following chapter. As the interpretation of the data depends on an appreciation of many of the physical properties of silver halide crystals and as no recent review has been published, Chapter II attempts to describe some of the more important properties. In the subsequent two chapters the theory of electron resonance spectroscopy and its application to transition ion systems is discussed. Chapter V briefly indicates the instrumentation which is used in E.S.R. studies and a short description is given of the spectrometer which has been built and used in the silver chloride experiments. An analysis is given of some aspects of the use of a slow wave helical structure as the absorption cell in a spectrometer; in particular the dielectric loading by samples is investigated. It has been found necessary to prepare and purify the silver chloride crystals fairly carefully and Chapter VI is devoted to a description of the preparation and handling of silver chloride.

CHAPTER II

PHYSICAL PROPERTIES OF SILVER HALIDES

2.1 Introduction

To provide some understanding of disorder and impurity processes in a crystal it is necessary to examine many of its properties. The silver halides are basically classed as ionic crystals, and both silver chloride and bromide, which are the two halides which will be discussed, have the same face-centred cubic structure as the majority of the alkali halides. Attention is restricted to the chloride and bromide as ~~it is on them that~~ most work has been concentrated on them and the fluoride and iodide are not nearly as "well behaved". The fluoride has a tendency to prefer the AgF_2 form and silver iodide has a disordered phase at high temperatures.

Many of the detailed properties of the alkali and silver halides differ considerably; this is often because the binding of the silver halides is not so completely polar as that of the alkali halides. A study of both crystal types is however of great use for contrast or comparison when the properties of one or the other are considered. Accordingly, there will be much reference in this chapter to the properties of alkali halide crystals, although no conscious attempt will be made to survey them. Many of the properties of ionic crystals in particular the alkali halides, are described, for example by Seitz (1, 2), by Kittel (3) and by Dekker (4).

The section on photographic sensitivity will be restricted primarily to physical volume effects, although much of the technical importance of this aspect of silver halides depends on the surface properties.

2.2 Binding of the Perfect Crystal

2.2.1 Binding Energy

The cohesive energy of an ionic crystal is divided into four parts in the Born Theory: the electrostatic, repulsive, Van-der-Waals and zero-point energy (1). These experimental and theoretical energies for sodium chloride and silver bromide are compared in table 2.1 (5).

Table 2.1 Various contributions to the cohesive energy per ion pair (in e.v.)

	AgBr	NaCl
Coulomb Energy	8.64	8.86
Repulsive Energy	-1.37	-1.02
Van-der-Waals Energy	1.18	0.12
Zero-point Energy	-0.04	-0.07
Total Energy	8.41	7.89
Experimental value	8.74	7.90

The agreement of the theoretical and experimental values for NaCl can be taken as an indication that its character is truly ionic at least when compared with AgBr.

In any ionic crystal, there will be overlap between nearest neighbours to provide the repulsive energy; this will distort the ions to some extent. This distortion will be important if the work required

to remove an electron from the negative to an adjacent positive ion (not to the conduction band) is small (see Section 4.3). This is the case with the silver halides to some extent. Examination of the ionization potentials of the alkali metals and silver shows that the first ionization potential for the alkali metals is lower than other metals; more than 2e.v. less than for silver. This allows an appreciable amount of covalent bonding between the halogen ions and their silver ion ligands.

Associated with this difference between the alkali and silver halides is the very large difference in the Van-der-Waals energy. Although the Van-der-Waals energy is properly described by a quantum mechanical treatment, classically the effect will be of the form $\frac{\alpha_1 \alpha_2}{r^6}$ for the dipole-dipole part of the interaction, where α_1 and α_2 are the atomic polarizabilities of nearest neighbours. These are large for the halogen ions but alkali metal ion polarizabilities are small due to the tight binding of the remaining electrons in the ion. In silver α is large compared with the alkali metals. This is due to the weaker binding of the 4d electrons to the silver ion relative to the crystal. It is worth noting that this is associated with the fact that silver is to be found in a divalent state in some complexes.

The case of AgCl is similar although the contrast is perhaps not quite so great.

2.2.2 The Dielectric Constant

The polarizability of a substance may usually be divided into three parts: electronic, ionic and dipolar. The electronic part is

figure 2.1

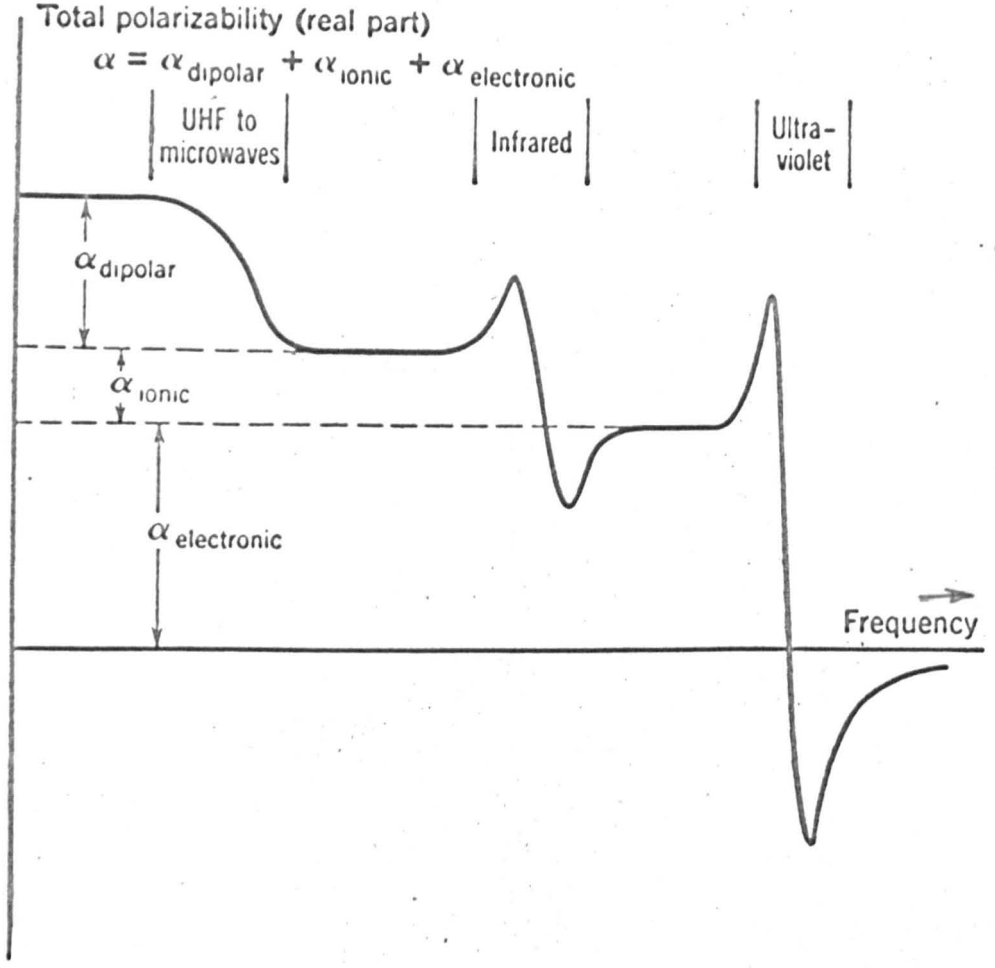

Figure 2.1

Diagramatic frequency dependence of possible contributions to the polarizability.

simply the α mentioned above. It describes the displacement of the electrons relative to the nucleus. The ionic polarizability α_{ionic} arises from the displacement and distortion of an ion relative to other ions. This is important in ionic crystals but the effect is small in covalent crystals (e.g. diamond) where all ions interact identically in an external electric field. The dipolar or orientational contribution, $\alpha_{dipolar}$, occurs if there is some permanent dipolar molecule or complex in the crystal, as is the case with many organic substances. This can also be found in ionic crystals when, for example, a vacancy is associated with a divalent impurity in AgBr (8). As far as the perfect lattice is concerned, there is no dipolar contribution in ordinary ionic crystals.

The three effects can be separated experimentally as is shown in Figure 2.1. Dipolar complexes are only able to follow a varying electric field to a limited extent depending on the surroundings of the complex and its symmetry. A similar effect occurs with the ionic displacement when an electric field of frequency greater than the optical phonon vibration frequency is used. This frequency usually lies in the far infrared (approximately 110μ in AgBr and 80μ in AgCl) and the actual frequency can provide some measure of the ionic nature of the crystal by effectively measuring the charge of oscillating ions through the Szigetti relations (p. 167 of Ref. 3, 9, 10). The magnitude of α_{ionic} will depend very strongly on the degree of ionic binding and in the limit of covalent crystals its effect disappears.

The electronic polarization, largest for the most weakly bound electrons, is able to follow an electric field until the associated energy is sufficient to lift a valence electron into the conduction band. This effectively destroys the ionic state of that constituent of the crystal. The high frequency dielectric constant (ϵ_∞) is the observed effect of α_e in the bulk crystal. To assess the local field on an ion due to an applied field, some assumptions must be made regarding the surroundings of the ion (3, p.155). Ignoring the dipolar contribution, the low frequency dielectric constant (ϵ_o) is a combination of α_e and α_i. Again, some local field must be postulated to allow a calculation of the dielectric constant. This difficulty is related to the polaron problem which is mentioned in the next section; in the case of the alkali and silver halides, there is a fairly localised distortion around a given centre, but it is not concentrated within its own radius. The polarization energy associated with the perfect lattice, and with distortions of it, is of very great importance.

As would be expected from the large atomic polarizability of the silver ion, the high frequency dielectric constant of the silver halides is much larger than that of the alkali halides as shown in table 2.2. The details of a number of other substances are included for comparison.

Table 2.2

	Dielectric Constants			Polaron Coupling Constants	
	ϵ_∞	ϵ_o(r.t.)	(77°K)	$\alpha(m=m_e)$	α
AgBr	4.62	13.1	(11.5)	3.6	1.6
NaCl	2.25	5.26		5.5	≈3 *
KCl	2.13	4.68	(4.35)	5.6	≈3 *
Cu_2O	4.0	10.5		2.5	
PbS	15.3	17.9		0.26	0.16
InSb	16.0	17.5		0.13	0.014

* assuming a band mass similar to that of AgBr.

2.3 Electronic Properties

2.3.1 Introduction

The fundamental electronic processes in an ionic crystal are observed primarily in optical absorption and in photoconductivity experiments. Interband electronic transitions are introduced by ultra-violet or more energetic radiation, allowing electronic or hole conduction, or perhaps both, to take place.

For the purposes of this thesis, it is useful to study the electronic properties and band structure of the silver halides because the ionic processes which take place on irradiation are a very direct result of photoconduction. The presence of photoelectrons in a crystal is the primary part of the formation of a photographic latent image in sensitized silver halides (6).

facing page 9

figure 2.2

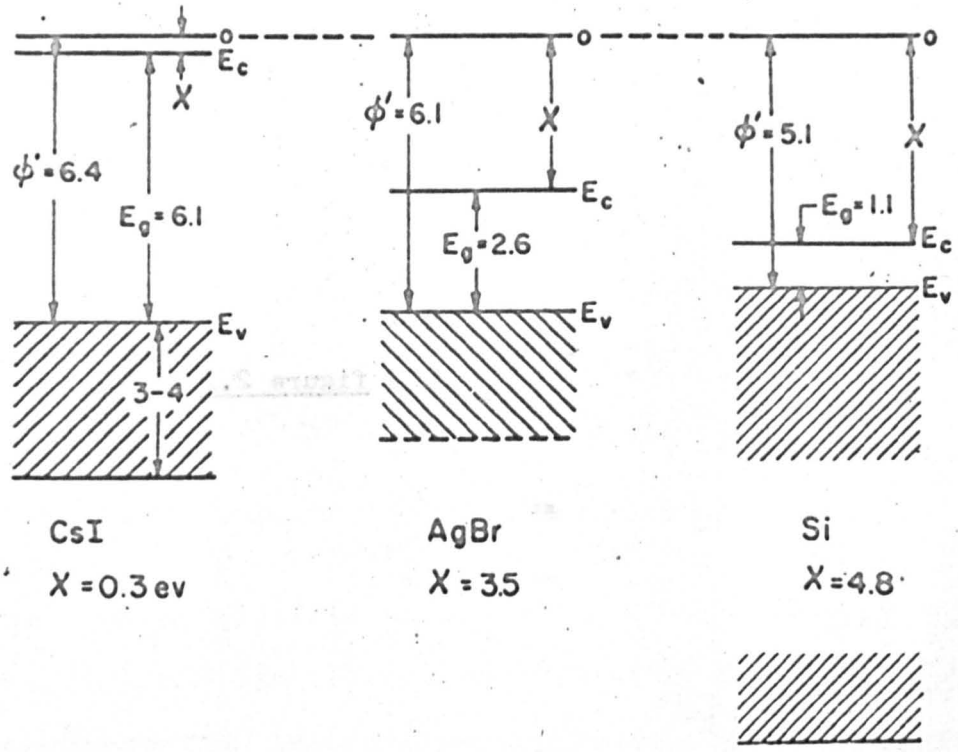

Figure 2.2

Simple Energy Diagram of three types of solids, χ is the electron affinity, E_g the band gap, and ϕ' the work function, all in e.v. (11).

facing page 9

figure 2.3

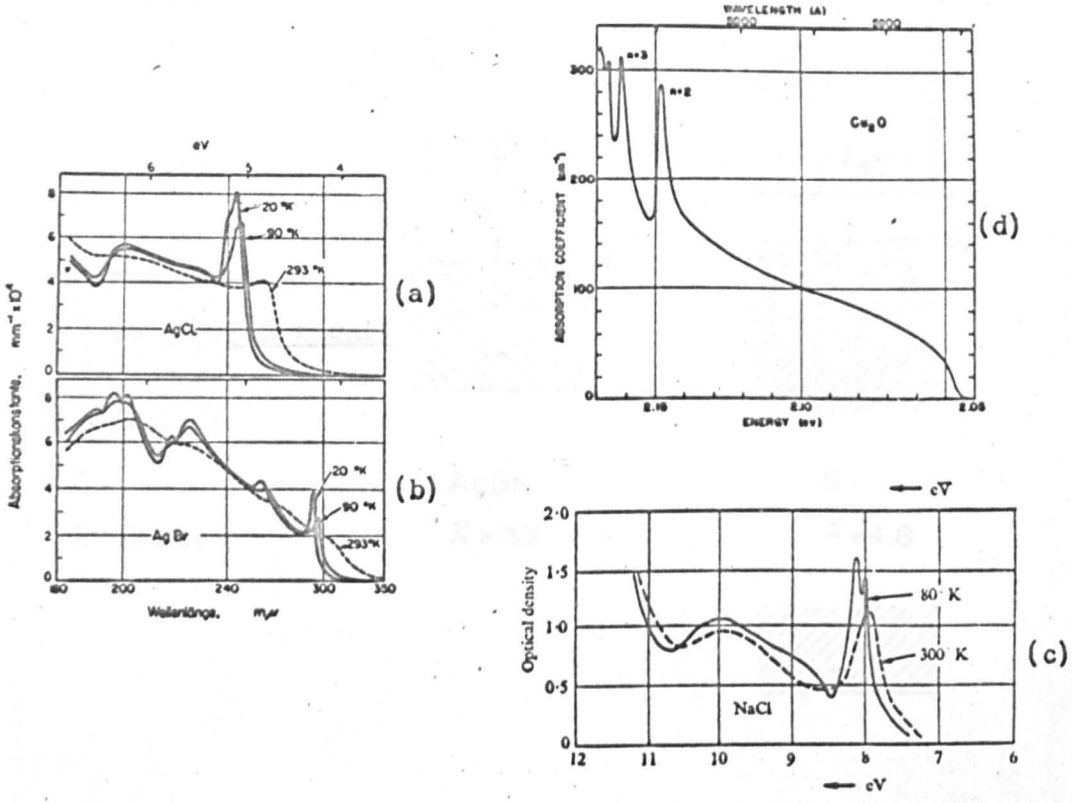

Figure 2.3

Comparison of fundamental absorption for thin films of AgCl, AgBr, NaCl and Cu_2O.

The fundamental properties of the silver halides have been extensively investigated, not only because of the relevance of such work to the photographic process, but because of some other interesting phenomena which occur.

The silver halides are an intermediate case as far as band gap is concerned, between the alkali halides and silicon as is shown in Figure 2.2 (11). In addition, their optical absorption possesses a low level tail which stretches into the visible region. More is probably known of their electronic properties than those of the alkali halides.

Single crystals of silver halides have been prepared (12) with the very high purity necessary for accurate observation of the optical absorption and electrical conductivity at low temperatures, when the effect of lattice vibrations is negligible and impurity effects can become very important. The preparation of silver halide crystals is described in Chapter VI.

2.3.2 Optical Absorption and Band Structure

The absorption spectra of silver chloride and bromide have been investigated over a wide range of wavelengths from the visible region to the far ultra-violet. Thin films have been prepared in various ways to provide values of the extinction coefficient in the ultra-violet where the absorption is characteristically very strong. At longer wavelengths, large single crystals can be used.

Figure 2.3 shows the fundamental absorption of thin films of AgBr, AgCl (13) and NaCl (14) for comparison. There is clearly a great

similarity between the spectra of silver and sodium chlorides, although the effect of thermal vibrations in smearing out the structure appears much more prominently for AgCl than for NaCl.

(a) The Conduction Band

The conduction and valence band structures of silver chloride and bromide have been studied extensively by Brown and his co-workers at Illinois. The conduction band is of standard form with a minimum at $k = 0$. This was shown to be the case by Tippins (11) using a magnetic field to reduce the spherical symmetry associated with electrical conductivity in a cubic crystal to a symmetry consistent with the crystal class. The results showed an agreement with the simple band structure and correspond to a Hall mobility in excess of 50,000 cm^2/volt.sec. at 2°K, at least in the case of one sample of AgBr. In this experiment ~~observed~~ the component of current density in the direction of an applied electric field is observed, in contrast to the situation in ~~rather than~~ the Hall experiment where the component of field is measured in the direction of the current density; thus there is no Hall potential developed across the sample. It is assumed that holes left in the valence band would not contribute appreciably to the current, due to their shorter drift range, especially at these very low temperatures.

(b) The Valence Band

The structure of the top of the valence band for the silver halides has been studied experimentally, particularly by Brown et al. (15) and theoretically by Bassani et al. (16, 23). Although the detailed shape is not certain, it is clear that there is a minimum

facing page 11

figure 2.4

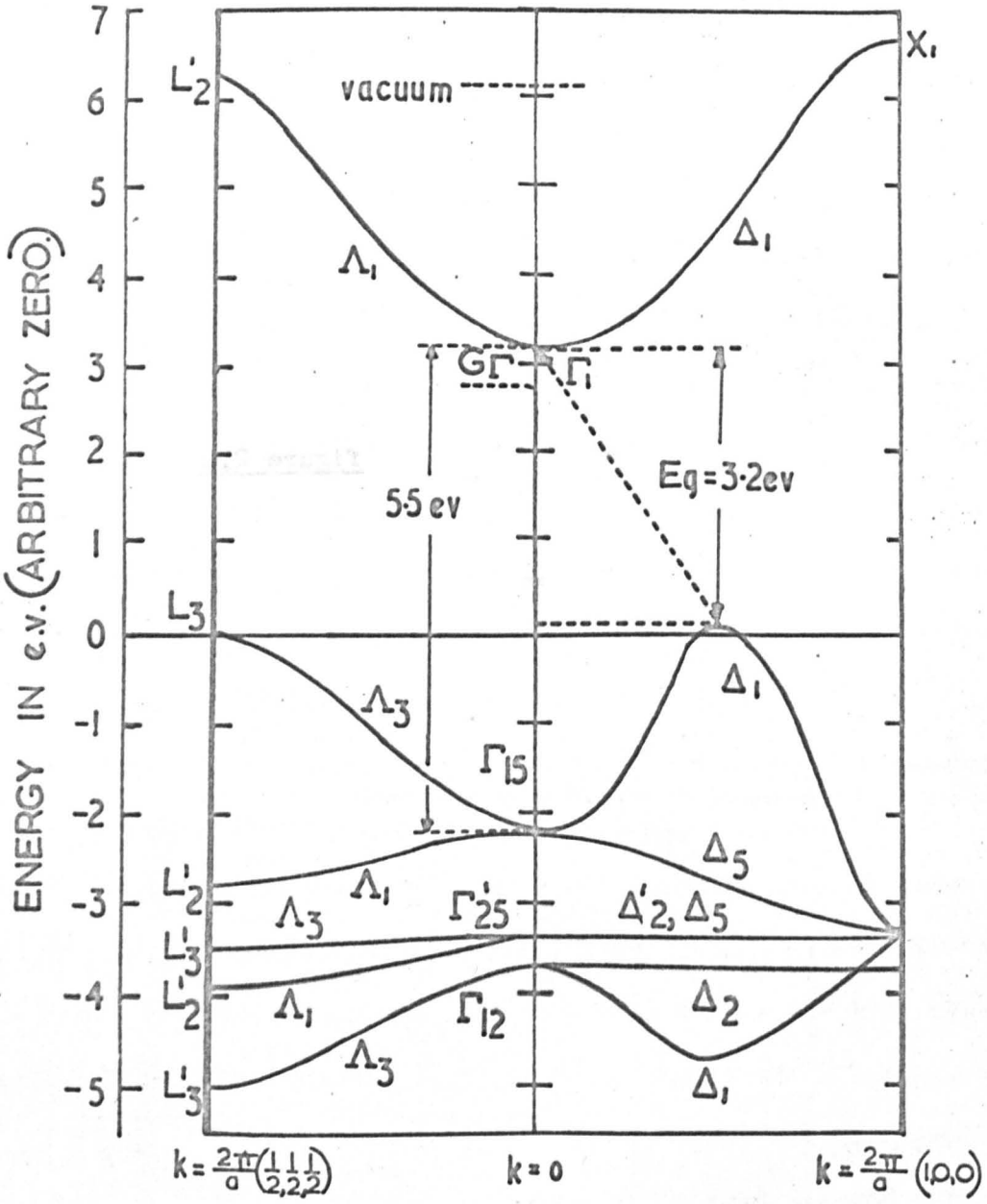

Figure 2.4

Probable Band Structure for AgCl in two of the principal directions, (neglecting the effect of spin-orbit coupling).

at $\underline{k} = 0$ in at least one crystallographic direction (Figure 2.4); this leads to the indirect transitions which are observed to stretch far into the visible part of the spectrum.

There is little doubt that the first strong absorption peak near 5e.v. in AgCl (Figure 2.3[a]), like that in NaCl at 8e.v. (Figure 2.3 [c]) is due to an exciton state which occurs when there is a direct excitation of an electron in a Cl^- ion. The exciton state is still bound to the halogen with a binding energy of a few tenths of an electron volt. In the silver and alkali halides, the electron is localized to the ligands of the chlorine ion due to the strong polarization of the lattice, whereas in much less polar crystals, such as copper oxide, the electron is highly delocalized because of the lack of lattice polarization. This leads to a hydrogenic exciton spectrum (Figure 2.3[d](19)) where the lines are narrow as a result of the small amount of interaction between excitons and their surroundings. The fairly large linewidths in the more polar crystals are due to strong interactions of the excitons with imperfections such as phonons and surfaces.

The exciton which occurs in the alkali and silver halides is really an intermediate between the Wannier case (e.g. Cu_2O) and the Frenkel case (occurring in molecular crystals) where the excited state is localized within the nearest neighbours and is simply a perturbation of the isolated molecular states. Clearly these two models can be considered theoretically without much difficulty, but the approximations

of either case are not applicable to the intermediate distorted lattice configurations associated with polar crystals; (the theoretical treatment of excitons is considered in some detail by Knox (17)). The problem of the theoretical treatment of excitons in polar crystals is in common with the difficulty of assessing theoretically all charged defects in these crystals, where the bulk dielectric constant cannot be used.

The exciton peak is split into a so-called halogen ion doublet which was first discussed by Mott (18, p. 95 of ref. 6). The excitation of the halogen ion leaves behind a halogen atom with an unfilled p shell. The effect of spin-orbit coupling will be to separate the $j = \frac{1}{2}$ and $j = \frac{3}{2}$ states and in the free atom the splitting is about 0.11e.v. in chlorine and 0.44e.v. in bromine. Since the electron is not set free but is bound to the halogen atom, only a lower limit can be established for the splitting. The energies associated with the splitting of the exciton peaks of longest wavelengths in most of the alkali and silver halides agrees quite well with predictions on this basis. This supports the viewpoint that the first optical absorption peaks in the silver halides are a consequence of direct transitions.

It is much more difficult to state the origin of the higher energy bands appearing within the absorption spectrum. The first fundamental absorption is due to the excitation of an electron from the p states associated with a Cl^- ion; and various d states of the Ag^+ ion lie below this in energy. This is discussed by Bassani (16), and

facing page 13

figure 2.5

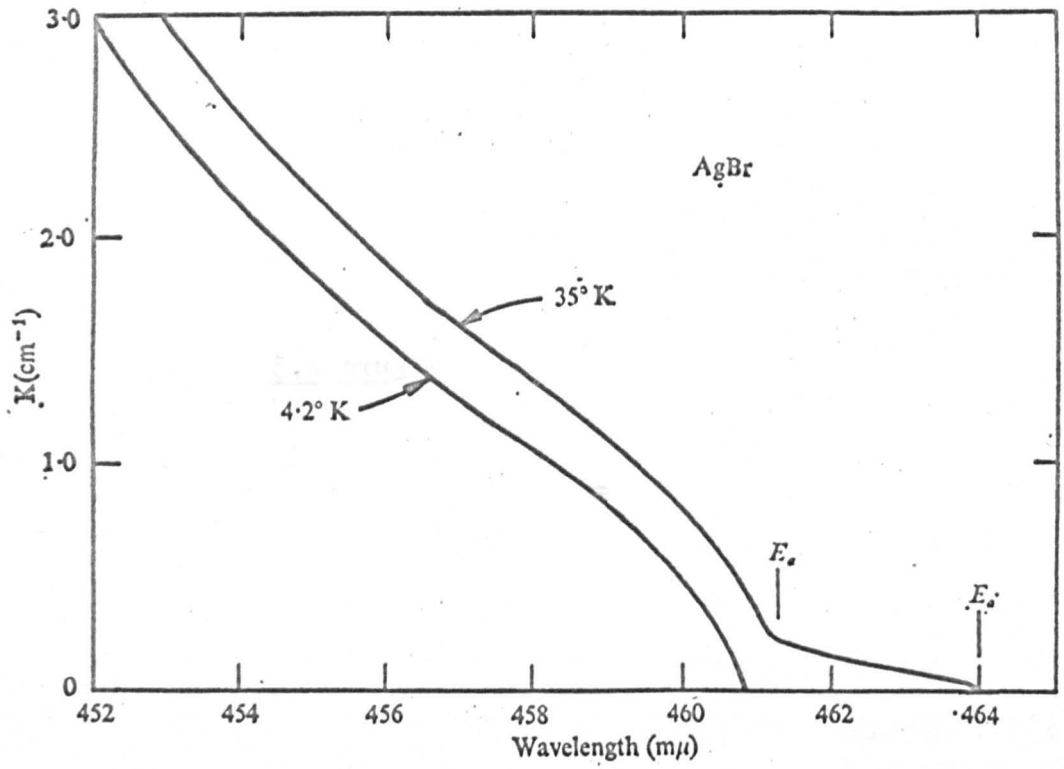

Figure 2.5

Long wavelength absorption edge of AgBr showing the effect of phonon emission and absorption on an indirect transition at low temperature. The phonon energy is $\frac{E_e - E_a}{2}$

the valence band part of Figure 2.4 is the result of their calculations.

The exciton can have a considerable mobility in the crystal lattice; it can migrate and interact directly with impurities in the lattice (2). Since photoconductivity occurs with a high probability in very pure silver halides when an exciton transition is irradiated, it can be assumed that the exciton is very likely to interact either with a phonon at least down to 77°K because of the strong polarization associated with electrons and holes (see 2.3.3 b) or with an imperfection during its lifetime (24).

The absorption in the exciton band is very high (about $10^6 cm^{-1}$) which is associated with an allowed, direct transition and a high yield of photoelectrons. The absorption in the long wavelength tail is low (10^3 to 10^4 cm^{-1}) but the quantum efficiency for the yield of photoelectrons from photons absorbed is high (21, 22) which suggests an indirect or forbidden transition associated with the low oscillator strength. In such a transition, a phonon must be either emitted or absorbed, emission occurring at low temperatures and both processes at sufficiently high temperatures.

The observations by Brown, Masumi and Tippins on the long wave absorption edge support the possible occurrence of indirect transitions (15, 11). Their results (Figure 2.5) are consistent with the emission E_e (or absorption E_a at sufficiently high temperatures) of a phonon with a characteristic temperature of about 90°K; other higher energy or two phonon processes are also possible. There is some structure in

the absorption at helium temperatures (15, 16) which is smeared out by vibrations at higher temperatures. It is not clear in which direction the most important indirect transitions occur; the structure on the absorption edge and the available phonons are discussed in reference 15. Figure 2.4 shows the band structure of two of the principal directions in AgCl, neglecting spin-orbit interaction. The beginning of interband transitions would then take place between states connected by the dotted arrow (this is the smallest gap).

The covalent character of the silver halides is particularly important as it is as a result of p-d mixing that the maxima in the valence band occur away from $\underline{k} = 0$. Such effects are much less marked in the alkali halides which do not possess this low level absorption extending to long wavelengths.

2.3.3 Electron and Hole Conduction

The conduction of electrons and holes is often limited by some sort of lattice imperfection. Such processes are of primary interest when studying the effect of lattice defects on the properties of the crystal. Before describing these processes, it is necessary to discuss the dynamics of electrons and holes in the otherwise perfect lattice. Extensive work has been done on the silver rather than alkali halides because of the relative ease with which they can be purified and also because they are sensitive photoconductors at low temperatures.

(a) Electron Mobility

Two physically distinct electron mobilities can be measured in a

facing page 15

figure 2.6

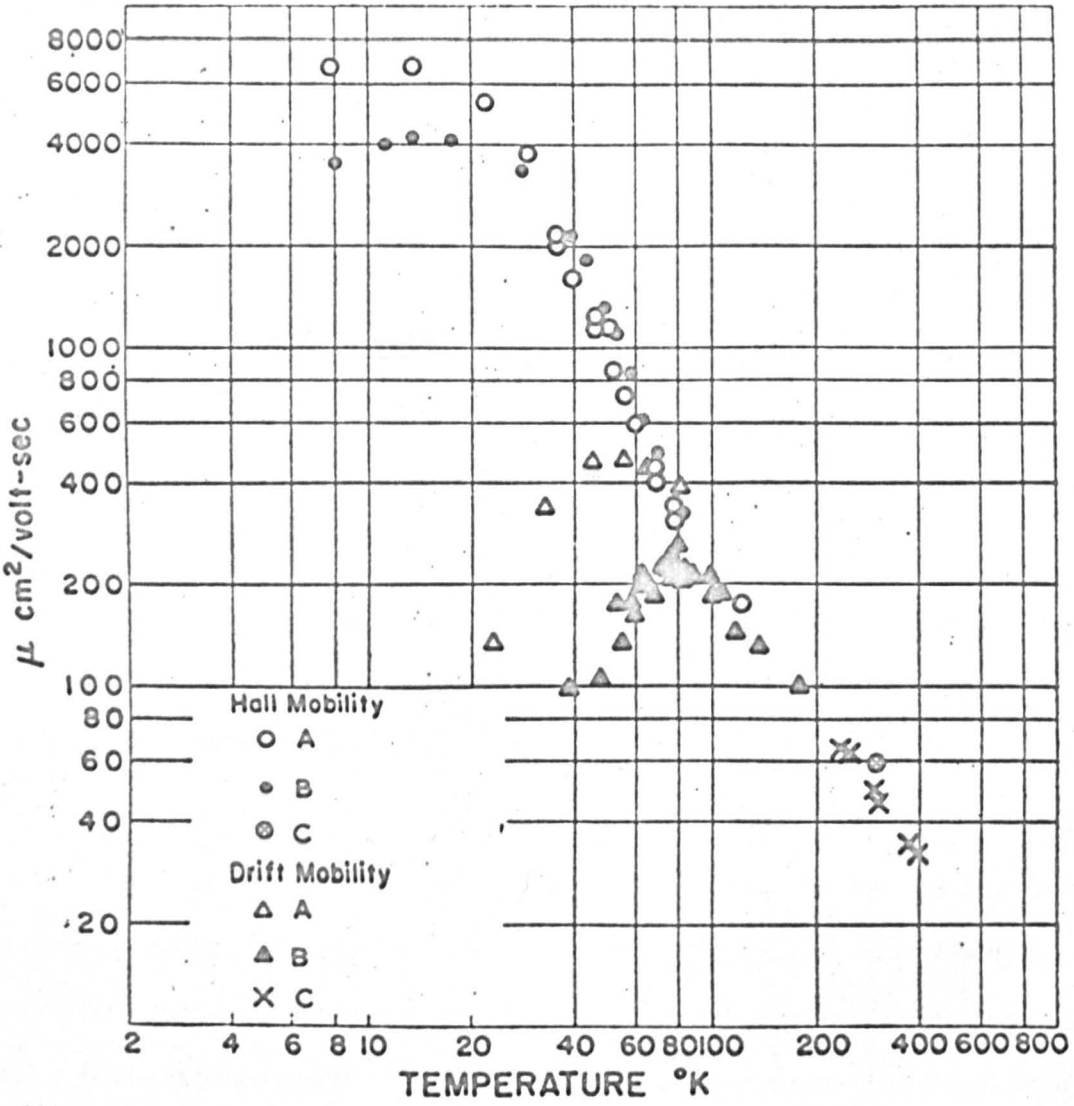

Figure 2.6

Drift and Hall mobilities as a function of temperature for electrons in AgCl. A and B are for different crystals and C are results given by Haynes and Shockley.

crystal and, by studying their variation with temperature, some insight can be obtained into the conduction process. Although the results of hole conduction are often abundantly clear, particularly in photochemically sensitized crystals, holes are much more difficult to detect directly than electrons.

The drift and Hall mobilities for electrons in silver chloride are shown as a function of temperature in Figure 2.6 (25). The drift mobility (triangular points) is found to be small at both high and low temperatures with a maximum in the vicinity of 50° to 90°K depending on the sample preparation. The decrease at low temperatures is not the result of scattering processes as the Hall mobility continues to rise to high values (circles). In zone refined specimens it is found to rise as high as 20,000 cm^2/volt. sec. in AgCl and 50,000 cm^2/volt. sec. in AgBr. This difference between the two mobilities is an excellent example of multiple trapping. Fitting of the data shows that these traps have a depth of about 0.03e.v. and there are about 10^{15} to 10^{16} per cm^3. The Hall mobility gives a far better measure of the true crystal mobility and the variation with temperature can be explained by assuming phonon interactions, particularly with longitudinal optical phonons of Debye Θ of the order of 195°K. This agrees well with the Restrahlen value of about 200°K. (10). At sufficiently low temperatures these phonons will become frozen out and one could expect only a small acoustical phonon effect. This may be partially responsible for the change in slope of the Hall mobility curve at about 35°K. As will be

facing page 16

figure 2.7

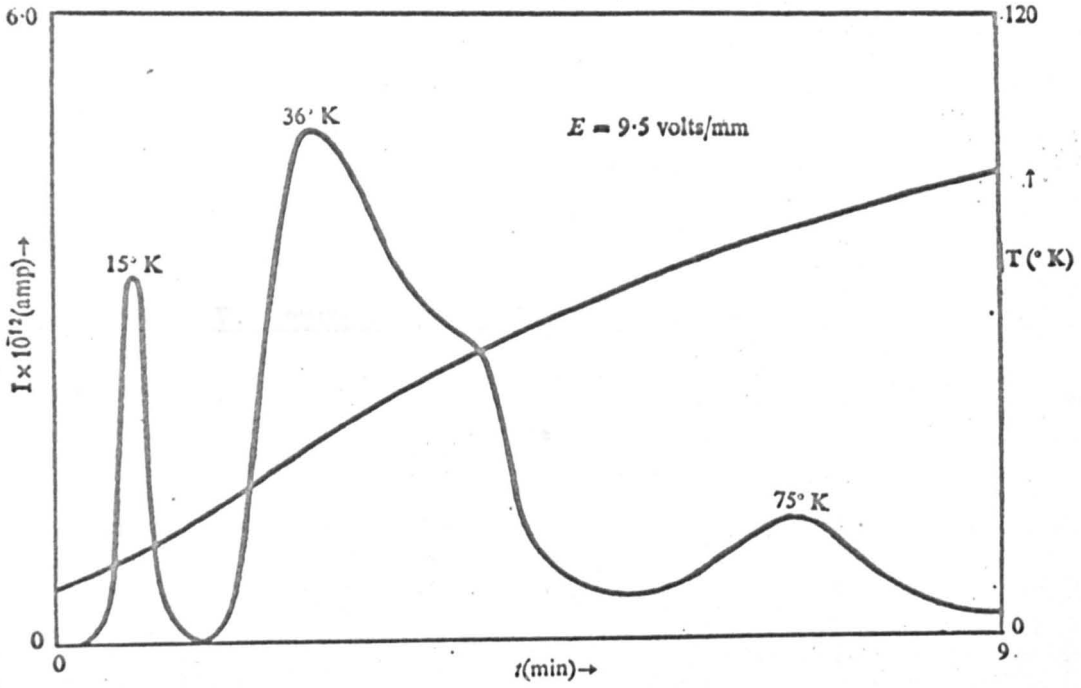

Figure 2.7

Electric Glow Curve for AgCl below 90°K. The crystal had been illuminated at 10°K without collecting voltage E and then warmed with the field on.

mentioned below, this could also be caused by an impurity trap. It would not be expected that the interaction with acoustical phonons would be very large because of the localised nature of the polarization around the conduction electron. At very low temperatures, impurities certainly become important and the mean electron range is drastically reduced (22).

The impurity trapping at low temperatures can be compared with electric glow data (Figure 2.7) (22). The increase of Hall mobility with falling temperature is reduced below $35^{o}K$ and again below $15^{o}K$ rather more sharply. The electric glow curve was obtained by irradiation at $10^{o}K$ without collecting voltage applied to the crystal; a monitoring potential was applied after irradiation and the crystal was warmed. Glow peaks were observed at about $15^{o}K$ and $35^{o}K$, apparently corresponding to the trapping centres responsible for the loss of conductivity. The $15^{o}K$ peak can be associated with a trap depth of about 0.03e.v. assuming a frequency factor of $10^{10}sec^{-1}$ which would correspond with the trap postulated as a result of the drift mobility experiment. This trap is apparently very important; bearing in mind its strong effect on the Hall mobility, it would appear that it has a large capture cross-section, but its structure remains obscure. The number of traps observed may be of about the same number as the number of chemical impurity atoms in the crystal, so that it is not clear if the trapping is due to impurities or to some centre with a character similar to that of the F-centre in alkali halides. However, the available information about Frenkel defects suggests that there will be only in the region of

10^{12} such defects per cm^3 at room temperature (27). This would not imply that the interstitial silver ion was responsible for the trapping unless the numbers are greatly increased by the presence of impurities or dislocations. The former possibility is a very likely one. Incipient silver ion vacancies on dislocations (Figure 2.12) will also provide a possible electron trap.

The above aspects of the problem will be discussed more fully later in this chapter.

(b) Polaron Effects

The strong dependence of the electron mobility on phonon scattering and the cyclotron resonance experiments of Ascarelli and Brown (24, 26, 28) provide excellent agreement with the polaron calculations of Feynman et al. (29, 24, 30, 21). The idea of a polaron has been developed from the proposal by Landau concerning self trapping of electrons in the alkali halides (31). The concept of a polaron (the conduction electron or hole together with the polarization of the lattice surrounding it) is of general significance and ionic crystals are a limiting case (see 32 for example). The lattice polarization around a conduction electron can be thought of as having a phonon-like character and the interaction between the electron and the lattice is described in terms of a coupling constant, α. This can be interpreted as being roughly equivalent to the number of longitudinal optical phonons associated with the electron. Transverse optical phonons will normally have less importance due to the weaker electric field associated with them.

The coupling constant thus depends on the lattice polarization which is associated with the differences between the static and optical dielectric constants ϵ_0 and ϵ_∞, on the momentum band mass of the electron m and also on the longitudinal frequency ω_L giving:

$$\alpha = \frac{e}{\hbar} \left(\frac{m_e}{2\hbar} \right)^{\frac{1}{2}} \left(\frac{1}{\epsilon_\infty} - \frac{1}{\epsilon_0} \right) \left(\frac{m}{m_e \omega_L} \right)^{\frac{1}{2}}$$

The value of α provides a rather good guide to the degree of the polar binding in ionic crystals as can be seen in table 2.2 (24). In highly polar substances such as the alkali halides, α is more than 3 . In intermediate cases such as the silver halides, α is about 1.5; and in weakly polar substances such as the compound semiconductors, α is much less than unity.

The cyclotron resonance experiments of Ascarelli and Brown on AgBr (28), ~~which~~ who observed the resonant electric dipole absorption in the plane of the conduction electrons in a magnetic field, measured the polaron mass m_p rather than the band mass m of the bare electron. This is because the cyclotron frequency (7.10^{10} cycles/sec.) was much less than the optical phonon frequency (5.10^{12} cycles/sec.), allowing the polarization to follow faithfully the cyclotron orbit. They found $m_p = 0.27\ m_e$ from the cyclotron data and $m = 0.20\ m_e$, taking into account the Hall data (21) and the polaron calculations (30). The cyclotron resonance experiments were difficult because of the severe limitation on electron lifetime below 16°K (see Figure 2.7) and Ascarelli's best results were obtained at 18°K. If it was possible to observe the electron mass at frequencies above as well as below the Restrahl frequency,

this should provide an excellent observation of the polaron effect. This range of frequencies has been covered in some of the compound semiconductors, but the effect is small due to the small coupling constant and the experimental results are not sufficiently precise (26). There is thus strong evidence that a slow conduction electron in AgBr is in fact a polaron and that this obeys polaron mobility theory.

As was mentioned in section 2.3.2 b, there is a possibility that the dissociation of an exciton may be assisted by the introduction of the polarization energy of a free electron and hole (24). The formation of an exciton is the result of an optical absorption which takes place in such a short time that the polarization of the lattice cannot follow. Thus, polaron effects are not initially present but the exciton can possibly dissociate into a free polaron in the conduction band and a hole polaron which might be considerably "heavier". The free polaron state may not be much above the exciton state in energy, taking advantage of the polarization gained from the distortion of the lattice.

The range or "Schubweg" of electrons has been measured at room temperature and below, primarily by transient photoconductivity experiments (33, 22). Haynes and Shockley find a unit range of electrons in AgCl of 5.10^{-4} cm^2 $volt^{-1}$, and Van Heyningen's results at low temperatures show a marked dependence on sample preparation. The maximum range at 80^oK was for an air grown sample (10^{-3} cm^2 $volt^{-1}$) and ranges as low as 10^{-6} cm^2 $volt^{-1}$ were obtained for samples which had been grown so as to avoid the possibility of silver oxide dissolving. The principal heavy

metal impurity is possibly iron in an amount of a few tenths of a part per million.

(c) Hole Mobility

While the effects of hole trapping are often observed in silver halides, it has proved very difficult to observe the conduction of holes directly in the silver halides, particularly at low temperatures.

In the experiments of Van Heyningen and Brown (22) did not observe any hole conduction in the silver halides at low temperatures. In silver chloride, and at low temperatures, Burnham measured a mobility of holes in AgBr about 400 times less than the electron mobility.

The diffusion of positive holes at room temperature was established by Stasiw and Teltow (34), who observed the bleaching of silver halides containing traces of silver sulphide. The best direct evidence came from measurements of the dark conductivity of silver bromides in an atmosphere of bromine (35, 36). The dark conductivity increases apparently because the crystal absorbs an excess of bromine; the excess appears in the form of silver ion vacancies and holes which are not trapped by the vacancies at room temperatures. The concentration of vacancies remains virtually unchanged for small bromine pressures because of the large Frenkel disorder normally present, so the increase of conductivity should be due almost entirely to the presence of holes. Hanson and Brown have measured the Hall mobility of holes in AgBr by this technique and have found a value of 1.7 cm^2/volt.sec at 27°C (37) which agrees quite well with other measurements (38).

The drift mobility of holes in AgBr is thus about 40 times smaller than the electron mobility at room temperature, which provides an explanation of why earlier experiments were unsuccessful. A combination of factors such as a high effective mass and a strong polaron effect could explain the low hole mobility.

More recently, the drift mobility of AgBr has been measured between 220° and 320°K by transit time techniques. The mobility varies from 0.8 $cm^2/v.sec$ at 310°K to 2.0 $cm^2/v.sec$ at 250°K. At lower temperatures, multiple trapping begins to set in and there is a characteristic downturn of the mobility. Below 220°K, deep trapping effects begin to predominate. Long hole lifetimes ($\approx$ 100μsec at room temperature) were observed in zone refined samples by allowing impurity or defect centres responsible for hole trapping to precipitate on dislocations (41).

It is generally accepted that some efficient hole trapping mechanism must exist in silver halide crystals if photographic silver is to be deposited in a crystal. A good example of this is the trapping of photoproduced holes in the silver halides by copper impurity in a monovalent state (39, 40).

4 Ionic Properties

Many of the physical properties of a crystal are associated with some sort of distortion or discontinuity in the perfectly periodic crystalline structure. Imperfections can be classed according to their spatial characteristics: as point defects (discussed in this section), linear defects or dislocations, planar defects or grain

facing page 22

figure 2.8

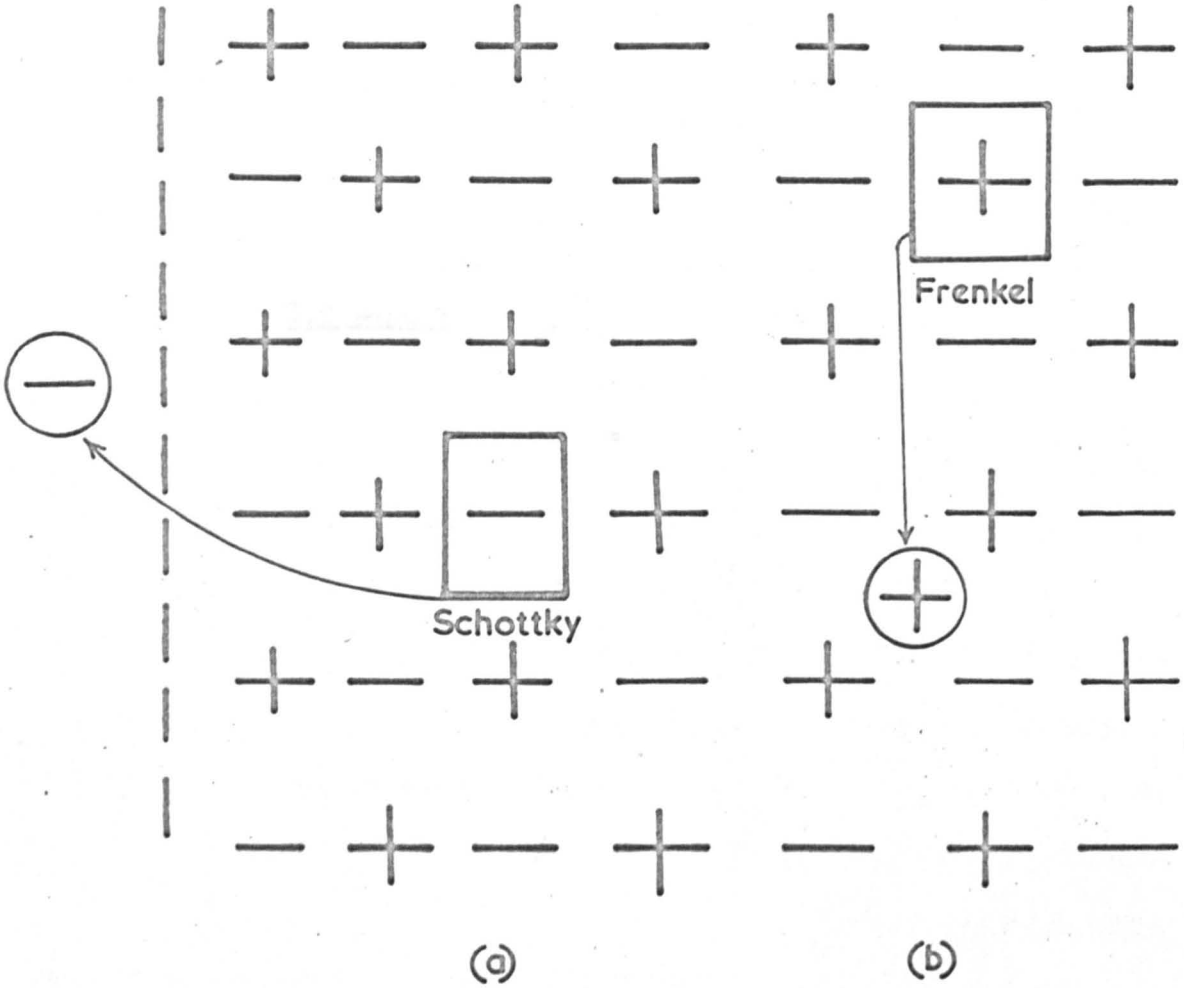

Figure 2.8

Diagramatic Schottky and Frenkel defects in a two dimensional array.

boundaries, and macroscopic disturbances, such as occluded particles. The mechanical strength of a crystal is usually controlled by these defects, (the effect of point defects is usually rather small). Electrical and optical effects, other than the ones described in the last section, are usually connected with a point defect. In a number of cases the defects are paramagnetic and it is possible to observe electron paramagnetic resonance from the unpaired electrons localised on these centres. Such measurements provide very detailed information about the nature of the defect and about its surroundings.

2.4.1 The Crystal in Thermal Equilibrium

In an otherwise perfect crystal lattice, containing no impurities, defects must occur for purely thermodynamic reasons. The Helmholtz free energy of the crystal must be a minimum if it is in thermodynamic equilibrium with its surroundings. Although energy must be expended to form a defect against the cohesive forces of the crystal, the increase in entropy resulting from it causes the free energy to be a minimum for a definite concentration at a given temperature.

The nature of the defects that occur clearly depends on the detailed nature of the crystal. In the alkali halides, Schottky disorder predominates. A Schottky defect comprises a disassociated pair of positive and negative ion lattice sites. This is shown symbolically in Figure 2.8.a for a two dimensional lattice; the square denotes a vacancy. The ions are thought of as migrating to surface sites and it is necessary to have, on average, approximately equal numbers of positive

and negative sites to provide charge neutrality; otherwise, electrostatic repulsion would inhibit the formation of further vacancies. The equality condition will only be fulfilled when the formation energies for positive and negative ion defects are equal.

The Frenkel defect (Figure 2.8 b) is a pair consisting of a positive ion vacancy and a positive interstitial ion, or similarly with negative ions. The silver halides are an example of the former case and calcium fluoride is an example of the latter.

If E_f is the energy required to form one Frenkel defect, then the increase in internal energy in the crystal on forming n such defects is nE_f. If there are N suitable lattice sites in the crystal, then n ions can be taken from these in $\frac{N(N-1)\text{----}(N-n+1)}{n!} = \frac{N!}{(N-n)!\,n!}$ ways (The n! occurs as order of selection is unimportant). They are put into n of the N' interstitial sites in $\frac{N'!}{(N'-n)!\,n!}$ ways. There are thus W ways of forming n Frenkel defects in a crystal, where

$$W = \frac{N!\ N'!}{(N-n)!(N'-n)!\ n!\ n!} \qquad 2.1$$

The increase in entropy (S) on forming n defects is given by the Boltzmann relation $S = k \log W$ 2.2

and the associated change in Helmholtz free energy is:

$$F = U - TS \qquad 2.3$$

The equilibrium state is found by minimizing this function at constant temperature, i.e.

$$\left(\frac{\partial F}{\partial n}\right)_T = 0$$

When 2.1 is substituted in 2.2, the factorial terms can be simplified by using Stirling's approximation, as large numbers are involved.

$$\log x! \approx x\log x - x$$

Substituting 2.2 in 2.3 and performing the partial differentiation yields:

$$E_f - k\,T \log \frac{(N - n)\,(N' - n)}{n^2} = 0$$

i.e. $$n \approx (N\,N')^{\frac{1}{2}} \exp(-E_f/2kT) \qquad 2.4$$

assuming $n << N, N'$

2.4 is in fact the result which would be obtained by using the chemical "Law of Mass Action", with the exponential term as the equilibrium constant.

The possibility of a process taking place depends very strongly on the magnitude of E_f (or in the case of a Schottky defect where the calculation is similar, on the formation energy of the defect pair). If the crystal lattice was completely rigid, the magnitude of the defect formation energy would be in the region of the cohesive energy of the lattice (i.e. above 8e.v. in table 2.1). The polarization energy of the surroundings of the defect can be almost as large as this, and the resulting energy of formation of defects is often in the region of 1 to 2e.v.

Schottky disorder occurs in the alkali halides because of their simple ionic nature - interstitial lattice sites are not available without

distorting the lattice unduly. According to Jost (42), the silver halides prefer the Frenkel mechanism. Here the Van-der-Waals forces are larger and these favour the occurrence of interstitial cations rather than anion vacancies. The existance of interstitials is very seriously affected by the difference in the symmetry of the closed d shell of the silver ion and the closed p shell of alkali metal ions. The difference between the shell and ionic radii could then be important (43). While it is possible for both Frenkel and Schottky mechanisms to occur, only Frenkel defects have been definitely observed even at temperatures near the melting point (44, 45). The activation energy for the formation of Frenkel defects in AgCl is 1.4e.v. (45) and in AgBr it is 1.1e.v. (46).

2.4.2 The Effect of Impurities on Thermodynamic Equilibrium

Once the Frenkel defects are formed the silver halide crystal becomes a good ionic conductor and by measuring the variation in conductivity with temperature, it is possible to assess the importance of this type of conduction. Impurities, particularly those with a valency different from that of the host constituents, will disturb the symmetry of the lattice and disturbance of the charge symmetry will have a very substantial effect at sufficiently low temperatures, depending on the impurity concentration of course.

If it is assumed that the crystal contains divalent positive impurity ions in the concentration n_x, that the concentration of silver ion vacancies is n, and of interstitial silver ions is n', then for

electrical neutrality,

$$n_x + n' = n \qquad 2.5$$

If the crystal is in thermodynamic equilibrium with its surroundings, then the Law of Mass Action is satisfied, i.e.

$$nn' = K_T \qquad 2.6$$

where K_T is the equilibrium constant and will take a form similar to that in equation 2.4. (This will be modified at low temperatures where effectively another constituent will occur due to the association of vacancies with the impurity ions (2); this is usually important only below room temperature).

Eliminating n' from 2.6 and 2.5 gives

$$n = \frac{n_x}{2} + \left(\frac{n_x^2}{4} + K_T \right)^{\frac{1}{2}} \qquad 2.7\ a$$

or eliminating n

$$n' = -\frac{n_x}{2} + \left(\frac{n_x^2}{4} + K_T \right)^{\frac{1}{2}} \qquad 2.7\ b$$

At low temperatures K_T is negligible so that $n = n_x$ and conductivity will depend on the diffusion of impurity induced silver ion vacancies. At high temperatures, K_T is large with respect to n_x^2 and the thermally generated vacancies determine the conductivity. This sort of effect is well known in many crystals (e.g. the alkali halides) and the electronic analogue is found in the case of semiconductors.

In the silver halides, however, electrolytic conductivity due to silver ion vacancies is far lower than the conductivity of interstitials. The diffusion of a defect can be thought of as overcoming a potential

facing page 27

figure 2.9

barrier between one site and the next. This potential is known as the activation energy E_a for migration of a defect and the probability of a jump will have a dependence on E_a and on the lattice temperature. The probability per second (γ) is given by (3):

$$\gamma = \gamma_o \exp (- E_a/kT) \qquad 2.8$$

when γ_o is the atomic vibrational frequency. In this way an expression for the diffusion taking place in a crystal can be found and on applying the Einstein relation which associates a mobility with the diffusion, the ionic conductivity is found to be:

$$\sigma = (N_o e^2 p \gamma a^2 / kT) \exp (- E_a/kT) \qquad 2.9$$

where N_o is the number of ions of the species in the crystal per unit volume, p is the fraction of atoms able to move and a is the lattice constant (3).

The values of E_a for the silver vacancy site are found to be 0.39e.v. in AgCl (47) and 0.25e.v. in AgBr (46), and for the interstitial site 0.10e.v. in AgCl (47) and 0.11e.v. in AgBr (46).

The effect of the very different conductivities for the two mechanisms is shown particularly well by such experiments as those of Teltow (47, 27) where Cd^{++} is introduced into substitutional sites in the crystal and instead of increasing the conductivity of the crystal it is reduced for small concentrations of cadmium at relatively low temperatures, as is shown in Fig. 2.9. This is because the effect of the cadmium is to reduce the equilibrium concentration of interstitial silver ions as is shown in equation 2.7 b and it is only at higher

concentrations of Cd^{++} that the lower mobility of a much greater quantity of vacant sites produces a larger conductivity.

2.4.3 Electron Trapping and Defect Centres

It is to be expected that impurity centres will have a marked effect on the crystal's electronic conductivity. A suitably charged centre would be expected to provide a trap for electrons or holes and even when no trapping can take place, the effect will be a strong scattering, which will reduce the electron or hole mobility.

Such trapping occurs very strongly in the alkali halides at the vacant lattice sites forming an F-centre, when an electron is trapped at a vacant halogen site and a V-centre when a hole is trapped at a vacant metal site. Many more complex centres can be formed on suitable treatment of the crystal, particularly when impurities are incorporated. In general, the centres are classified according to optical absorption bands which correspond to electronic excitation of the centres. A very considerable amount of work has been carried out on imperfections in the alkali halides; references 2 and 48 review the state of this subject.

While similar centres must exist in the silver halides, no direct identification has been made either of the thermally induced centres or of these when electrons or holes are trapped, even at low temperatures. There appear to be no characteristic absorptions in the optical absorption spectrum although it is doubtful if the investigations have been carried far enough into the infra-red. The only absorption which

can be observed is that of colloidal silver particles in suitably prepared crystals - this is discussed in the following section.

Silver chloride and bromide exhibit an efficient characteristic visible luminescence at low temperatures; this is quenched by thermal activation above 180°K in AgCl and above 77°K in AgBr. This effect is not as yet well understood but it is of considerable interest and has been investigated quite extensively. Wiegand (58) suggests that the process is possibly connected with the transport of carriers since irradiation leads to electrons and holes in the crystal. The holes are first trapped at silver ion vacancies which later act as recombination centres for the conduction electrons. The luminescent emission spectrum has been investigated by Vacek and others (59) in pure and doped AgCl and they observe a doublet structure in the band extending from 450 to 550 mμ which could be due to an exciton on a lattice vacancy, and on a dislocation jog (59) or else it may reflect the exciton structure seen in optical absorption (11). Sonoike and Akimoto have observed a number of bands which are common to various impurities and so would appear to be connected with crystal defects rather than impurity sites (60). Various emission bands are attributed to silver vacancies (545 mμ), interstitial silver ions (520 mμ); one possibly due to thermally decomposed silver atoms (620 mμ) and a peak at 485 mμ which may be due to shallow electron traps at dislocation sites.

2.4.4 The Colloidal Band

Optical colloid absorption bands are well known in many ionic crystals including the alkali halides; conduction electron spin resonance has been observed in many of them - in particular when the spin-lattice relaxation of the conduction electrons is sufficiently long, in Li, Be, Na and K. Lithium colloids form very easily on the irradiation of lithium hydride and this was the first occasion when conduction e.s.r. in such colloids was observed (49). The case of lithium in lithium fluoride is particularly useful as a "g-value marker" in e.s.r.; Kaplan and Bray (50) found that Li colloids formed when crystals were given very heavy neutron doses ($\approx 10^{20}$ per cm^2) and on annealing at 730°C the single e.s.r. line narrowed to not more than ·03 gauss with a g-value of $2.00229 \pm \cdot 00001$, extremely close to the free spin value.

Conduction e.s.r. of silver colloids in AgBr has been claimed (51) but all attempts to repeat this have been completely unsuccessful. It should be noted that these results were obtained using a highly impure AgBr powder sample (the impurity would probably be in the region of 1%, but no measurement was made of this).

The optical absorption by colloidal particles was originally treated by Mie in 1908 (52, 53) who applied his results to suspensions of gold particles in liquids. The "latent image" or colloid absorption in the silver halides was first observed by Hilsch and Pohl (54) and has been extensively investigated since then. Some dichroism

facing page 31

figure 2.10

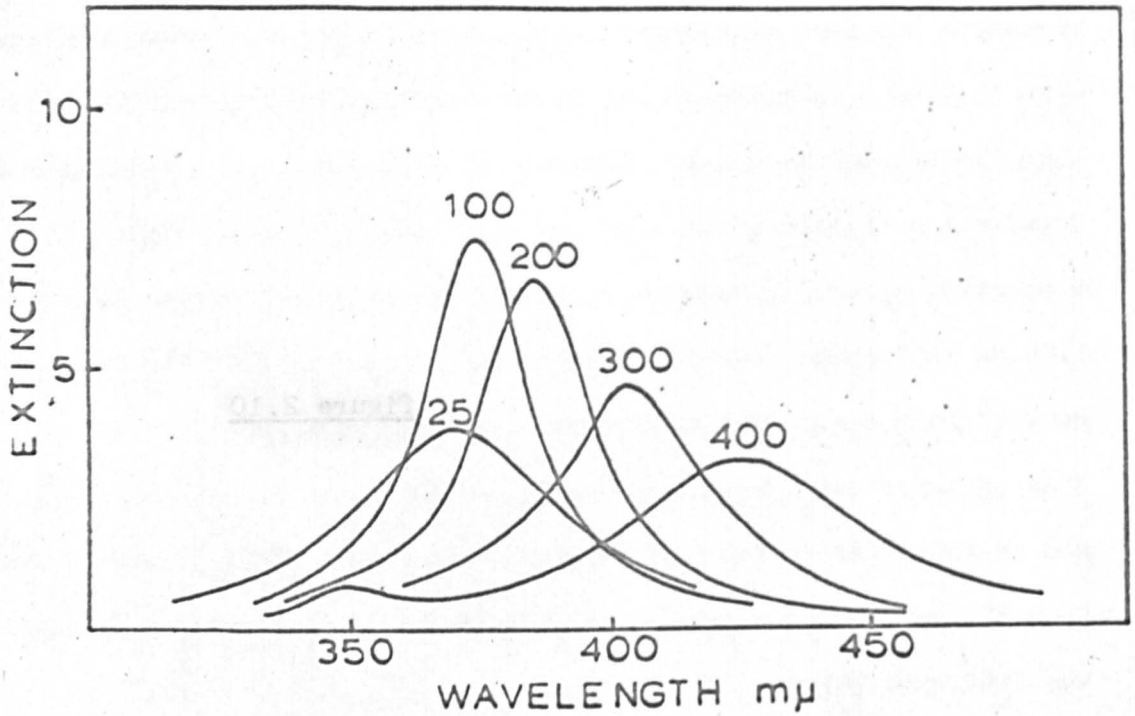

Figure 2.10

Wavelength dependence of optical extinction calculated as a function of particle radius (given in Å) for sodium spheres (57).

was observed by Rohloff on rolled specimens of AgCl, where the colloidal silver particles would be distorted (55). A similar effect would presumably occur if preferred orientation of non-spherical particles took place.

A physical explanation of the colloid absorption process has been put forward by Doyle (56, 57). It is due to a frequency dependent local field within the particle which is a result of the variation of the internal dielectric constant with frequency. Doyle also put forward the alternative explanation that the absorption is due to a bound plasma resonance of the conduction electrons in the colloidal particles as a whole. He points out that conditions are the same (i.e. depending on the real part of the complex dielectric constant of the metal which falls to zero at the frequency of onset of the u.v. transparency). Doyle's theoretical results for sodium, which is electrically "well behaved" are shown in Figure 2.10. The wavelength dependence of optical extinctions is given as a function of particle radius in Å.; the absorptions are of an electric dipole character but he predicts that for the largest particles there will be some electric quadrupole contribution at shorter wavelengths.

2.4.5 Properties of Certain Metallic Ions as Impurities

The effect of many different ions in the silver halides have been investigated, particularly in relation to the photographic process. Much of this work has been of a phenomenological or chemical nature and the physical processes involved have remained quite obscure.

A commercial photographic emulsion is exceedingly complex and is often only accessible for investigation after the system has been drastically simplified. Most of the important processes which take place occur on the surface of the crystal grains in the emulsion and it is in general on the surface that sensitization of the grains for absorption of radiation occurs. Important processes can however take place away from the grain surface, and it is in such processes that experiments with large crystals, or crystal plates can be of considerable importance. Many of the physical processes taking place in photographic systems are discussed by Mitchell (61) and although this work is very incomplete, and some of the conclusions may be inadequate, it provides an excellent guide to the physical nature of the problem. Some mention of Mitchell's approach to the subject is given in 2.6.

The effect of anions such as oxygen, sulphur, selenium and tellurium in the silver halides has been investigated extensively by Stasiw and his co-workers (62), but the details of this work are beyond the scope of this thesis. Among the many cations which have been investigated are copper, iron, manganese, gold, cobalt (63) and nickel (63, 64); of these the first four will be described.

(a) Copper

It is found that when copper is incorporated in silver chloride crystals which are annealed in a reducing atmosphere, the crystal is highly sensitized for the formation of an internal latent image (i.e. on irradiation in the exciton or conduction band at room temperatures,

there is a large amount of colloidal silver formed in the crystal) (65, 66, 67). Annealing the crystal in an oxidising atmosphere (chlorine) removes this photosensitivity.

Tucker observed the e.s.r. spectra of Cu^{++} in freshly chlorinated samples (68). He found that three complexes could occur: in samples cooled quickly from room temperature to liquid nitrogen temperature, the dominant one is that of a Cu^{++} ion substituted for an Ag^{+} ion. Apparently all of the surrounding lattice sites are occupied and there is a Jahn - Teller distortion along a <100> axis. One of the other centres has a similar but larger distortion and this is attributed to a vacant next-nearest neighbour silver ion lattice site (<100> direction) The third centre is due to Cu^{++} with the nearest neighbour silver lattice site vacant (<110> direction). Larger numbers of the latter two types of complex can be obtained by cooling the crystal slowly from room temperature. This allows the thermally dissociated silver ion vacancy to associate with the charged copper ion - the binding energy of this complex is only about 0.2e.v. (27). Palma and his co-workers found that irradiating Cu^{+} doped crystals with the 436 mμ Hg-line at room temperature formed centres similar to those described by Tucker (39, 69). They found that darkening increased on irradiation but afterwards the e.s.r. signal decayed over some hours and could be restored on reirradiation. The Cu^{+} ions apparently act as a hole trap and electrons combine with silver ions at suitable sites to provide the darkening. This is in agreement with the mechanism put forward

by Mitchell for photographic sensitivity (2.6). This work showed the importance of using light which would penetrate the crystal for irradiation; earlier experiments using u.v. radiation produced much less stable centres on or close to the crystal surface. The decay of the e.s.r. signal is probably associated with a loss of resolution implying an interaction with other Cu^{++} ions (70).

More recent work by Burnham and Moser has shown that in well prepared crystals with a relatively low concentration of Cu^{+} (less than $10^{17}/cm^3$; Palma's samples contained about $3 \times 10^{18}/cm^3$), the e.s.r. signal obtained on irradiation is fairly stable at room temperature and the lifetime is short only above $180^{o}C$ (40). It would appear that Cu^{+} ions provide a deep hole trap, while in halogenated crystals Cu^{++} ions act in some ways as an electron trap (71) (presumably the process where an electron associated with the interstitial Ag^{+} liberated when a hole is captured by Cu^{+} is more probable in the Cu^{+} doped specimens until sufficient Cu^{++} centres are formed).

The stability of the e.s.r. signal from the Cu^{++} ions in irradiated Cu^{+} doped crystals and in Cu^{++} doped crystals is destroyed by straining the samples and this presumably accounts for the lower stability of Palma's and Tucker's signals.

Apparently an aggregation of Cu^{++} centres takes place ~~and~~ it would appear that this is related to crystal dislocations at room temperature and/that some process ~~must~~ occurs where the Cu^{++} ions may be redispersed by

optically bleaching the absorption attributed to them, restoring the e.s.r. signal (72).

In conclusion, the investigations on the system AgCl : Cu have demonstrated the relevance of hole trapping mechanisms to darkening of the silver halides and the importance of dislocation processes as well as purely electronic and ionic phenomena.

(b) Iron

There has recently been some investigation of the effect of iron dissolved in the silver halides. This has some importance principally because it has proved difficult to remove it from otherwise pure samples of the host. There is thus likely to be present (perhaps in quantities of about 0.1 p.p.m.) some iron in nominally pure crystals and it must be remembered that some of the properties described in 2.3 are perhaps the result of iron impurity in the crystal as much as properties of the silver halide itself. This will be particularly important in the case of low temperature mobility experiments.

Brown and his co-workers have observed an increase of electron trapping in crystals doped with iron (73). Recent work has been to investigate the nature of Fe^{3+} centres in the silver halides using e.s.r. techniques. These centres were obtained by annealing doped crystals in the halogen at around 400°C and quenching them to liquid nitrogen temperatures (74, 75). One state has been observed: that of $^6S_{5/2}$ in a cubic environment. There is a partly resolved hyperfine

interaction with the halogen ligands in the $M_s = -\frac{1}{2} \rightarrow +\frac{1}{2}$ fine structure transition (Figure 7.1). Maximum resolution is in the <100> crystallographic direction and Hayes has fitted the absorption line-shape using an independent bonding model to an interstitial Fe^{3+} ion co-ordinated with four tetrahedrally placed halogen ions on normal lattice sites $(FeCl_4)^-$ (Figure 8.1). It is necessary to include a large quadrupole contribution to obtain the correct type of splitting. The ENDOR spectrum of $(FeCl_4)^-$ has been observed by Garth (76); his results essentially confirm those predicted by Hayes (table 2.3).

Table 2.3 Parameters (i) of the Spin Hamiltonian of Fe^{3+} in AgCl and AgBr.

Lattice	g (ii)	a (ii)	A (ii)	A (iii)	B (ii)	B (iii)	P (ii)	P (iii)
AgCl	2.0156 ±0.0004	+75.0 ± 0.3	3.3 ±0.5	3.85 ±0.06	2.0 ±0.5	+2.28 -0.04	(-)1.0 ± 0.5	1.91 ±0.04
AgBr	2.045 ±0.005	(iv)	16.2 ±1.5		7.8 ±1.5		(+)3.8 ± 1.5	

(i) The various parameters have their usual meaning and a, A, B and P are in units of $10^{-4}cm^{-1}$. The sign of a is from measurements at 1.3°K (76).
(ii) From reference 75.
(iii) From reference 76.
(iv) No fine structure has been observed, possibly because of crystal imperfections.

There is apparently a considerable amount of covalent bonding in the ion $(FeCl_4)^-$ and supporting this model, this complex is found to exist in molecules with a high stability.

Hayes proposed the model which is shown in Figure 8.1 for this centre; the Fe^{3+} ion is in an interstitial site with the tetrahedron of four nearest neighbour Ag^{+} absent. This is supported by measurements of the room temperature ionic conductivity as predicted by Hayes et al. and more recent measurements by Slifkin with large annealing pressures further support the interpretation (77). ENDOR studies of the chlorine (76) and silver (78) nuclei surrounding the complex have confirmed this model.

Apparently the stable state of iron in the silver halides is the ferrous one (Fe^{2+}) in a substitutional site, as is the case with Cu^{2+}, Ni^{2+}, Co^{2+}, and Mn^{2+} (68, 64, 63, 79). The measured ionic conductivity of crystals also corresponds to one silver ion vacancy associated with each Fe^{2+} ion (75, 27). Bottger (8), claims to have observed dipolar absorption in AgBr, due to an Fe^{2+} ion with an associated silver ion vacancy (2.2.2). Koswig and Kunze have observed the optical absorption spectrum of Fe^{2+} in AgCl and AgBr in both low and high concentrations (where aggregation occurs). Their results for the dilute phase agree with the Fe^{2+} model with an associated distortion (80). No observation has been reported of e.s.r. of Fe^{2+} in AgCl, perhaps because of the likelihood of line broadening by lattice defects (81).

Hayes proposes a process for the conversion of Fe^{2+} to Fe^{3+} during a high temperature anneal in chlorine. This will be described in Chapter VIII where the results obtained with irradiated AgCl : Fe will be discussed.

(c) Manganese

A number of workers (82, 83, 79) have studied the S-state ion Mn^{++} in AgCl using e.s.r. techniques. The results are not significantly different from those with Mn^{2+} in alkali chlorides (84). Daehler (79) observed isolated Mn^{2+} centres and centres distorted by a next-nearest neighbour silver ion vacancy in a <100> direction, depending on how the crystal was cooled, as with copper. He also observed a very broad absorption ($\approx$ 750 gauss near g = 2) which he attributed to an aggregation of the manganese centres. This work has been pursued with AgBr : Mn^{++} but so far no results are available due to the large line width of the manganese resonance in this host.

Some e.s.r. studies were made on AgCl : Mn during the investigations on silver chloride which are the subject of this thesis. The results obtained appear to agree with Daehler's, but they were not continued in detail because of Daehler's almost identical work.

(d) Gold

Little work has been done on the physical properties of gold dissolved in the silver halides. It is used extensively in commercial photographic emulsions to increase the sensitivity of the emulsion for incomplete development. It apparently acts on the emulsion grains surface and is probably associated with sulphur ions, i.e. adsorbed as aurous sulphide (61). It is unlikely that the subject would be directly useful in this thesis, particularly because it has been studied empirically as a surfaces chemical phenomenon with little

reference to the physical processes involved.

Mitchell has investigated the decoration of dislocations (2.5.1) by Ag and Au in the silver halides (85) and a brief description of the use of gold in this context will be given.

Chemically, gold occurs in a monovalent (aurous) state or in a trivalent (auric) state. A divalent form, analogous with divalent copper or silver does not normally occur as a stable chemical species; e.s.r. of divalent gold complexes ~~may have~~ has been observed under special conditions (92). Gold forms chlorides in both its states, and in such substances as chloroauric acid ($HAuCl_4$) the planar complex $(AuCl_4)^-$ is quite stable.

Bartlett and Mitchell prepared their crystals by adding up to 0.1 Mol% of auric chloride to molten AgCl under an atmosphere of hydrogen chloride. They expected it to go into the crystal as aurous chloride. Before examination, they annealed the crystals for 6 to 12 hours under 200 to 300 mm. Hg of chlorine at $350^{o}C$. Annealed crystals containing 10^{-1}Mol% of AuCl which had been briefly irradiated through an AgCl filter (to remove strongly adsorbed wavelengths), darkened in exposed areas in a matter of a few weeks at room temperature and in a few minutes at about $150^{o}C$. The darkening was apparently due to the separation of platelets of gold. Later experiments with lower concentrations produced no such separation probably because the gold diffused out of the crystal in the anneal. They then annealed the crystal in chlorine in the presence of gold

which on exposure and thermal development produced excellent decoration of dislocations.

Mitchell points out that the system is in a metastable state of high free energy at room temperature, and that the free energy is lowered by the separation of platelets and the liberation of the halogen. This would occur when the AuCl had a much lower solubility in AgCl at room temperature than at 400°C. It would appear that the sort of mechanism which occurs on thermal development is analogous to that of chemical development to produce silver (61). The irradiation forms some nucleus, similar to the latent image (2.6), and gold ions which probably diffuse through the crystals by way of the interstitial positions are adsorbed to the nuclei to charge them positively. This is followed by the transfer of electrons from halide ions with the creation of positive holes. Gold atoms are thus added to the nuclei and positive holes and vacant silver ion lattice sites diffuse to the surface where halogen molecules are formed and can escape (85).

The best decoration was observed within a fraction of a millimeter of the crystal surface. In the interior, the contrast was not good due to a general separation of fine particles of gold as well as the decoration.

The optical colloid absorption of AgCl : Au is described in Chapter VII.

facing page 41

figure 2.11

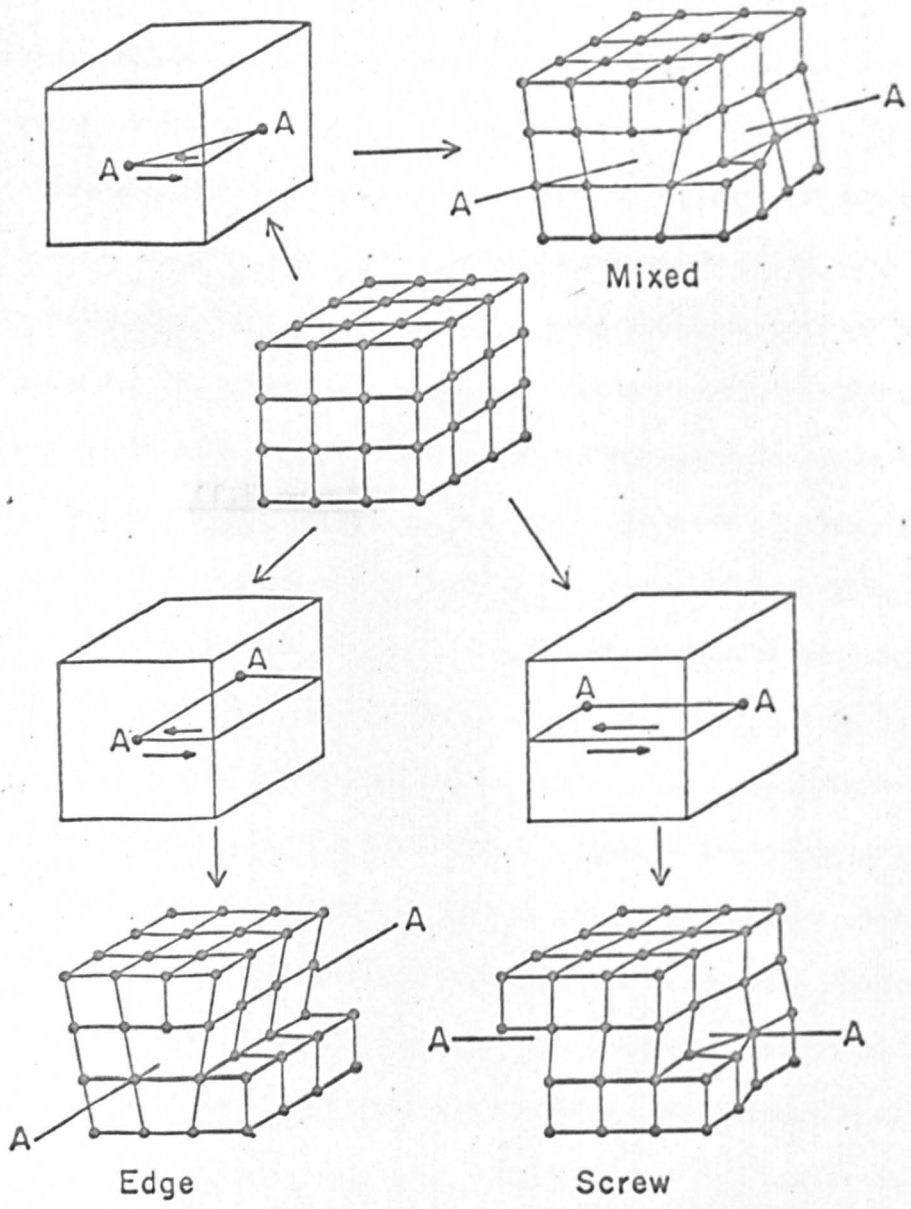

Figure 2.11

The Creation of an Edge, Screw and a Mixed Dislocation.

2.5 Dislocations

Although crystal lattice dislocations have their greatest significance when such subjects as lattice strength and crystal growth are being studied, they can have considerable effect on the character of ionic processes which occur in the crystal. A brief description of dislocations will be given to indicate the sort of processes which may be important.

2.5.1 General Description (3, 86)

The concept of a dislocation in a lattice is of a linear defect in the cubic array. Its best description is obtained from a study of its formation. In the centre of Figure 2.11 is the starting material, a perfect, undeformed simple cubic lattice (taken for the sake of clarity). Suppose this lattice is cut along any of the planes indicated in the auxiliary cubes, then the atoms on one side of the cut are shifted in a direction parallel to the cut surface through a distance equal to one atom spacing relative to the corresponding atoms on the other side. The atoms on either side of the cut are then rejoined and the new, distorted lattice is shown in the outer figures. The lattice structure itself is actually almost perfect except near the lines AA of the various figures. The line AA is the dislocation line. If the atoms over the cut surface are shifted in a direction perpendicular to the line AA an edge dislocation is created; if the shift is parallel to AA, a screw dislocation is created; if the shift is at some other arbitrary angle to AA, the result is a dislocation

of mixed character. In general, the line AA need not be straight and the dislocation can vary between the two extremes.

An edge dislocation can be simply visualized by inserting an additional half plane of atoms in the crystal. A screw dislocation can be thought of as a spiral ramp about the dislocation line.

The planar lattice defect which is called a small angle or sub-grain boundary can be constructed from arrays of dislocations. A tilt boundary is made up of a series of edge dislocations and a twist boundary is an array of screw dislocations. Such boundaries are likely to exist in a nominally single crystal. They can be observed using X-ray crystallographic techniques or else the distortion of the lattice can be observed in polarized light in the transparent crystal when the boundary angle is sufficient.

As was previously mentioned, the prime importance of dislocations is connected with the mechanical strength of crystals. Plastic slip processes can occur many orders of magnitude more easily when dislocations are present in a crystal than in a perfect crystal; the silver halides are an excellent example of this. They have a consistency akin to ~~stiff~~ cheese and clearly the lattice energy is not directly playing much part in maintaining the lattice as the melting points are over 400°C. It is not possible to cleave the crystals and these properties lead to many problems in handling single crystal specimens.

Frank has proposed mechanisms which greatly increase the speed

of growth of crystals - the presence of screw dislocations on a crystal surface mean that no new lattice planes need be formed; the crystal grows on the "ramped" single plane.

Dislocations can be observed directly in a number of ways: by direct observation in metal films using electron microscopy; by decoration techniques, which were originally developed by Mitchell in his work on the silver halides; and by observing the etch pits which occur where dislocations emerge on crystal surfaces which have been treated with some etching solution. The latter two techniques have been used very extensively on the silver halides and much has been learned about the properties of dislocations from this work.

2.5.2 Interactions with Point Defects

(a) Mechanical Effects

Dislocations are surrounded by a mechanical stress field whose magnitude decreases as a function of distance. An impurity atom, having a radius some-what different from that of the normal atoms, will produce a local disturbance of the lattice, i.e. a stress field. In this way, an interaction between the dislocation and the impurities will occur. Cottrell (88) proved that in first approximation, only edge dislocations interact with impurities and that a cloud of impurities, the so called "Cottrell Atmosphere", will be formed around them. Naturally, migration is only possible when diffusion is possible and if the temperature is too high, thermal agitation makes the number of atoms leaving the atmosphere the same as the number entering and

the Cottrell atmosphere more or less vanishes. Cottrell calculated that, in a well annealed, undeformed crystal, with about 10ppm. of impurity, all the dislocations (about $10^5/cm^2$) will be saturated. The Cottrell atmosphere has important effects on the mechanical strength of the crystal.

It should be noted that dislocations are not created under conditions of thermodynamic equilibrium, so that, once they have been created, correct annealing will not restore the perfect lattice. Annealing will, however, allow some opportunity for associated point and near point defects to minimise their free energy.

It may also be possible that impurities can migrate along dislocation lines with a lower activation energy for diffusion than in the crystal lattice.

(b) Electrical Effects

Two dislocations can intersect in any one of a large number of ways. There are a variety of ways in which one dislocation can move past another but the result is often that a trail of vacancies or interstitials is created. The crossing of two screw dislocations at right angles produces a row of vacancies. Another case is ~~where~~ one in which two parallel edge dislocations of opposite sign meet and annihilate one another. If they fail to meet by one lattice spacing, for example, then a row of vacancies is again produced. (This latter case is not a very likely one but it is very simple to visualize). The interaction of dislocations in a straining process will thus produce many vacancies

and interstitials in the lattice. They will presumably diffuse away subject to the thermodynamic state of the crystal. It was pointed out by Seitz (89), that a row of negative ion vacancies is indistinguishable along an edge dislocation from a row of interstitial positive ions which have condensed at the edge of the dislocation. Annealing the crystal should restore the thermodynamic equilibrium to some extent.

Another result of the interactions between dislocations is that discontinuities or steps in the dislocation lines can occur. These are known as jogs when the step moves the dislocation from one slip plane to another and as kinks if the dislocation remains in the slip plane; a jog can only be eliminated at temperatures high enough to permit "climb" of the dislocation (i.e. when the dislocation can become a source or sink for vacancies). There will be a large number of jogs and kinks immediately after plastic deformation but in time the number will fall considerably.

A very important property of dislocation jogs and kinks in ionic crystals is that they carry an electrical charge of $\pm e/2$, where e is the ionic charge (89), so that they can take part in the trapping of electrons and holes, and of mobile ions in the crystal.

Figure 2.12

Figure 2.12 is a simple demonstration of the fact that what is called an "incipient halogen ion vacancy" has a charge of e/2. The row of ions represents an extra strip on the edge of an edge dislocation in a crystal of the NaCl type, running in the <100> direction. The squares represent two incipient halogen ion vacancies at the points where the dislocation jogs. The row possesses an extra charge of +e which may be regarded as being evenly divided between both ends and hence the incipient vacancies.

Dislocations as a whole will be charged if their surroundings are in thermal equilibrium and there is an excess of incipient vacancies of one sign. This will occur whenever the energies of formation of vacancies (or interstitials) of both signs are different. For electrical neutrality to occur, the dislocation will be surrounded by a "Debye-Hückel" cloud of vacancies or interstitials having a net charge equal and opposite in sign to that of the dislocation. This can be described as an "electrical Cottrell atmosphere". When divalent impurities are present, the magnitude of the charge of the dislocation is modified and can even be reversed (90).

McGowan (91), has demonstrated that moving dislocations in AgCl carry a negative charge, using an indentation technique to produce a strong inhomogeneous stress field.

It is a matter for speculation what effects dislocations will have on the electronic properties of silver halides. The distortion will relax electronic transition selection rules (89), as well as

disturbing the band structure. The 75°K peak in the glow curve (Figure 2.7) may be associated with dislocations in some way (22).

2.6 Photographic Sensitivity

As has been previously mentioned, the silver halides, often as mixed crystals of chloro-bromide or bromo-iodide, form the basis of all photographic emulsions. The crystal grains are suitably "sensitized" which usually means they are treated chemically to form the sulphide on the surfaces and also with dyes to convert the lower energy (red) radiation to some form with which the surface will interact. The emulsion is then formed by suspending the sensitized grains in gelatine.

It is not intended to describe the sort of very complex processes which must take place in such an emulsion. The theories put forward, however, principally by Mitchell (61, 92), go some way to providing an explanation of both surface and volume effects although it is not in place to give a criticism of them.

Two properties of silver halide crystals are particularly important in their ability to form a photographic image, which is the accumulation of very small particles of silver. Of prime importance is the ease of formation and the high mobility of interstitial silver ions (2.4.1 and 2); following this is the ability to absorb relatively low energy radiation (2.3.2) with the efficient formation of electrons and holes (Gurney - Mott theory). In some way, electrons and silver ions combine within the lifetime of the conduction electrons and a

"latent-image speck" is formed. At some stage of the process, this speck is stable and is "developable", i.e. it can be developed chemically from microscopic to macroscopic dimensions.

Following on the suggestion by Seitz regarding the half ionic charge on incipient vacancies (2.5.2 b), Mitchell has evolved a largely qualitative theory which appears to fit many of the properties of silver halide crystals (61). His theory is based on the parts of the Gurney - Mott theory mentioned above with a recognition of the importance of crystal dislocations as sites for the formation of the image. He further assumes that it is in the incipient vacancy beside the silver ion jog sites (or similar surface sites) with the charge e/2 that the latent image starts to form. Seitz suggests that this will trap an electron, but Mitchell proposes that in fact an electron will only be efficiently trapped after an interstitial silver ion has diffused into the vicinity of the jog. This is perhaps not too unlikely as the +e/2 trap will be very shallow at room temperature due to the polarization of the surrounding lattice; (Mitchell (61) estimates 0.05 to 0.02e.v.). This small repulsion may well be balanced by a mechanical Cottrell attraction (2.5.2.a). The lifetime of this silver atom in a site next a jog is apparently limited (Mitchell estimates in the region of 1sec) and this process must be repeated to form a more stable pair of silver atoms. A latent image speck is formed by the further addition of an interstitial Ag^{+} ion and a conduction electron in that order. This will decay on prolonged storage. Mitchell then postulates that at room

temperature, groups of three or more silver atoms adsorb adjacent jog sites silver ions and thus become positively charged. The compensating negative charge is provided by vacant silver ion lattice sites in the neighbourhood.

Crucial to Mitchell's argument is the fate of positive holes. If they are likely to be trapped by the image as it builds up, a regression will occur and the quantum efficienty is drastically reduced below what is often observed. Holes have a considerably higher mobility than the interstitial ions $\approx 1\ cm^2 volt^{-1} sec^{-1}$ compared with $5 \times 10^{-4} cm^2 volt^{-1} sec^{-1}$ for Ag^+ interstitials in AgBr (2.4.2).

It is thus essential that very efficient hole traps should exist; in the pure silver halides they do not, so that their photosensitivity is very low. When a hole is trapped by a suitable site, to maintain charge neutrality, a silver ion will be released which can diffuse by the interstitialcy mechanism to a point where it can contribute to the latent image. When the hole is trapped on or is close to the surface of the crystal, it can join with another trapped hole and silver ion vacancy to allow the formation of a halogen molecule. While gas may under some circumstances form within the crystal (perhaps on internal imperfections) this would not seem very likely and it would appear that the release of halogen depends on the ability of silver vacancies to diffuse to the surface. This matter is not at all clear but it may be a limitation on the formation of the internal latent image. Even if image formation takes place in pure crystals,

it will only occur very slowly at room temperature due to the relatively small number of Frenkel defects in the crystal ($\approx 10^{12}/cm^3$ in AgBr).

The case of Cu^{+} doped AgCl described in 2.4.5.a is an excellent example of the action of a hole trap assisting the formation of a latent image. On the other hand, Cu^{++} in AgCl acts as an electron trap and this inhibits formation of the image.

CHAPTER II - REFERENCES

1. F. Seitz, "Modern Theory of Solids", McGraw-Hill (1940).
2. F. Seitz, Rev. Mod. Phys., 18, 348 (1946); 26, 7 (1954).
3. C. Kittel, "Introduction to Solid State Physics", Wiley (1956).
4. A.J. Dekker, "Solid State Physics", McMillan (1960).
5. G. Chiarotti, "Radiation Damage in Solids", p. 398, ed. D.S. Billington, Italian Physical Society (1962).
6. N.F. Mott and R.W. Gurney, "Electronic Processes in Ionic Crystals", Oxford (1948).
7. L. Pauling, "The Nature of the Chemical Bond", Cornell (1945).
8. H. Bottger, Phys. Stat. Sol., 4, 669 (1964).
9. M. Born and K. Huang, "The Dynamical Theory of Crystal Lattices", Oxford (1954).
10. G.O. Jones et al., Proc. Roy. Soc., A261, 10 (1964).
11. F.C. Brown, J. Phys. Chem., 66, 2368 (1962).
12. F. Moser, D.C. Burnham and H.H. Tippins, J. Appl. Phys., 32, 48 (1961).
13. Y. Okamoto, Nachr. Akad. Wiss. Gottingen (IIa) 14, 275 (1956).
14. J.E. Eby, K.J. Teegarden and D.B. Dutton, Phys. Rev., 116, 1099 (1959).
15. F.C. Brown, T. Masumi and H.H. Tippins, J. Phys. Chem Solids, 22, 101 (1961).
16. F. Bassani, R.S. Knox and W.B. Fowler, Phys. Rev., 137 A1217 (1965).

17. R.S. Knox, The Theory of Excitons, Solid State Physics, Suppl. 5, eds. F. Seitz and D. Turnbull, Academic (1963).

18. F.C. Brown and F. Seitz, "Scientific Photography", p. 13, ed. H. Sauvenier, Liege Symposium (1959).

19. P.W. Baumeister, Phys. Rev., 121, 359 (1961).

20. F.C. Brown and F. Seitz, "Photographic Sensitivity", 2, 11, ed. S. Fujisawa, Maruzen (1957).

21. D.C. Burnham, F.C. Brown and R.S. Knox, Phys. Rev., 119, 1560 (1960).

22. R.S. van Heyningen and F.C. Brown, Phys. Rev., 111, 462 (1958).

23. R.S. Knox, F. Bassani and W.B. Fowler, "Photographic Sensitivity" ed. S. Fujisawa, Maruzen, 3, 11, (1963).

24. F.C. Brown, "Excitons and Polarons", p. 323, (ref. 32).

25. K. Kobayashi and F.C. Brown, Phys. Rev., 113, 507 (1959).

26. G. Ascarelli, "Excitons and Polarons", p. 357, (ref. 32).

27. I. Ebert and J. Teltow, Ann. Phys. Lpz., (6), 15, 268 (1955).

28. G. Ascarelli and F.C. Brown, P.R.L., 9, 209 (1962).

29. C. Kittel, "Quantum Theory of Solids", Wiley (1963).

30. R.P. Feynmann et al., Phys. Rev., 127, 1004 (1962)

31. L. Landau, Physik. Z. Sowjetunion, 3, 664 (1933).

32. C.G. Kuper and G.D. Whitfield (editors), "Polarons and Excitons", Oliver and Boyd (1963).

33. J.R. Haynes and W. Shockley, Phys. Rev., 82, 935 (1951).

34. O. Stasiw and J. Teltow, Nachr. Akad. Wiss., Gottingen, 155 (1944).

35. C. Wagner, Z. Physik. Chem., B 32, 447 (1936).

36. G.W. Luckey and W. West, J. Chem. Phys., 24, 879 (1956).

37. R.C. Hanson and F.C. Brown, J. Appl. Phys., 31, 210 (1960)

38. F.A. Hamm, "Scientific Photography", p. 172, ed. H. Sauvenier, Pergamon (1962).

39. I.S. Ciccarello, M.B. Palma-Vittorelli and M.U. Palma, Phil. Mag., 5, 723 (1960).

40. D.C. Burnham and F. Moser, Phys. Rev., 136, A 774 (1964).

41. R.K. Ahrenkiel and R.S. Van Heyningen, Bull. Am. Phys. Soc., 10, 394 (1965).

42. W. Jost, "Diffusion in Solids, Liquids and Gases", p. 109f., Academic (1952).

43. J.C. Slater, J. Chem. Phys., 41, 3199 (1964).

44. B.N. Dutta and B. Dayal, Phys. Stat. Sol., 5, 73 (1964).

45. R.D. Fouchaux and R.O. Simmons, Phys. Rev., 136, A 1664 (1964).

46. W.D. Compton, Phys. Rev., 101, 1209 (1965); W.D. Compton and R.J. Maurer, J. Phys. Chem. Solids., 191 (1965).

47. J. Teltow, Z. Physik. Chem., 195, 197, 213 (1950); Ann. Physik, 5, 63 (1949).

48. J.H. Schulman and W.D. Compton, "Color Centers in Solids" Pergamon (1963).

49. W.T. Doyle, D.J.E. Ingram and M.J.A. Smith, Proc. Phys. Soc., 74, 540 (1959).

50. R. Kaplan and P.J. Bray, Phys. Rev., 129, 1919 (1963).

51. M.J.A. Smith, Ph.D. Thesis, University of Southampton (1961); M.J.A. Smith and D.J.E. Ingram, Proc. Phys. Soc., 80, 139 (1962).

52. G. Mie, Ann. Physik., 25, 377 (1908).

53. H.C. van de Hulst, "Light Scattering by Small Particles", Wiley (1957).

54. R. Hilsch and R.W. Pohl, Z. Phys., 64, 606 (1930).

55. E. Rohloff, Z. Phys., 132, 643 (1952).

56. W.T. Doyle, Proc. Phys. Soc., 75, 649 (1960).

57. W.T. Doyle and A. Agarwal, J. Opt. Soc. Am., 55, 305 (1965).

58. D.A. Weigand, Phys. Rev., 113, 52 (1959).

59. K. Vacek, Czech. J. Phys., B 13, 424 (1963) and B 10, 66 (1960).

60. S. Sonioke and K. Akimoto, J. Phys. Soc. Japan, 18, Suppl. 2, 320 (1963).

61. J.W. Mitchell, Rep. Prog. Phys., 20, 433 (1957).

62. O. Stasiw, Bull. Acad. Sci. U.S.S.R. Phys. Ser., 24, 209 (1960);
A. Scholz, Ann.Der. Phys., 7, 179 (1961);
A. Scholz and O. Stasiw, Z. Phys., 164. 431 (1964);
M. Stasiw, Phys. Stat. Sol., 7, 893 (1964); 8, 139 (1965).

63. T.R. Sliker, Phys. Rev., 130, 1749 (1963).

64. J. Busse, Phys. Stat. Sol., 3, 1892 (1963).

65. P.V. McD. Clark and J.W. Mitchell, J. Photo. Sci., 4, 1 (1956).

66. A.S. Parasnis and J.W. Mitchell, Phil Mag., 4, 171 (1959).

67. F. Moser, N.R. Nail and F. Urbach, J. Phys. Chem. Solid., 3, 153 (1957).

68. R.F. Tucker, Phys. Rev., 112, 725 (1958).

69. L. Bellomonte, M.B. Palma-Vittorelli and M.U. Palma, P.R.L., 9, 84 (1962); Paramagnetic Resonance Vol. 2, ed. W. Low, p. 790 (1963).

70. M.U. Palma, Private communication.

71. R.S. Van Heyningen and F. Moser, Bull. Am. Phys. Soc., 8,230 (1963).

72. F. Moser and D.C. Burnham, Bull. Am. Phys. Soc., 10, 349 (1965).

73. T. Masumi, R.K. Ahrenkiel and F.C. Brown, Phys. Stat. Sol., 11, 163 (1965); also ref. 22.

74. K. Hennig, Phys. Stat. Sol., 3, K 458 (1963).

75. W. Hayes, J.R. Pilbrow and L.M. Slifkin, J. Phys. Chem. Sol., 25, 1417 (1964).

76. J.C. Garth, Ph.D. Thesis, University of Illinois, Urbana, Illinois (1964); Phys. Rev., 140, A656 (1965).

77. L.M. Slifkin, Private communication.

78. M. Satoh and C.P. Slichter, Phys. Rev., 144, 259 (1966).

79. M. Daehler, Ph.D. Thesis, University of Wisconsin, Madison, Wisconsin (1963).

80. H.D. Koswig and I. Kunze, Phys. Stat. Sol., 8, 319 (1965).

81. F.H. McMahon, Phys. Rev., 134, A 128 (1964).

82. H. Abe, J. Phys. Soc. Japan, 12, 435 (1957); "Photographic Sensitivity" 2, 103, Maruzen (1958).

83. J. Schneider and S.R. Sircar, Z. Naturforschz., 17a, 155 (1962).

84. P.A. Forrester and E.E. Schneider, Proc. Phys. Soc., B69, 833 (1956); E.E. Schneider, Arch. Sci. Geneva, 10, 120 (1957); G.D. Watkins, Phys. Rev., 113, 79, 91 (1959).

85. J.T. Bartlett and J.W. Mitchell, Phil. Mag., 3, 334 (1958); J.W. Mitchell, Disc. Farad. Soc., 28, 242 (1959).

86. J. and J.R. Weertman, "Elementary Dislocation Theory", McMillan (1964).

87. J.M. Hedges and J.W. Mitchell, Phil. Mag., 44, 223, 357 (1953).

88. A.H. Cottrell, Rep. Bristol Conf. on Strength of Solids, 1947, p. 30 (1948).

89. F. Seitz, Rev. Mod. Phys., 23, 328 (1951).

90. W. Maenhout-Van der Vorst and W. Dekeyser, "Scientific Photography" p. 31, ed. H. Sauvenier, Liege Symposium (1959).

91. W. McGowan and L. Slifkin, Bull. Am. Phys. Soc., 9, 263 (1964).

92. J.H. Waters and H.B. Gray, J. Am. Chem. Soc., 87, 3534 (1965); T. Vanngard and S. Akerstrom, Nature 184, 183 (1959), and R. Petterson and T. Vanngard, Arkiv Kemi, 17, 249 (1961).

CHAPTER III

THE PRINCIPLES OF E.S.R. SPECTROSCOPY

3.1 The Resonance Condition for an Isolated Electron

Since an electron is a charged particle, its motion in an applied magnetic field constitutes an electric current with a related magnetic moment. There is thus a magnetic moment $\underline{\mu}$ associated with the angular momentum $\underline{J}$ such that

$$\underline{\mu} = -\gamma \underline{J}$$

where the constant of proportionality γ is called the "gyromagnetic ratio". Quantum mechanically, the justification of this proportionality for all states with given $\underline{J}$ is by the Wigner-Eckhart theorem.

This angular momentum need not have an entirely spatial character and in general it is a combination of the spatial moment with the intrinsic spin of the electron and its corresponding magnetic effect. For the sake of simplicity, a description will first of all be given of the interaction of an isolated electron in a steady magnetic field with a perturbing oscillating magnetic field. Such a situation is correctly described using a quantum mechanical treatment but a classical treatment is of great use in some applications especially when considering relaxation and rapid passage effects. The classical description succeeds because the spontaneous emissions which can occur from the excited states of a quantized system are negligible in the practical conditions of a typical resonance experiment.

Induced absorption and stimulated emission processes are completely

dominant due to the large numbers of photons emitted even from a relatively low power source.

(a) Quantum Mechanical Treatment

The application of a magnetic field $\underline{H}$ to an electron with magnetic moment $\underline{\mu}$ leads to the Hamiltonian

$$\mathcal{H} = -\underline{\mu} \cdot \underline{H} \qquad 3.1$$

For an electron with spin angular momentum $\underline{s}\ \hbar\,(s = \frac{1}{2})$ this takes the form

$$\mathcal{H} = g\beta\underline{s}.\underline{H} \qquad 3.2$$

where g is the spectroscopic splitting factor and β is the Bohr magneton. The components of $\underline{H}$ are

$$\underline{H} = (2H_1 \cos \omega t, 0, H_0) \qquad 3.3$$

$$(H_1 \ll H_0)$$

where H_0 is the static magnetic field in the z direction of the laboratory frame. It is the axis of quantization of the spin moment and in the absence of the microwave field $2H_1 \cos \omega t$, the Hamiltonian ($\mathcal{H}_0$) has the two eigenvalues $\pm \frac{1}{2}g\beta H_0$ corresponding to the two values of s_z ($= \pm \frac{1}{2}$).

The microwave field can now be included as a small, time dependent perturbation to induce transitions between the two states. The perturbation Hamiltonian $\mathcal{H}_1$ will have the form

$$\mathcal{H}_1 = g\beta s_x H_x \qquad 3.4$$

and the eigenfunction of the electron at time t will be

$$\psi(t) = a_1(t)/-\tfrac{1}{2}\rangle \exp(-iW_1 t/\hbar) + a_2(t)/+\tfrac{1}{2}\rangle \exp(-iW_2 t/\hbar) \qquad 3.5$$

where W_1 and W_2 are the eigenvalues of H_0, $a_1(t)$ and $a_2(t)$ are the normalized probability amplitudes. It is the variation of these probabilities with time that is of interest here and this will follow from the application of the time dependent Schrodinger equation:

$$(\mathcal{H}_0 + \mathcal{H}_1) = i\hbar \frac{d\Psi}{dt}$$

The probability of finding the system in the $|+\frac{1}{2}\rangle$ state at a time $t > 0$ is to the first order

$$P_{-\frac{1}{2}\to\frac{1}{2}} = |a_2(t)|^2 = 4g^2\beta^2 H_1^2 \langle +\tfrac{1}{2}|S_x|-\tfrac{1}{2}\rangle^2 \left[\frac{\sin^2(\omega_{21}-\omega)t/2}{(\omega_{21}-\omega)^2}\right] \qquad 3.6$$

where $\omega_{21} = (W_2 - W_1)/\hbar$

The function [ ] only has an appreciable value when $\omega \approx \omega_{21}$ for times which are not too short. This then is the condition for resonance; the matrix element $\langle +\frac{1}{2}|s_x|-\frac{1}{2}\rangle$ leads to the selection rule $\Delta m_s = \pm 1$ for magnetic dipole transitions. The Hermitian character of the Pauli spin matrix s_x means that $P[(m+1) \to m] = P[m \to (m+1)]$, i.e. that induced absorption and emission are equally likely.

The above conditions will be disturbed if the microwave field H_1 is too large and the conditions of the perturbation are not justified. Higher order theory will then allow double quantum transitions.

(b) Classical Treatment

Classically, a spinning electron with magnetic moment $\underline{\mu}$ will precess about an applied (steady) magnetic field $\underline{H}_0$ according to the equation of motion

facing page 60

figure 3.1

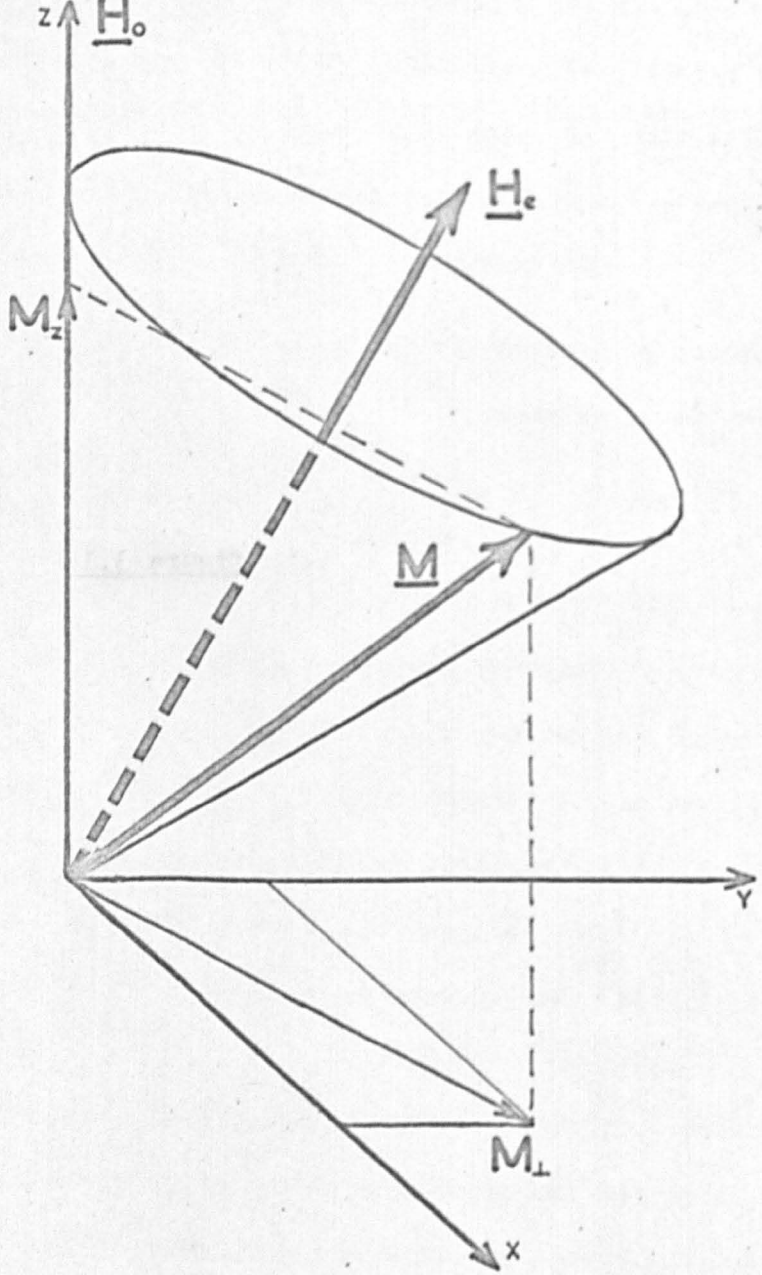

Figure 3.1

Precession of $\underline{M}$ about $\underline{H}_e$ in the Rotating Coordinate System. The Moment $\underline{M}$ is the Combined Effect of the Individual Moments $\underline{\mu}$.

$$\frac{d\underline{\mu}}{dt} = \underline{\mu} \times \gamma \underline{H} \qquad 3.7$$

This describes the Larmor precession with a frequency $\underline{\omega}_o$ given by $\gamma\underline{H}_o$.

In a magnetic resonance experiment, a circularly polarized field of amplitude H_1 rotates about $\underline{H}_o$ with a frequency $\underline{\omega}$ in the same sense as the precession. The effect of H_1 on the precessing electron is most easily observed from a frame rotating with H_1 (i.e. so that H_1 is stationary in the rotating frame). In this frame equation 3.7 then becomes

$$\left[\frac{d\underline{\mu}}{dt}\right]_{rot} = \underline{\mu} \times (\gamma\underline{H} + \underline{\omega}) \qquad 3.8$$

Equation 3.8 shows that the motion of $\underline{\mu}$ in the rotating system obeys the same equation as in the laboratory system, provided the actual field $\underline{H}$ is replaced by an effective field

$$\underline{H}_e = \underline{H} + \frac{\underline{\omega}}{\gamma}$$

The resonance condition is, as before,

$$\gamma H_o = \omega, \quad \text{i.e. } \omega = \omega_o$$

and this is detected by the r.f. field H_1.

The spin vector precesses now about the effective field $\underline{H}_e$, at an angle θ to $\underline{H}_o$

$$|\underline{H}_e| = \left[(H_o - |\underline{\omega}/\gamma|)^2 + H_1^2 \right]^{\frac{1}{2}}$$

and

$$\tan\theta = \frac{H_1}{H_o - |\underline{\omega}/\gamma|}$$

This is shown in Figure 3.1.

At resonance $\underline{H}_e$ coincides identically with $\underline{H}_1$, so we see from equation 3.7 that the spin now precesses about $\underline{H}_1$ according to

$$\underline{\omega}_p = \gamma \underline{H}_1 \qquad 3.9$$

in the rotating frame. This model agrees with the conclusions derived quantum mechanically; the angle θ describes the relative probabilities of the electron being in the spin states $|-\frac{1}{2}\rangle$ and $|+\frac{1}{2}\rangle$ and the transition probability can be assessed geometrically.

3.2 An Assembly of Electrons

In general, when the static susceptibility is measured or the resonance is observed for a set of paramagnetic electrons, they are within some host, whether it be solid, liquid or gas. It is useful to talk of a "spin temperature" which describes the relative populations of the electron spin states in a magnetic field. This must be related to the temperature of the host, or the lattice, and in conditions of thermal equilibrium, the two temperatures will be equal, due to some coupling between the two systems. In many cases, the interaction between electrons is small and Boltzmann statistics will be satisfactory (in the case of conduction electrons in a metal, Fermi-Dirac statistics must be used, leading to a much lower temperature independent susceptibility for temperatures below the Fermi temperature). The relative populations of the two states of an electron in a field H will normally be of the form $\exp(-g\beta H/kT)$ which leads to Curie's Law at most normal temperatures. In a paramagnetic resonance experiment, one will observe a net absorption of power by the spin system dependent on the population

excess in the lower energy state as the probabilities of absorption and emission from the lower and higher energy states are equal. It is now essential to introduce some mechanism to remove this energy from the upper state, otherwise the populations will equalize and the resonance will "saturate". Normally the electron spins are weakly coupled to the lattice by way of the spin-orbit coupling. The ability of this mechanism to de-excite the electrons allows a spin-lattice relaxation time T_1 to be defined. This is the time it takes for a given excess of energy in the spin system to fall to 1/e of its initial value.

Bloch (1) took account of this spin-lattice interaction and also of possible spin-spin interactions when he modified the basic form of equation 3.7 to include these two effects. Introducing a total magnetization vector $\underline{M}$ which is the resultant of all the electronic magnets, equation 3.7 now is

$$\frac{d\underline{M}}{dt} = \gamma \underline{M} \times \underline{H} \qquad 3.10$$

The effect of the two spin relaxation interactions will be quite distinct as can be seen if it is considered what happens to the case in 3.1.b if the exciting field H_1 is suddenly turned off after a nonequilibrium situation has been achieved. M will tend to precess at $\underline{\omega}_0 = \gamma \underline{H}_0$, the z component of $\underline{M}$ (parallel to $\underline{H}_0$)will grow as individual moments making up $\underline{M}$ flip to bring M_z towards M_0, the unperturbed magnetization. This process which is shown in Figure 3.1 ,

requires the moments to give up their energy to the lattice and so the time constant T_1 is applicable.

The second process involves the individual moments in the local dipolar field of their neighbours. This will alter the field $\underline{H}_o$ which each moment experiences and so there will be a distribution in precession frequencies for each moment and the coherence in the individual components making up $M_\perp$ (normal to $\underline{H}_o$) is lost, causing $M_\perp$ to decay with the characteristic spin-spin relaxation time T_2 (Figure 3.1).

Taking account of these effects we can now modify equation 3.10 to the Bloch equations (expressed in the laboratory frame)

$$\frac{d M_z}{dt} = \gamma (\underline{M} \times \underline{H})_z + \frac{M_0 - M_z}{T_1} \qquad 3.11a$$

$$\frac{d M_{x,y}}{dt} = \gamma (\underline{M} \times \underline{H})_{x,y} - \frac{M_{x,y}}{T_2} \qquad 3.11b$$

These equations can be solved for a number of cases. Certain "fast passage" situations where the resonance is observed in a time short compared with T_1 have been solved. A discussion of these is given by Abragam (2). The simplest case and the one normally applicable in the experiments described in this thesis, is the slow passage approximation where the magnetic field $\underline{H}_0$ is swept slowly through the resonance in a time long compared with T_1. The solution of the equations 3.11 is then obtained by expressing them in the rotating frame

facing page 64

figure 3.2

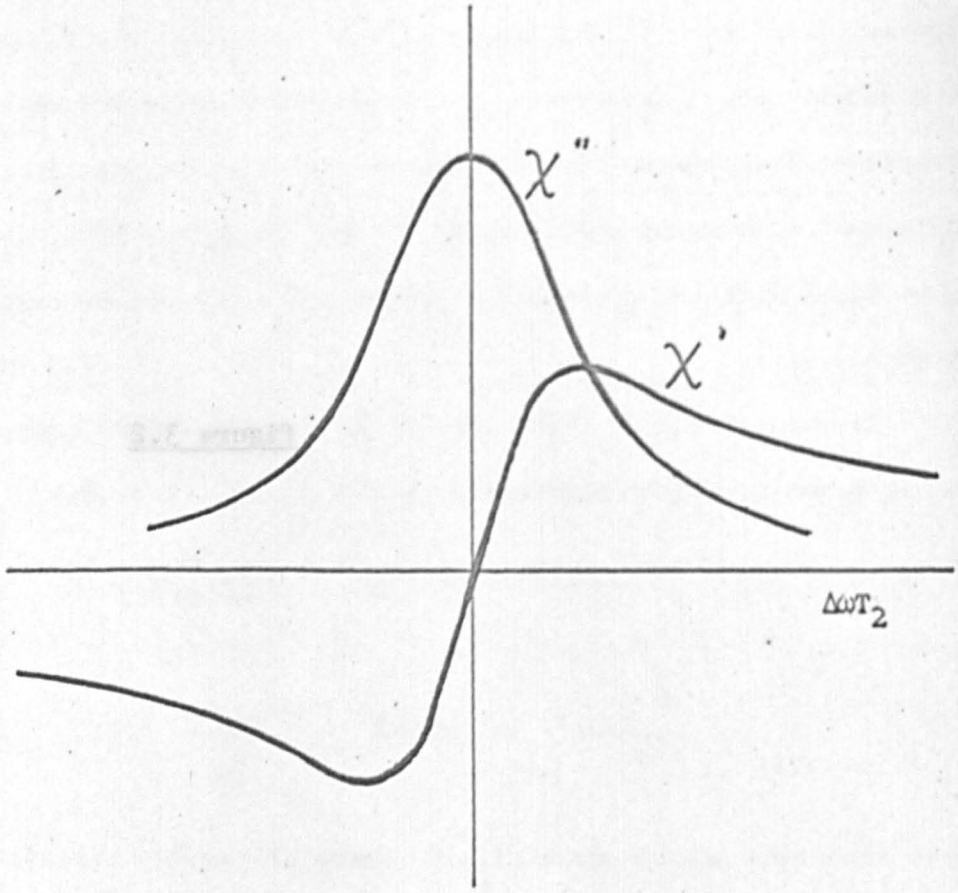

Figure 3.2

The Bloch Susceptibilities

and equating all the time derivatives to zero. A resonance experiment observes the effect of the magnetization on $\underline{H}_1$, and the out-of-phase component leads to an absorption of energy from the r.f. field. These effects are described by a complex susceptibility, $\chi = (\chi' - i\chi'')$ where

$$\chi' = \tfrac{1}{2}\chi_o \omega_o T_2 \frac{\Delta\omega T_2}{1 + (\Delta\omega)^2 T_2^2 + \gamma^2 H_1^2 T_1 T_2} \qquad 3.12\ a$$

$$\chi'' = \tfrac{1}{2}\chi_o \omega_o T_2 \frac{1}{1 + (\Delta\omega)^2 T_2^2 + \gamma^2 H_1^2 T_1 T_2} \qquad 3.12\ b$$

χ_o is the static susceptibility, given by $M_o = \chi_o H_o$

and $\Delta\omega = \omega_o - \omega$.

A plot of χ' and χ'' against $\Delta\omega$ is given in Figure 3.2 for the case

$$\gamma^2 H_1^2 T_1 T_2 \ll 1 \qquad 3.13$$

When the condition 3.13 does not hold, saturation of the resonance occurs as mentioned above when the concept of a spin-lattice relaxation is introduced. Saturation will thus occur if the r.f. field is too large or if T_1 is too long.

When $(\gamma H_1)^2 T_1 T_2 \gg 1$, the steady state description can no longer be used as $\underline{H}$ no longer varies quasi-statistically; this affects the behaviour of χ' especially.

3.3 Electron Resonance Line Shapes and Line Widths

Under the steady state conditions discussed in the previous section an absorption line with a shape described by the Lorentzian

function is obtained. The width is expressed in a variety of ways, the most common being the frequency separation between the half power points or between points of maximum slope (the first differential of the absorption line is usually displayed in an e.s.r. experiment). Remembering the sort of interactions which paramagnetic electrons have with their surroundings in a real lattice it is not surprising that the Lorentzian line predicted by the Bloch equations is seldom realised. In many cases, the line shape is far closer to the form of the Gaussian error function which would be expected for static dipolar interactions.

An e.s.r. line can be "homogeneously broadened" when the width is controlled by the lifetime of the spin in one of the states involved in the transition. The energy uncertainty in the transition will then be given by the Heisenberg principle. The line is said to be "inhomogeneously broadened" if the interactions of some spins differ from those of others due to differing local fields, and such differences are not resolved from the total line shape.

A number of effects can be distinguished and the more important ones are mentioned below. It should be noted that the natural line width does not contribute significantly to the overall line width in the microwave region due to the very low probability of spontaneous emission.

(a) Spin-Lattice Effects (3)

Often the value of T_1 is sufficiently short to cause severe broadening of the e.s.r. line and in these cases, it is necessary to take advantage of the temperature variation of T_1 and perform the experiments at low temperatures. The dominant mechanism for spin-lattice relaxation is in most cases that proposed by Kronig (4). Energy in the spin system is coupled to the electron orbital motion by the spin-orbit interaction. The orbital motion is coupled energetically to the lattice as a whole by lattice or local vibrations.

The phonon spectrum at the particular lattice temperature is very important and this critically controls the temperature dependence of the effect. There are two distinct effects; a direct process which will involve the emission of a phonon of the appropriate energy and an indirect or Raman process which is the inelastic scattering of a higher energy acoustic phonon with the consequent spin relaxation. Although this process is indirect, it is dominant above liquid helium or hydrogen temperatures due to the much larger number of higher energy phonon modes available in the lattice. The paramagnetism which is observed is often associated with some defect in the crystal. This can cause a large local variation in the mode distribution.

A variety of other processes have been observed through excitation to and then relaxation from an intermediate level (an Orbach process). A number of cross relaxation processes, typically controlled by a dipolar coupling between two spin systems are sometimes important.

(b) Spin - Spin Effects (3)

These take on a number of forms. The basic spin-spin relaxation process is simply a magnetic dipole effect of the type that was postulated in introducing T_2. Often closely related to this are exchange effects which occur when the wavefunctions of two paramagnetic electrons overlap either directly or through a common ligand (super-exchange).

The dipolar spin-spin effect has a dependence on the inter-electronic distances of the form $(1/r^6)$. The broadening which is caused can thus be made negligible by diluting the paramagnetic ions with "similar" diamagnetic ones. A number of distinct cases can be distinguished. The broadening due to ions in inequivalent sites is somewhat smaller than from ions in equivalent sites due to the symmetry distribution. When the surrounding dipoles are tumbling rapidly compared with the lifetime of the spin states, as is usually the case in liquids, the electron sees an average field and this often produces a spectacularly narrower line than for the same spins in a rigid lattice.

Hyperfine interactions, while smaller owing to the much smaller moments associated with nuclei, often produce an important contribution to the spin-spin broadening; indeed, it is such effects that often ultimately limit the width of an electron resonance line. It is in such cases that ENDOR (Electron-Nuclear Double Resonance) techniques became invaluable. The subject of electron-nuclear interactions will

be described in section 4.4 c. It is sufficient to mention at the moment that direct electron-nuclear interaction of the Fermi Contact type provides an isotropic interaction (often resolved), whereas dipolar effects and interactions with other nuclei produce as anisotropic effect, depending on the symmetry of the ion site.

Exchange only takes place between two ions, atoms or molecules when the electronic wavefunctions overlap. If the two paramagnetic ions are not similar, or if they are not in equivalent sites, the general effect will be to combine the resonances, if these occur at slightly different fields, into a single broader one. When the sites have the same orientation and symmetry, the electron exchange between the two leads to an averaging somewhat analogous to the dipolar averaging occurring in liquids. The result is a narrower line near the peak, although the wings of the line are larger with the second moment of the line remaining constant. Another narrowing process occurs when the paramagnetic electron is delocalised as in a molecular orbital which averages the local magnetic field over the extended wavefunction.

(c) Saturation Broadening (5,6)

~~Under the conditions~~ When an electron resonance transition is saturated (i.e. H_1 too large and T_1 too long), a homogeneously broadened line will be further broadened due to the higher probability of absorption of energy close to the centre of the line than in the wings. An examination of the Bloch susceptibilities demonstrates this

effect, although it is generally true for all homogeneously broadened lines (5). Using equation 3.12 b, the peak of the absorption (χ_o'') is given by $\Delta\omega = 0$, so that

$$\chi_o'' = \tfrac{1}{2}\chi_o\omega_o T_2 \frac{1}{1 + \gamma^2 H_1^2 T_1 T_2} \qquad 3.14$$

Defining the line width ($2\Delta\omega_1$) in terms of the separation of the half-power points $\chi_o''/2$ gives

$$\chi_o''/2 = \tfrac{1}{2}\chi_o\omega_o T_2 \frac{1}{1 + (\Delta\omega_1)^2 T_2^2} \frac{}{+ \gamma^2 H_1^2 T_1 T_2} \qquad 3.15$$

Eliminating χ_o'' from 3.14 and 3.15 and rearranging

$$2(\Delta\omega_1) = 2\sqrt{\frac{1 + \gamma^2 H_1^2 T_1 T_2}{T_2}}$$

so that, if the condition $\gamma^2 H_1^2 T_1 T_2 \ll 1$ (3.13) does not hold the line is broadened. The intensity of the dispersion line is not so seriously affected by saturation as the absorption line which can be seen from equation 3.12 a.

Inhomogeneously broadened lines will not be broadened by saturation as the individual resonances making up the envelope will be reduced in proportion to their initial intensities.

(d) Other Mechanisms

Inhomogeneities in the applied magnetic field lead to a spread in the position of resonance. Although of some importance in narrow line e.s.r. experiments, it is of far greater importance in nuclear resonance and ENDOR work.

High frequency modulation is often used in the observation of e.s.r. lines. A small amplitude is usually used in differentiating the line, but for maximum sensitivity, a modulation amplitude comparable with the line-width is used (7); this and larger amplitudes broaden and distort the line shape.

The frequency of the modulation, if sufficiently high, will cause a lifetime broadening when the line-width (in units of frequency) has the same order as the frequency.

3.4 The Unpaired Electron

Paramagnetic resonance can be observed in very many different substances. In solids and liquids particularly, electron orbital motion is often effectively "quenched" at least to a first order, and the paramagnetism is in these cases dominated by the electron spin. In ionic crystals such as the silver halides, there are a number of possibilities where e.s.r. techniques would be of great assistance. It should be possible, at least from a very simple viewpoint, for electrons and holes to be trapped by interstitial silver ions and silver vacancies respectively. However, all attempts at identifying such centres through their expected paramagnetism has apparently been unsuccessful. Various impurities, in particular, members of the various transition series can clearly be observed using e.s.r. This is the principal subject of this thesis and the following chapter deals fairly generally with the energy levels of transition ions in crystals. Later chapters deal with the spectra associated with the

S-state ion Fe^{3+} in silver chloride. The interpretation of the properties of these spectra makes it possible to infer some of the effects of iron impurity on electronic and ionic processes in silver chloride.

It is possible in principle to ~~observe~~ detect conduction electron spin resonance for electrons in the conduction band (polarons). Such electrons would obey Boltzmann statistics and although the coupling of the electronic motion to the lattice is very strong (see section 2.3.3.b), the orbital character of the electronic motion should be effectively quenched. A small amount of angular momentum will probably be admitted from silver 4d levels close to or contributing to the conduction band. The magnitude of this effect will probably decide whether the experiment is feasible. Silver chloride would be an excellent crystal in which to attempt such an experiment due to the ease with which large numbers of conduction electrons can be produced. On the other hand, crystals with a lighter metal forming the conduction band states would introduce less orbital character into the electronic wave function.

CHAPTER III - REFERENCES

1. F. Bloch, Phys. Rev., 70, 260 (1946).

2. A. Abragam, "Principles of Nuclear Magnetism", Oxford (1961).

3. G.E. Pake, "Paramagnetic Resonance", Benjamin (1962).

4. R. de L. Kronig, Physica, 6, 33 (1939).

5. D.J.E. Ingram, "Free Radicals as Studied by E.S.R.", Butterworths (1958).

6. A.M. Portis, Phys. Rev., 91, 1071 (1953).

7. G.W. Smith, J. Appl. Phys., 35, 1217 (1964).

CHAPTER IV

INTERPRETATION OF THE E.S.R. SPECTRA OF TRANSITION ION COMPLEXES

4.1 The Electronic Structure of an Isolated Transition Atom

As this thesis is primarily concerned with the properties of transition ions dissolved in the silver halide lattice, attention will be restricted to a description of the energy levels expected for this case.

The electronic states of the transition ion which are of principal interest in a paramagnetic resonance experiment are those of the unfilled d shell. The effect of the surrounding lattice on these states is always extremely marked and gives a lot of information concerning the state of the ion and its environment.

The usual starting point of a calculation to find the energy levels of the ion in a lattice is the free ion Hamiltonian ($\mathcal{H}_f$) describing the motion of the electrons in the field of the nucleus and the other electrons. The effect of nuclear magnetic and quadrupole interactions is ignored at this stage for the sake of simplicity. If the effect of an external magnetic field $\underline{H}$ is included, the Hamiltonian is:

$$\mathcal{H}_f = \sum_i \left[\frac{1}{2m} \left(\underline{p}_i + \frac{e}{c} \underline{A}_i \right)^2 - e\phi_i - \frac{e\hbar}{2m^2c^2} \underline{s}_i \cdot \underline{E}_i \times \underline{p}_i + 2\beta \underline{s}_i \underline{H} \right] + \sum_{i<k} \frac{e^2}{r_{ik}} \qquad 4.1$$

The momentum term includes the vector potential $\underline{A}_i$ arising from the application of the static external field at the electron and ϕ_i is the scalar potential at the electron. β is the Bohr Magneton. The term $(e\hbar/ 2m^2c^2)\underline{s}_i.\underline{E}_i x\underline{p}_i$ can be reduced to the form $(e\hbar^2/2m^2c^2)\langle\frac{E}{r}\rangle\underline{s}_i.\underline{l}_i$ for a central field; here $\hbar\underline{l}$ is the angular momentum $\underline{r}$ x $\underline{p}$. This term which expresses the spin-orbit coupling energy of the electrons is often written in the form $\sum_i \zeta_i \underline{s}_i.\underline{l}_i$ where ζ_i is called the one-electron spin-orbit coupling constant. It is important to note that this parameter implicitly includes some information concerning the radial nature of the electronic wavefunction as it depends on the expectation value $\langle 1/r^3\rangle$ for a Coulomb field. The magnitude of the parameter is thus most sensitive to the value of the wavefunction close to the nucleus and is relatively insensitive to changes in the outer part of an electron's range.

The term $2\beta\underline{s}_i.\underline{H}$ (more correctly $2.0023..\beta\underline{s}_i.\underline{H}$) is the Zeeman interaction between an electron spin and the applied field. The terms involving spin follow from a relativistic treatment of the electron. A number of smaller terms arising from this treatment but not involving spin have been neglected (1). Small terms expressing magnetic interactions between the electrons are also excluded (2).

Expressing $\underline{A}$ in terms of the magnetic field as $\frac{1}{2}\underline{H}$ x $\underline{r}$ the kinetic energy term in $\mathcal{H}_f$ becomes

$$\frac{1}{2m}\left(\underline{p} + \frac{e\underline{A}}{c}\right)^2 = \frac{p^2}{2m} + \frac{e}{2mc}\,\underline{H}.\underline{r} \times \underline{p} + \frac{e^2}{8mc^2}\,(\underline{H} \times \underline{r})^2$$

$$= \frac{p^2}{2m} + \beta \underline{H}.\underline{l} + \frac{e^2}{8mc^2}\,(\underline{H} \times \underline{r})^2$$

The second term describes the influence of a field $\underline{H}$ on the orbital magnetic moment and contributes to the Zeeman interaction. The final term leads to a diamagnetic effect which can usually be neglected.

The calculation of the eigenfunctions and eigenstates of $\mathcal{H}_f$ leads to a description of the atom which is usually used as a starting point for calculating the energy levels involved in electron resonance spectroscopy. For many purposes the strongly bound electrons which form the core of an atom can be regarded as contributing a modification to the potential "seen" by the outer electrons. The energy difference between the outer electrons and the atomic core is such that the effect of any matrix elements between the states is very small. It is convenient to define "core" as those levels which are not materially altered by chemical effects. In a 3d transition series atom this would include 3p and all lower states. (The closest states are about 500,000cm^{-1} below the upper occupied levels). The "outer" electrons are those in the incomplete transition shell, 3, 4, 5 or 6d, 4 or 5f together with the levels close to these. In the 3d series the 4s levels are usually occupied in the free atom and the 4p levels are not far above the 4s and can also contribute

to the essentially 3d states.

In general, the incomplete shell will cause the atom to have a finite orbital and spin angular momentum and hence also a magnetic moment; this is the origin of the atomic paramagnetism.

(a) Hund's Rules

In a hydrogen-like atom all one-electron n, l states are degenerate but much of the degeneracy is lifted in a many electron atom by the electronic interactions. The calculation of the energy level scheme for the various ways of combining the one-electron states in a transition series is a complex problem but the ground state of a given ion or atom is found from Hund's Rules. These can be stated as follows. For a given atomic configuration, an energy level with largest total spin S lies deepest and, of these, the level with largest total orbital angular momentum L lies deepest. For a set of N equivalent electrons (i.e. within a given shell), the total angular momentum J of the lowest level is given by $J = |L - S|$ for N less than or equal to a half filled shell and $J = L + S$ otherwise. These rules indicate Russell-Saunders (LS) coupling and although they apparently indicate a magnetic effect, such forces are two or three orders of magnitude less than electrical interactions which lead to a similar effect. The first criterion, for maximum S, is a consequence of the electrostatic repulsion between the electrons making the spatially antisymmetric combination of wavefunctions most favourable. For the

total wavefunctions to be antisymmetric the spin state must be symmetric in the interchange of electrons. This is just the criterion for maximum S (3). The condition for maximum L consistent with this is again a consequence of electrostatic repulsion. In this case, the m states of the electrons orient themselves to prefer a maximum L as explained by Karayianis (3). The coupling of $\underline{L}$ and $\underline{S}$ vectors to form $\underline{J}$, the total angular momentum, is a consequence of spin-orbit coupling. The breakdown of this simple description and of Russell-Saunders coupling ~~is~~ occurs because of the restriction of this model to the consideration of classical forces and of the importance of spin-orbit coupling.

Hund's Rules can give some idea of the order of excited state levels in an atom. For example, in manganese (II) which has the electronic configuration $3d^5$, the ground state has S = 5/2, L = 0 (i.e. ^6S) and the first excited state within the d shell is ^4G ($\approx 30{,}000cm^{-1}$) which would be the next possibility after relaxing Hund's Rule: S = 3/2, L = 4. The doublet levels lie higher still and the lowest of these is the ^2I at about $50{,}000cm^{-1}$ above the ^6S.

When considering the paramagnetism of an ion it is very often possible to ignore the effect of these excited levels to a good approximation as they are not populated at normal temperatures ($200cm^{-1}$ is equivalent to a value of kT with T = 287°K) and the energy splittings are so large as to make interaction with the ground state very small. This approximation is inadequate in the

case of S-state ions (e.g. Mn^{2+}) and in some cases when the crystal field is very strong. It however forms a basis for the idea of a spin Hamiltonian which is the subject of section 4.4 where it is indicated how these difficulties are overcome.

4.2 The Crystal Field

When an atom is fitted into a solid lattice, it is not surprising to find that the states of the outer electrons can be drastically altered. Some sort of chemical bond is formed between the atom and its surroundings if the arrangement is to be at all stable. If the bond is essentially ionic, some electrons are transferred between the atom and its surrounding atoms; a charged ion rather than an uncharged atom is left as the "building block". Restricting the discussion to the essentially ionic case for the moment, the main concern in an electron resonance experiment is to assess the effect of the surroundings on the initially free paramagnetic ion or atom. This model, where the atomic electrons are classified as "core" and "outer", is a useful starting point to appreciate the physical interactions which take place in an ionic crystal. In a transition series, where Russell-Saunders coupling is effective, the energies associated with the atomic states L and S (i.e. the coupling of the one-electron functions described in the last section) is in the region of $10^5 cm^{-1}$. For the 3d series the spin-orbit coupling energy which makes J a good quantum number in the free atom is about $10^2 cm^{-1}$ ($10^3 cm^{-1}$ for the rare earths).

In an electron resonance experiment at microwave frequencies, the Zeeman interaction is about $1cm^{-1}$.

The effect of the ionic surroundings in a crystal is to place the ion in a strong electric field. It is the energy associated with the strength of this field, compared with the spin-orbit coupling and compared with the separate L and S coupling that decides the state of the paramagnetic levels. For the rare earths, the unfilled 4f shell is rather well screened from the surroundings as it is localized within the atom with other electrons outside it. The energy of interaction between the crystal field and the 4f shell is usually in the region of 10^2cm^{-1}, so that the spin-orbit coupling is more important than this weak crystal field. In the 3d transition series, ~~the crystal field~~ this energy lies in the region 10^4 to 10^5cm^{-1}. When the strength of the field is greater than the spin-orbit coupling energy but less than the L and S coupling, the field is called a medium crystal field. When it is greater than the L,S coupling, it is called a strong crystal field. Both the medium and the strong cases, particularly the latter, indicate an appreciable degree of covalent bonding; the simple model of an ionic crystal with no overlap between neighbouring atoms is often rather inadequate in such circumstances and the methods for treating such a system are described in the following section.

The value of a simple classification of the strength of the crystal field is that it provides a guide for the starting point of a perturbation calculation on a "free" ion. In the rare earths the atomic J quantum number is initially good and the problem first of all is to calculate the effect of a weak crystal field on the atomic state. This will not be considered further.

When the crystal field is stronger than the spin-orbit coupling, J can no longer be a good quantum number; it is the result of an essentially magnetic or internal Zeeman interaction, while the crystal field is a very strong electric or Stark field. When a magnetic field interacts with an orbital state L, the degeneracy of the state is removed and individual levels are described by values of M which express in units of $\hbar$ the component of angular momentum in the direction of the magnetic field field ($|M| \leq L$). This is the Zeeman effect. When the orbital state L is placed in an electric field, M no longer describes the separate states and individual levels are of the form $\frac{1}{\sqrt{2}}[\,|M\rangle \pm |-M\rangle]$ where M takes the values $0 \leq |M| \leq L$. This is the Stark effect. Clearly the state L can no longer possess a permanent magnetic moment as each level is an equal combination of moments + M and - M. An atom placed in an electric field such that the orbital state interacts more with this field than with the spins (i.e. medium or strong crystal field) has the magnetic alignment with the spin overruled and the orbital magnetic moment

is quenched. This quenching is a purely spatial effect so that the electron spin states are not affected.

The detailed way in which the "Stark levels" split is purely a function of the symmetry of the surrounding electric field. The magnitude of the splitting depends on the nature and size of the interaction. The degeneracies are provided in a straightforward way by group theory; the detailed calculation of splittings is very complex in general and a difficult quantum mechanical problem.

Looking first of all at the way in which a single d electron eigenfunction splits in an electric field, the Stark levels would be states of the form $\frac{1}{\sqrt{2}}(d_2 \pm d_{-2})$, $\frac{1}{\sqrt{2}}(d_1 \pm d_{-1})$, d_o where the subscript is the m quantum number. Using the phase convention of Condon and Shortley (4) these states are usually written in a form in which they are real, viz:

$$\left.\begin{aligned} d_{xy} &= \frac{1}{i\sqrt{2}}(d_2 - d_{-2}) \\ d_{xz} &= -\frac{1}{\sqrt{2}}(d_1 - d_{-1}) \\ d_{yz} &= -\frac{1}{i\sqrt{2}}(d_1 + d_{-1}) \end{aligned}\right\} t_{2g}$$

$$\left.\begin{aligned} d_{z2} &= d_o = d_{(3z^2-r^2)} \\ d_{(x^2-y^2)} &= \frac{1}{\sqrt{2}}(d_2 + d_{-2}) \end{aligned}\right\} e_g \qquad 4.2$$

In these eigenfunctions, the subscripts indicate the function in Cartesian space with which each one transforms. They can be

facing page 82

figure 4.1

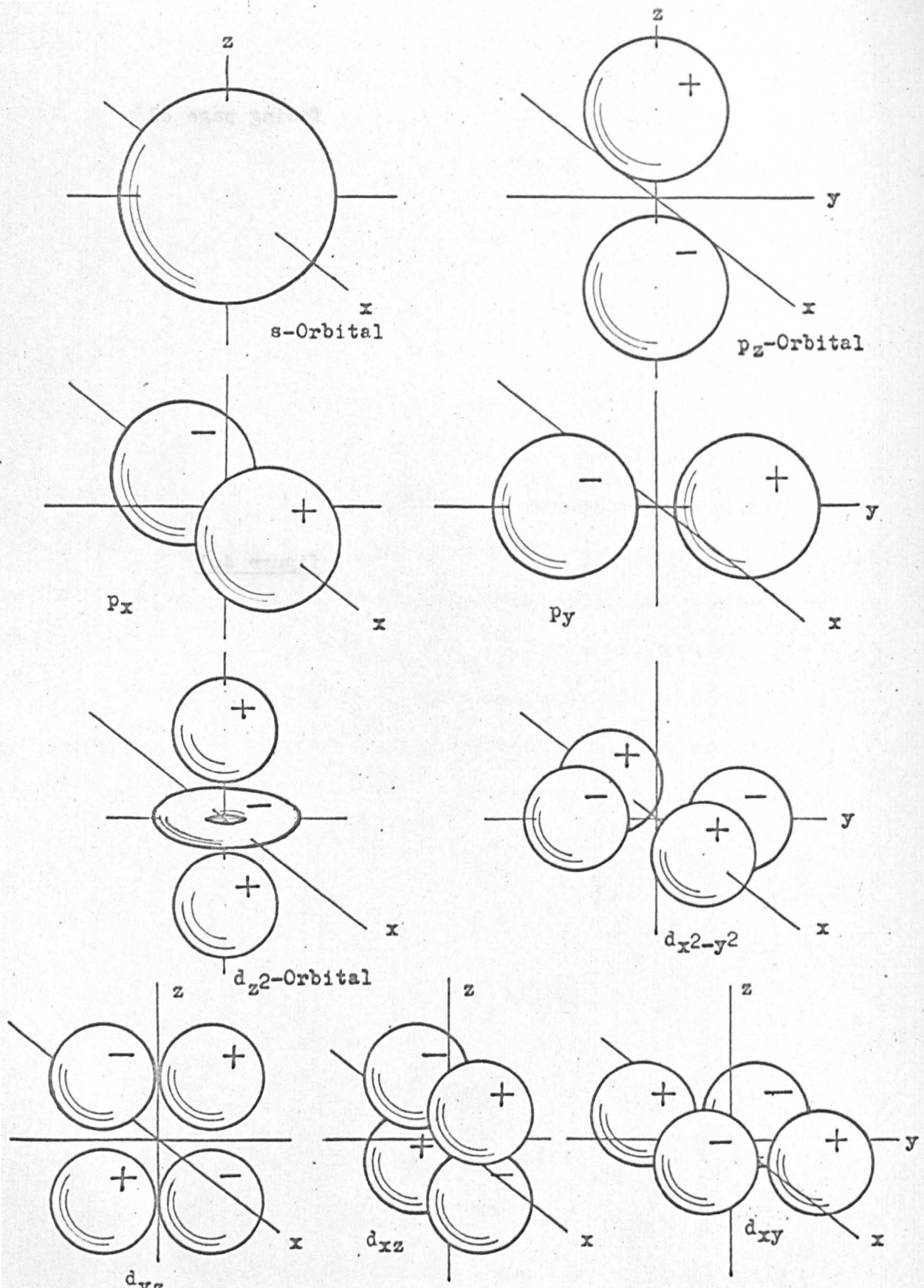

Figure 4.1

Diagram of s,p and d Orbitals

represented diagrammatically in real space by surfaces (called orbitals) within which the electron is, say, 90% likely to be found. This is shown in Figure 4.1 along with the s and p functions.

$$\left.\begin{aligned} p_x &= -\frac{1}{\sqrt{2}}(p_1 - p_{-1}) \\ p_y &= -\frac{1}{i\sqrt{2}}(p_1 + p_{-1}) \\ p_z &= p_o \end{aligned}\right\} t_{1u} \qquad 4.3$$

The diagram shows 1s, 2p and 3d orbitals; increasing the n quantum number alters the radial function (introducing nodes) but the angular distribution remains unaltered. The orbitals 4.2 and 4.3 are bracketed to indicate the irreducible representation (i.r.)* of the octahedral group (O_h) for which they provide a basis.* Physically, this means that an electric field of octahedral symmetry (provided for example by six equal ions, equally situated along positive and negative coordinating axes), will split the five degenerate d levels into two sets, one with a degeneracy of 3 and the other 2. Group theory tells that this is all an octahedral field could do. To lift the degeneracy further, an additional distortion would be necessary. The texts 5, 6, 7 and 8 provide

---

* The Mulliken notation is used to denote i.r's of single groups, the Bethe notation is used to distinguish i.r's of double groups. Small letters in the Mulliken notation indicate one-electron states, large letters indicate atomic states.

* Any set of orthonormal linear combinations would of course be equally acceptable.

useful sources for the application of group theory to transition ion and general molecular problems.

Group theory gives no information as to the direction or size of the splitting. In the example given above, taking it specifically as $Ti^{3+}(3d^1)$, it is in general a problem of quantum mechanics to calculate the splitting between the E_g and the T_{2g} levels. The value of group theory is that it shows that no physical process can produce more than two sets of levels in an octahedral field and so only one energy splitting (Δ or 10Dq) need be calculated in this case. The simplest model which is used to represent the crystal field is the point charge model where the surroundings of the ion are represented by a suitable arrangement of point charges or dipoles arranged with the correct symmetry around the ion. This model is quite successful for the rare earths but it appears that accurate quantitative agreement with experimental measurements for the 3d series is often rather more fortuitous than real. This subject is discussed more fully in section 4.3. The model is however satisfactory for qualitative argument. It indicates for example, that in the case of the single d electron introduced above, for negatively charged ligands, the E_g levels will lie above the T_{2g} set (looking at the orbitals in Figure 4.1 and placing a negative charge at the same place on each coordinate axis, the E_g orbitals will be repelled electrostatically more than the T_{2g} orbitals). The reverse will be true for one hole in a closed shell,

facing page 84

figure 4.2

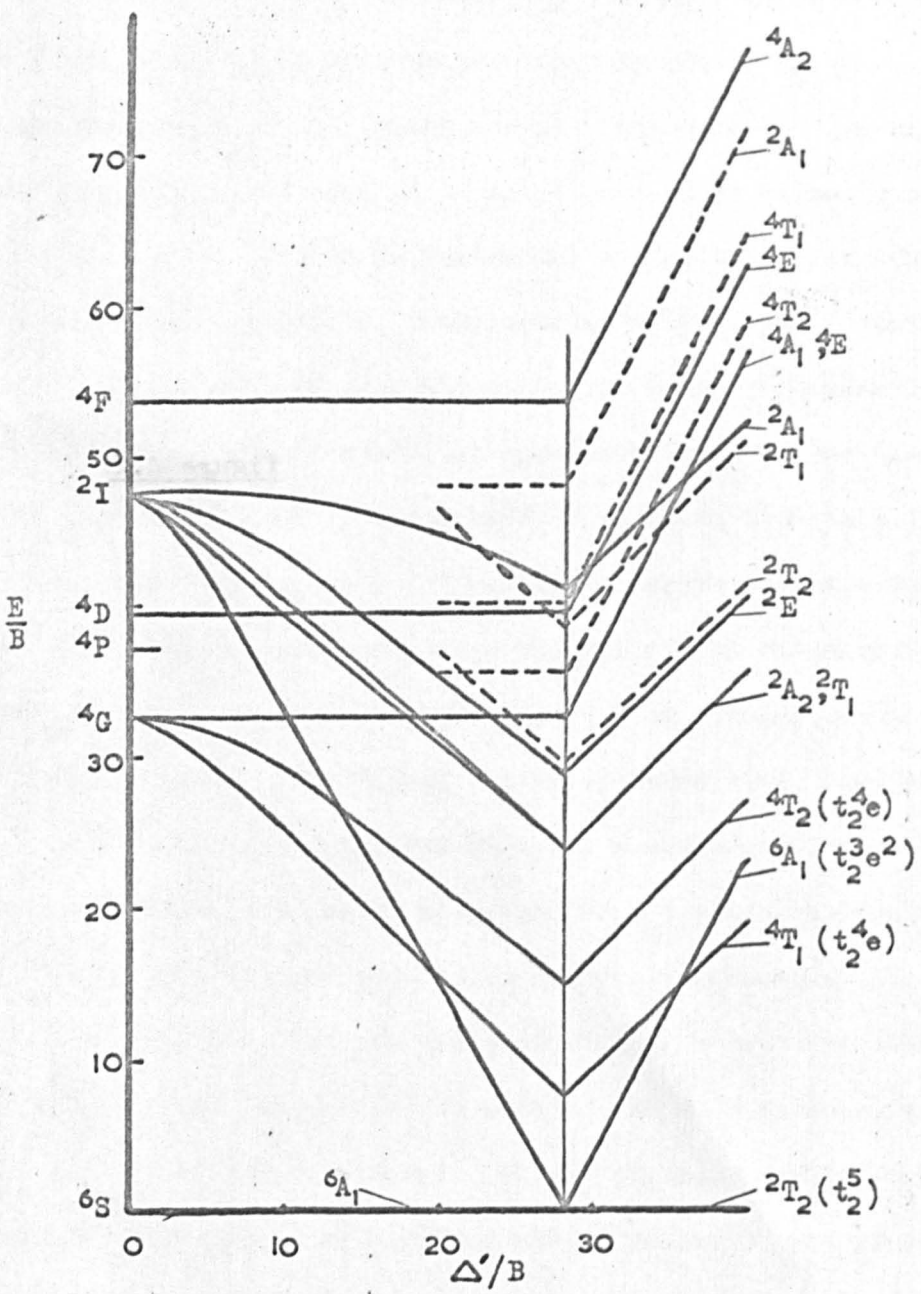

Figure 4.2

Tanabe-Sugano Diagram for Fe^{3+}. The Strong Field Assignments are for an Octahedral Field. For a Tetrahedral Field: $(t_2^5) \rightarrow (t_2e^4)$; $(t_2^4e) \rightarrow (t_2^2e^3)$. B ~ 1100cm^{-1}.

e.g. $Cu^{2+}(3d^9)$, or for one electron in tetrahedral symmetry where the 4 point charges would be at alternate corners of a cube.

When the crystal field is very strong, the splitting between the one electron e_g and t_{2g} levels becomes so large that Hund's Rules break down. Taking $Fe^{3+}(3d^5)$ in an octahedral field as an example, the five one-electron states will split to make the t_{2g} levels lowest. According to Hund's Rules, the ground state of the free ion is $^6S_{5/2}$ (This is really a special case in the transition series but it indicates rather well how the strength of the crystal field can alter the ground state of the ion). When the interaction between the 3d electrons and the crystal is very much stronger than the atomic interactions which make L and S good quantum numbers, all five electrons will be in t_{2g} states (the one-electron functions have an extra degeneracy of 2 because of spin), this is denoted by t_{2g}^5 in the strong field limit. The first excited state is $t_{2g}^4 e_g$ and so on. The ground state must now be a spin doublet as all but one of the electrons are forced to pair off; the strong field ground state is a $^2T_{2g}$ state, whereas the weak field ground state is a $^6A_{1g}$; the ^6S is not split. Figure 4.2 shows the effect of an increasing octahedral crystal field (Δ') on some of the more important free ion states (left-hand side); the right-hand side represents a strong electric field. This type of diagram has been constructed by Tanabe and Sugano for all cubic 3d configurations and it is quantitatively very useful (6). For the d^5 case it is

unlikely that the strong field levels in an octahedral field will coincide with the strong field levels in a tetrahedral field, but Tanabe and Sugano's calculations are made for a strong electric field with no particular reference to the importance of σ or π bonding. If Δ' is assumed to be an experimental parameter, the diagram can be applied to d^5 in octahedral or in tetrahedral symmetry, provided the strong field assignments are altered, as is indicated in Figure 4.2. A more accurate diagram would require specific assumptions about the ligands and it would not be generally applicable to all $3d^n$ ions. The construction of this type of diagram is described by Griffith (6). It is of particular value when analysing strong field e.s.r. spectra, and in the study of S-state ion spectra. Optical absorption transitions can often be observed between the ground and lower excited states, providing a fairly direct measurement of the strength of the crystal field. (Electric dipole transitions between d levels are forbidden but the absorptions are allowed by "vibronic" interactions - lattice vibrations destroy the inversion symmetry allowing dipole transitions.)

At this stage, having described the splitting of free ion levels under the action of the crystal field, one must carry on to the next most important effect energetically, namely, spin-orbit coupling. Group theory indicates how levels split under the influence of spin-orbit coupling and calculation of the splittings and their effect on e.s.r. spectra has in general been very

successful. As was mentioned previously, the energy associated with this effect is in the region 10^2 to $10^3 cm^{-1}$ and the indirect effect on g-values in e.s.r. spectra is often large. This is described in section 4.4.

At this point it is valuable to mention two theorems which provide further information about the ground states of ions.

(a) Kramer's Theorem states that a level which is characterized by a half-integral J and of degeneracy 2J + 1 cannot have all of the degeneracy removed by an electric field. The most that an electric field can do is to split the level into a series of doublets. This is a consequence of the invariance of a physical system under time reversal in the absence of a magnetic field. When the system is placed in an external magnetic field, it no longer retains this invariance relative to the field and the doublets are split. This result is of great value in e.s.r. as it shows that a singlet level cannot be the ground state of an odd electron system (9).

(b) Jahn-Teller Theorem indicates that a molecule with an orbitally degenerate ground state (indicating a fairly high symmetry) may spontaneously distort so as to remove all or part of this degeneracy (7). This does not apply to linear molecules or to a Kramers degeneracy which is not a spatial degeneracy. For example, Cu^{2+} in an octahedral field has an E_g ground state and a tetragonal distortion along any of the octahedral ones removes the degeneracy, splitting it into an A_{1g} and a B_{1g} level of the tetragonal group D_{4h}.

The Cu^{2+} ion will prefer the level with lowest energy and the distortion resonates between the three symmetry axes of the octahedron (dynamic Jahn - Teller effect) (10).

In this section an attempt has been made to indicate the way in which a crystal field is likely to affect the levels of a 3d transition ion. The extension to heavier ions is at least from a qualitative point of view fairly straightforward. The crystal field typically becomes more important for d-transition series of heavier atoms.

4.3 Covalency Effects

In the last section, little mention has been made of the physical processes which connect the crystal field with the energy levels of the ion immersed in it. It is essential to appreciate the origin of these interactions if the parameters used to describe electron resonance spectra are to be understood. Clearly, the first theoretical problem is to calculate the splitting (Δ) caused by the crystal field on the ground states of various ions. Early calculations used the point charge model as a classical electrostatic field in which the ion was placed. It was possible to produce fairly good agreement with measurement by choosing suitably diffuse wavefunctions for the 3d ions. It now appears likely that the fit was largely fortuitous (references 11 and 12 describe briefly the evolution of crystal field calculations). Attempts to refine the calculations by taking the charge delocalization of the ligands into

account classically were disastrous, producing the wrong sign for Δ. The situation was improved when small admixtures of ligand functions were admitted to the d functions, retaining the ionic model (i.e. no overlap), but more recent calculations have ~~found~~ shown it necessary to include the effect of overlap between the central ion and ligands. The first consequence of this is an important one, namely that the ionic model is not fully reliable and even in nominally ionic complexes, there is likely to be at least a few percent of covalent character in the bonds. The paramagnetic d electrons are therefore not fully localized ~~on~~to the central ion to which they nominally belong. This result is likely to be of importance in calculating theoretically and in understanding physically the meanings of parameters which are used to descibe e.s.r. spectra. The various calculations of the crystal field splitting are described in a number of publications (11 to 14) but the description here is restricted to a simple indication of the electron eigenfunctions which have to be used to obtain a fair fit for Δ with experiment.

(a) Molecular Orbital (LCAO) Approach

This treatment is initially due to Van Vleck (15) and simple applications of it are given, for example, in refs. 7 and 8. The linear combination of atomic orbitals (LCAO) method assumes that various atomic orbitals can be combined to form molecular orbitals $\psi(\Gamma)$, where

$$\psi(\Gamma) = N\left[\alpha\, \phi(\Gamma) + \beta \sum_i a_i(\Gamma)\phi_i\right] \qquad 4.4$$

$\phi(\Gamma)$ is a wave function of the central atom transforming in the molecular point group as the i.r. Γ and $\sum_i a_i(\Gamma)\phi_i = \chi(\Gamma)$ is a linear combination of ligand wavefunctions (i) transforming as the same i.r. Γ. N is a normalizing constant. If the various wavefunctions are correctly normalized, α and β are coefficients which describe the relative amount of central ion and ligand character in the wavefunction. $\alpha = \beta = \frac{1}{\sqrt{2}}$ describes a fully covalent bond and $\alpha = 1$, $\beta = 0$ or $\alpha = 0$, $\beta = 1$, an ionic bond if it is true for all possible Γ. The latter case is really the starting point and one parameter is first of all accepted as small compared to the other for transition metal complexes. Usually the initial ligand functions χ lie at lower energies than the metal functions ϕ and interaction causes the formation of an essentially ligand bonding orbital ψ_b which is orthogonal to the essentially metallic antibonding orbital ψ_a where

$$\psi_b = N_b(\chi + \gamma\phi) \qquad 4.5a$$

$$\psi_a = N_a(\phi - \lambda\chi) \qquad 4.5b$$

The orthogonality condition $\langle\psi_a|\psi_b\rangle = 0$ relates the admixing parameters λ, γ with the overlap between ϕ and χ.

i.e. $\lambda = \gamma + S$ where $S = \langle\phi|\chi\rangle$ and λ, γ, S are small 4.6

The new wavefunctions are properly orthogonalized and can be introduced as a better approximation for the central ion and ligand functions. In an e.s.r. experiment on the central ion, the paramagnetic electrons occupy the eigenstates ψ_a rather than ϕ, and in

an n.m.r. experiment on the ligands, the electronic states ψ_b interact with the nuclei rather than the purely ligand functions χ.

In general this model can be extended to cover other central ion states, particularly the empty 4s and 4p levels of the 3d ion and also unoccupied ligand states. The electron-hole approximation which is used within the 3d shell to treat d^n ions with n>5 must be applied with rather more caution to avoid confusion of central ion hole and ligand electron states.

The molecular orbital method is usually applied to a rigid core matrix and this is perhaps one of its most serious shortcomings. In principle, the method could be extended to take account of changes in the configuration of various states but it is physically more meaningful to examine the atomic rather than single electron states to appreciate the difficulties which can occur. The molecular orbital (MO) treatment of transition metal complexes combined with the more successful aspects of the point charge crystal field theory is often called "ligand field theory".

(b) Configuration Interaction Approach (13, 14, 16)

An alternative approach to admixing one-electron ligand functions with the central ion states is to look at the molecular states as basically ionic, with a certain probability that a ligand electron will be transferred back to the central ion (i.e. that there is really still some degree of the atomic states which would have existed before the ionic bond was formed). It is simple

to show that this is really only a different way of assessing the same thing, namely the covalency.

The correspondence between the MO and this approach is shown by taking a three electron system with bonding and antibonding orbitals ψ_b and ψ_a; the antisymmetrical wavefunction of the system Ψ will be

$$\Psi = |\psi_b(\alpha), \psi_b(\beta), \psi_a(\alpha)| \qquad 4.7$$

where $\psi(\alpha)$ and $\psi(\beta)$ are spin-orbitals for up and down spin respectively and $|\ - - - - - -\ |$ indicates a Slater determinant with its normalization factor. The ψ_a and ψ_b are given by equations 4.5 and using the condition 4.6, substitution for ψ_a and ψ_b in 4.7 gives

$$\Psi = \frac{N_b}{\sqrt{1-S^2}}[|\chi(\alpha), \chi(\beta), \phi(\alpha)| + \gamma|\chi(\alpha), \phi(\beta), \phi(\alpha)|\ ] \qquad 4.8$$

This is the Heitler-London scheme for representing the covalency. It physically means that the simple ionic ground state of the system has admixed into it a certain amount of a state where an electron is spatially transferred to the central ion. In this approximation, where λ, γ and S are assumed small, the MO and the Heitler-London approaches are not physically different. At this stage it is possible to take into account a configurational interaction between the central ion and the ligands which the simple molecular orbital method cannot easily accept. Taking a specific example as $KNiF_3$, where Ni^{2+} is octahedrally coordinated by six F^-

ligands ($Ni^{2+}F_6^-$), the configuration interaction method admixes some ($Ni^{+}FF_5^-$) with rather different radial wavefunctions. This sort of approach can affect many quantitative predictions and can be appreciated as a physically more realistic situation.

The techniques which have been described above have been used principally on $KNiF_3$ and $KMnF_3$ as many careful measurements have been made on these crystals. Good wavefunctions are available for these calculations. The MO treatment has been successfully employed in g-value calculations and it is used fundamentally to interpret ligand hyperfine structure in e.s.r. spectra. These interactions are perhaps the best indication of the necessity for this type of study.

4.4 The Spin Hamiltonian

(a) The Concept of a Spin Hamiltonian

The preceeding sections have described what sort of energy level scheme one can expect for a transition ion in a crystal and how this can be found in principle. After taking into account the effect of the crystal field, a new set of energy levels are left and the Zeeman splitting has to be calculated. Pryce has shown that, by restricting attention to a single orbitally non-degenerate level, the usual perturbation procedure can be simplified and at the same time be made to include the spin-orbit coupling (17, 18). The Hamiltonian of the system, called a "spin Hamiltonian", is expressed purely in the terms of spin operators with all the other spatial

operators already integrated over the spatial functions. These matrix elements are then effectively numerical parameters. The eigenfunctions of the system are simply a set of spin functions and electron resonance absorption is observed between these states. The measurement of an e.s.r. spectrum usually amounts to a fitting of values to the parameters. The problem is then one of relating these parameters to physical processes.

The spin-orbit coupling and the influence of the external field are treated as perturbations; the part of the Hamiltonian 4.1 which is left after the examination of the crystal field is

$$\mathcal{H}_1 = \lambda \underline{L}.\underline{S} + \beta(\underline{L} + 2\underline{S}) \ .\underline{H} \qquad 4.9$$

where $\underline{L}$ and $\underline{S}$ are appropriate to atomic rather than one-electron states and λ is the spin-orbit coupling constant, coupling $\underline{L}$ and $\underline{S}$ (it is related to ζ_{nl} by $\lambda = \pm \frac{\zeta_{nl}}{2S}$, + for the first half of the shell and - for the second (4)). The correct classification of the atomic and crystal field states means that the rest of 4.1, plus a crystal field term has been diagonalized and a set of appropriate eigenvalues E_o have been found (the Hamiltonian is $\mathcal{H}_o$). These eigenvalues are the result of a zero-order perturbation calculation and in the first order, using the perturbation $\mathcal{H}_1$ (4.9) only, the term in 2β $\underline{S}.\underline{H}$ will provide a non-zero term. (The splitting of states of different M_s gives the free spin g-value of 2). In first order the contribution of the spin-orbit coupling vanishes if the unperturbed orbital level is non-degenerate and, as the orbital

angular momentum is quenched, the term in $\underline{H}.\underline{L}$ ~~also~~ does not contribute at this order either. Second order perturbation theory is necessary to account for the effect of the $\lambda\, \underline{L}.\underline{S}$ and $\beta\underline{H}.\underline{L}$ terms. It is only the interplay between them that causes the magnetic field to slightly "polarize" the orbital states like 4.2 and 4.3. (i.e. $\underline{H}$ slightly disturbs the Stark states making a slight orbital Zeeman effect. The pure electric field quantum states are no longer strictly "good"). This small amount of orbital magnetic moment is added to the spin moment only by way of the spin-orbit coupling which is energetically much stronger than the Zeeman term (section 4.1). The $\underline{L}.\underline{S}$ interaction apparently loses its direct effect because of the orbital quenching and second order perturbation theory is necessary to include the non-zero spin-orbit and orbital matrix elements which will exist between the ground and various excited states. The result of this is that the electron spin "g-value" is shifted from its free electron position.

Although second order theory is required to include all of the effect of $\mathcal{H}_1$, the energies of the second order terms may in some cases be larger than the first order terms and Pryce's method allows both first and second order calculations to be carried out without the approximations which are necessary when progressing from first to second order in normal perturbation theory. The simplification is possible because attention is restricted to a single non-degenerate orbital level, and the influence of higher

levels is included in orbital matrix elements.

The spin Hamiltonian is set up by recognising that the spin operators in 4.9 can only act on the spin part of the spin-orbitals describing the states and the orbital operators can only operate on the spatial functions. The consequence of this is that $\mathcal{H}_o + \mathcal{H}_1$ can be written as $\mathcal{H}_s$ where

$$\mathcal{H}_s = E_o + 2\beta(\delta_{ij} - \lambda\Lambda_{ij}) S_i H_j - \lambda^2 \Lambda_{ij} S_i S_j - \beta^2 \Lambda_{ij} H_i H_j \qquad 4.10$$

The spin Hamiltonian $\mathcal{H}_s$ involves only spin variables as the orbital matrix elements are included in Λ_{ij}. The indices i, j refer to Cartesian coordinates and a summation is assumed for all the combinations of i,j. The real, symmetrical, positive definite tensor Λ_{ij} is defined by

$$\Lambda_{ij} = \sum_{n=0} \frac{\langle 0 | L_i | n \rangle \langle n | L_j | 0 \rangle}{(E_n - E_o)} \qquad 4.11$$

where $|0\rangle$ is the orbital state under examination and $|n\rangle$ are other orbital states; E_o, E_n are their eigen-values.

The term $2\beta(\delta_{ij} - \lambda\Lambda_{ij}) S_i H_j$ is the magnetic energy of a spin system with a g-factor represented by the tensor

$$g_{ij} = 2(\delta_{ij} - \lambda\Lambda_{ij}) \qquad 4.12$$

The term

$$\lambda^2 \Lambda_{ij} S_i S_j \qquad 4.13$$

is a result of spin-orbit coupling alone and if Λ_{ij} is anisotropic, it will produce a splitting of the spin levels, even in

the absence of a magnetic field. The final term corresponds to a temperature independent paramagnetic susceptibility from the orbital levels and is spin-independent.

A more general discussion of the spin Hamiltonian and its application to transition ions states has been given by Abragam and Pryce (19) and by many authors since (e.g. 20, 21). This spin Hamiltonian which includes interactions between the paramagnetic electrons and the nucleus when it has a magnetic dipole and electric quadrupole moment, is of the form

$$\mathcal{H}_s = D_{ij}S_iS_j + \beta g_{ij}H_iS_j + A_{ij}S_iI_j + Q_{ij}I_iI_j - \gamma\beta_N\underline{H}.\underline{I} + \beta^2\Lambda_{ij}H_iH_j + \sum_n \mathcal{H}_L^n \qquad 4.14$$

The operator I_i is appropriate to nuclear states and the final term is similar to the central ion nuclear terms but accounts for the interaction of the spin states with n ligand nuclei (L). The first tensor parameter D_{ij} includes a spin-spin term and $\lambda^2\Lambda_{ij}$(4.13). A_{ij} includes all the physical processes coupling the electron and nuclear spins and Q_{ij} contains the effect of the nuclear quadrupole moment (when $I > \frac{1}{2}$). $\gamma\beta_N\underline{H}.\underline{I}$ is the direct interaction of the nucleus in the magnetic field and $\beta^2\Lambda_{ij}H_iH_j$ is the final term in 4.10.

The tensorial form of the parameters in 4.14 is dependent on the symmetry of the centre and specific examples are used later. The physical meaning of the parameters is also discussed later for

some particular cases, as is the specialized application of the spin Hamiltonian concept to S-state ion complexes.

(b) Generalized Spin Hamiltonians

When the symmetry of the crystalline environment of an ion is taken into account the parameters in the Hamiltonians 4.10 or 14 are simplified. As an example, if the centre has tetragonal or trigonal symmetry, the various tensors in 4.14 are characterized by two principal values each, parallel and perpendicular to the symmetry axis (z). The central ion terms, ignoring the spin-independent paramagnetism, are

$$\mathcal{H}_S = D(S_z^2 - \tfrac{1}{3}S(S+1)) + \beta\, g_{\parallel} H_z S_z + \beta\, g_{\perp}(H_x S_x + H_y S_y) + A S_z I_z$$

$$+ B(S_x I_x + S_y I_y) + Q(I_z^2 - \tfrac{1}{3}I(I+1)) - \gamma\beta_N \underline{H}.\underline{I} \qquad 4.15$$

A number of authors have examined the detailed properties of the symmetry of the crystal field as an initial step in the setting up of a spin Hamiltonian. This is in a way the opposite approach from that of Abragam and Pryce who carried out a perturbation calculation on the properties of a given state. The symmetry treatment is more general; it introduces new parameters to explain effects which are physically unspecified but are possible for the symmetry of the crystal field state of the ion and its ligands. This generalized treatment provides the maximum number of parameters which would be consistent with the symmetry of the complex.

Koster and Statz (22) have given a group theoretical analysis of the Zeeman splittings of ions and more recently a number of authors have examined the same problem by studying the decomposition of spherical tensors with the appropriate symmetry properties (23, 24, 25). Although the techniques of the two methods are different, the final result is the same. In an ordinary spin Hamiltonian, eigenfunctions are used which are linear combinations of the magnetic sublevels of a total effective spin S (2S + 1 levels); this treatment does not allow for the possibility that some of the states split by a D term in 4.15, say, are modified differently from others. This difference can occur if higher lying excited states of the free atom, or ligand states, are differently admixed into the ground sets of spin states. Physically, this sort of effect is very reasonable as spin-orbit coupling can, for example, split the ground spin levels, introducing a zero-field splitting. The separate sets of spin levels which are left will have distinct properties with respect to other electronic levels.

This type of argument is essential to produce a spin Hamiltonian for S-state ions, the Pryce treatment reduces the Hamiltonian 4.9 to the form

$$\mathcal{H}_S = g\beta \underline{H}.\underline{S} \qquad 4.16$$

and a number of other terms have been found necessary to explain observed spectra. In a cubic field, the splittings of spectra are usually well explained by using a term

$$\frac{a}{6}\left[S_{\xi}^4 + S_{\eta}^4 + S_{\zeta}^4 - \frac{1}{5} S(S+1)(3S^2 + 3S - 1)\right] \qquad 4.17$$

(ξ , η , ζ are the cubic axes).

Qualitatively, this term is a result of the effect of spin-orbit coupling and its linking with excited state levels, but high orders of perturbation theory are necessary to produce a value for a. When there is a distortion along an axis, z say, a term

$$D\left[S_z^2 - \frac{1}{3} S(S+1)\right] \qquad 4.18$$

is appropriate. The calculation of the parameters a and D has not been particularly successful and as these terms are necessarily included in a generalized treatment, it is certainly superior ~~for~~ in (for S-state ion) spin Hamiltonians. The criticism that the generalized treatment does not indicate a physical meaning of the parameters is not appropriate in this case as the conventional treatment fails even to predict necessary terms. There are unfortunately a number of problems attached to the use of a generalized spin Hamiltonian. It tends to predict a large number of parameters with no discrimination as to the magnitude. (The advantage of the method is that it does not require the use of perturbation theory which is really the reason for the shortcomings mentioned above). Because there are a large number of parameters, in general more e.s.r. measurements would be necessary - for example, at a wide range of frequencies.

It is generally true that the ordinary spin Hamiltonian concept has been very successful in explaining e.s.r. spectra with

the reservations regarding S-state ion spectra which have been mentioned above. It has apparently not been necessary to use the additional terms which can be predicted, even in the case of S-state ions; ~~so~~ it would appear that ~~the magnitudes of~~ the additional parameters in a generalized Hamiltonian are ~~such as to make their effect usually~~ so small that they are negligible. This subject is discussed further in Chapter VIII.

(c) The Interpretation of Spin Hamiltonian Parameters

McWeeny (26) has discussed the general form of spin Hamiltonian parameters in terms of various density functions. This type of treatment clarifies many of the physical processes which are obscured in the usual deductions, showing common properties of the different parameters. The use of density functions means that the theory is not restricted to free ion wavefunctions and the most suitable basis may be used. The density functions show a great simplicity, even when they emerge from very complex wavefunctions.

The description which is given below refers to the more usual treatment of the parameters.

(i) The g-value The change in g-value from the free electron position (2.0023---) is explained in section 4.4a. The most significant deviations from the expected value appear to be a consequence of covalent bonding (27). Replacing purely metal ion wavefunctions by orbitals of the form 4.5b will reduce the density

of the paramagnetic electrons on the central ion (through the coefficient λ and the normalizing constant N_a in 4.5b) and hence reduce the effect of spin-orbit coupling on the central ion, reducing the g-shift (27, 28). Misetich et al. (29) have shown that this is only half of the effect and that a one electron spin-orbit Hamiltonian can be set up which takes account of spin-orbit coupling on the ligand ions as well as on the central ion. Because of the dependence of the spin-orbit coupling constant on approximately $\langle 1/r^3 \rangle$ (section 4.1), it is possible to transport the spin-orbit coupling operator between the various nuclei and use the spin-orbit coupling constant appropriate for the degree of ionization of the particular ion. The matrix elements of $\beta \underline{H}.\underline{L}$ for each ligand are also found and the g-shift appears to agree well with the experimental measurements, at least for the case of $KNiF_3$. The g-shift of the $(FeCl_4)^-$ complex is discussed in Chapter VIII.

(ii) Hyperfine Interactions The magnetic interaction between a paramagnetic d electron and the nucleus would be expected to be a simple dipolar effect. The magnitude of the observed interaction shows a far larger interaction than this would predict and this has been explained by including a certain amount of unpairing of s electron states due to the unpaired d electrons. There is a finite probability of finding s electrons within the nucleus and clearly they must have a very large interaction with the nuclear

moments over the small proportion of the electron density which overlaps the nucleus. A number of mechanisms have been suggested for this "polarization" of the s states; the most important is that it is possible to preferentially admix some lower s states because of the differing exchange with up and down spin 3d wavefunctions. Hubbard et al. have pointed out that covalency between the central and ligand ions will make the 4s level contain a different proportion of up and down spin states (14). This effect, which is really a consequence of the Pauli Exclusion Principle, might provide an important contribution to the "Fermi Contact" interaction of paramagnetic electrons with their nucleus.

The hyperfine interactions between transition ion electrons and ligand nuclei gives a direct measurement of some of the bonding parameters when some covalency exists. The interaction between 3d electrons and ligand nuclei is often far larger than would be expected using an ionic model and only allowing magnetic dipole interaction. The paramagnetic resonance spectra are usually interpreted using a spin Hamiltonian of the form $\sum_n \mathcal{H}_L^n$ (4.14) where

$$\mathcal{H}_L^n = A\, S_z I_z^n + B(S_x I_x^n + S_y I_y^n) + P(I_z^{n2} - \tfrac{1}{3} I^n(I^n + 1)) - g\beta_N \underline{H}.\underline{I}^n \qquad 4.19$$

This is the interaction with the n^{th} ligand (L). The z-direction coincides with the line joining the n^{th} ligand to the magnetic ion and I_n is the spin of the n^{th} ligand nucleus. In practice, this

type of interaction leads to an e.s.r. spectrum with many lines which very often overlap and are not individually resolved. It is under conditions such as this that the Electron-Nuclear Double Resonance (ENDOR) technique (30) is invaluable. In this technique transitions are induced between nuclear as well as electron states. An inhomogeneously broadened e.s.r. transition is power saturated (section 3.3) and transitions are separately induced in the nuclear spin states. The r.f. frequency of the nuclear resonance is swept, and a reduction in e.s.r. saturation is observed when the nuclear resonance transitions couple with states involved in the electron resonance. In this way the resolution of the spectra can be greatly increased, allowing a determination of parameters which are not distinguished in a ~~purely~~ simple e.s.r. experiment.

In the cubic $(FeCl_4)^-$ complex in AgCl, the extrahyperfine structure described by 4.19 is only partially resolved, and Hayes (31) has used this Hamiltonian to explain the spectrum. Garth's ENDOR results provide much higher accuracy for the parameters (32).

The values of A and B which are measured lead to a value for the amount of s bonding and in general to the difference between σ and π bonding. Nuclear resonance studies of the ligands give the same parameters, but neutron scattering measurements (33) provide a sum of s, σ and π effects allowing an absolute determination. The results of this type of measurement are invaluable for the

further understanding of spectra. Interaction with the nuclear electric quadrupole moment is a consequence of the distortion of the d wavefunctions by the crystal field.

(iii) Fine Structure Parameters The theoretical calculations of the fine structure parameters in the spin Hamiltonian has, on the whole, been much less reliable than the calculation of g-values and hyperfine constants. The calculations are particularly difficult for S-state ions as high orders of perturbation theory are necessary to obtain the effects which are observed. Watanabe (34) has used a point charge model for the crystal field and considering interaction with the quartet excited states (see Figure 4.2) calculated values of (a) which were far smaller than the observed values. Calculations by Powell et al. produced much better values for (a) by including matrix elements with doublet states (35). In these calculations, spin-spin terms appear to be negligible compared with spin-orbit contributions. More recently, Sharma, Das and Orbach have calculated D and E for Mn^{2+}: ZnF_2 claiming equal importance for spin-orbit and spin-spin effects (36). This calculation takes account of overlap and change transfer covalency and claims good agreement with experiment.

The mechanisms for appreciating the meaning of the fine structure parameters are qualitatively fairly clear but the details of the calculations are difficult because the high orders of perturbation necessary make available many complex effects which may be important.

The reason for the overall success of the spin Hamiltonian is a result of the Wigner-Eckhart theorem which allows a matrix element to be factorized into two parts: one depends on the symmetry alone while the other depends on the physical processes involved. It is the latter which is treated as an adjustable parameter, which is usually found by experiment rather than by calculation.

CHAPTER IV - REFERENCES

1. H.A. Bethe and E.E. Salpeter, "Quantum Mechanics of One and Two-Electron Atoms", also in Encyclopedia of Physics 35, 142. both are Springer Verlag (1957).

2. R.E. Watson and M. Blume, Phys. Rev., 139, A1209 (1965).

3. N. Karayianis and C.A. Morrison, J. Am. Inst. Phys., 32, 216 (1964), and N. Karayianis, ibid., 33, 201 (1965).

4. E.U. Condon and G.H. Shortley "Theory of Atomic Spectra", Cambridge (1935).

5. R. McWeeny, "Symmetry; An Introduction to Group Theory", Pergamon (1963).

6. J.S. Griffith, "The Theory of Transition Metal Ions", Cambridge, (1961).

7. C.J. Ballhausen "Introduction to Ligand Field Theory", McGraw-Hill, (1962).

8. F.A. Cotton, "Chemical Applications of Group Theory", Wiley (1963).

9. P.H.E. Meijer and E. Bauer, "Group Theory", North-Holland (1962).

10. M.C.M. O'Brien, Proc. Roy. Soc., A 281, 323 (1964).

11. R.G. Shulman and S. Sugano, Phys. Rev., 130, 506, (1963) also preceding articles p. 506 and 512.

12. R.E. Watson and A.J. Freeman, Phys. Rev., 134, A1526 (1964).

13. S. Sugano and Y. Tanabe, J. Phys. Soc. Japan, 20, 1155 (1965).

14. J. Hubbard, D.E. Rimmer and F.R.A. Hopgood, to be published.

15. J.H. Van Vleck, J. Chem. Phys., 3, 803 (1935).

16. F. Keffer, T. Ogouchi, W. O'Sullivan and J. Yamashita, Phys. Rev., 115, 1553 (1959).

17. M.H.L. Pryce, Proc. Phys. Soc., A63, 25 (1950).

18. C.P. Slichter, "Principles of Magnetic Resonance", Harper and Row, (1963).

19. A. Abragam and M.H.L. Pryce, Proc. Roy. Soc., A205, 135 (1951).

20. B. Bleaney and K.W.H. Stevens, Repts. Prog. in Phys., 16, 108, (1953); K.D. Bowers and J. Owen,ibid., 18, 304, (1955).

21. W. Low, Solid State Physics, Suppl. 2, Academic Press (1960). W. Low and E.L. Offenbacher, ibid., vol 17, 135, (1965).

22. G.F. Koster and H. Statz, Phys. Rev., 113, 445, (1959); also 115, 1568 (1959).

23. W.C. Grant and M.W.P. Strandberg, J. Phys. Chem. Solids, 25, 635, (1964).

24. T. Ray, Proc. Roy. Soc., A277, 76, (1964).

25. Huang Wu-Han, Lin Fu-Cheng and Zhu Ji-Kang, Proc. Phys. Soc., 84, 661, (1964).

26. R. McWeeny, J. Chem. Phys., 42, 1717, (1965).

27. M. Tinkham, Proc. Roy. Soc., A236, 535, (1956).

28. K.W.H. Stevens, Proc. Roy. Soc., A219, 542, (1953).

29. A.A. Misetich and T. Buch, J. Chem. Phys., 41, 2524, (1964); A.A. Misetich and R.E. Watson, Phys. Rev., 143, 335, (1966).

30. G. Feher, Phys. Rev., 103, 500, 834, (1956).

31. W. Hayes, J.R. Pilbrow and L.M. Slifkin, J. Phys. Chem. Solids, 25, 1417, (1964).

32. J.C. Garth, Phys. Rev., 140, A656, (1965).

33. R. Nathans et al. Proc. Int. Conf. Mag., Nottingham, p. 327, Inst. of Phys. (1965); J. Hubbard and W. Marshall, Proc. Phys. Soc., 285, 542, (1965).

34. H. Watanabe, Prog. Theor. Phys. (Kyoto), 18, 405, (1957).

35. M.J.D. Powell, J.R. Gabriel and D.F. Johnston, Phys. Rev. Letters, 5, 145, (1960); Proc.Roy.Soc. A264, 503 (1961).

36. R.R. Sharma, T.P. Das and R. Orbach, Bull. Am. Phys. Soc., 11, 313, (1966).

CHAPTER V

INSTRUMENTATION AND TECHNIQUES

5.1.1 The General Design of E.S.R. Spectrometers

It is usually convenient to operate electron resonance spectrometers at microwave frequencies in the range of 8 to 36 Gc/s. This is generally a consequence of finding the best conditions of sensitivity and resolution, consistent with the available techniques. It is sometimes necessary to carry out experiments at different frequencies because of the specialized nature of the systems under investigation, but these shall not be described here.

The overall sensitivity of a paramagnetic resonance spectrometer is of primary importance for many applications and systems have been built which have a sensitivity under suitable conditions of 10^{11} spins for 1 gauss line width and a bandwidth of 1 sec. The specific conditions of sensitivity and design have been studied by a number of authors (1 to 4) and will not be specifically discussed here.

The layout of an electron resonance spectrometer is basically similar to that of any spectrometer, i.e. a source of power, feeding into an absorption cell in which the sample is situated and finally a detector where the effect of the radiation on the sample is observed. No dispersive element is required as power sources in the microwave region produce essentially monochromatic radiation. Usually the Zeeman energy levels of the paramagnetic substance can be altered

by varying an external magnetic field until the splittings coincide with the quantum energy of the microwave radiation.

(a) The Power Source

In a microwave system, the power source is usually a klystron oscillator, which is convenient because of its flexibility, reasonable inherent stability and power output. It is often necessary to ~~further~~ stabilize the klystron frequency further; this is possible in one of two basic ways. The klystron frequency can either be compared with the resonant frequency of a high Q microwave cavity and, by using a good feedback loop, stabilizations of about 1 part in 10^5 can be attained. Alternatively, it can be compared with a suitable harmonic from a crystal controlled oscillator. The latter system provides stabilizations of 1 part in 10^9 although the arrangement may not be tuned as easily over a small range.

(b) The Absorption Cell

The absorption cell of a spectrometer may be a standing or a travelling wave arrangement. The reflection cavity is most commonly used and it is compared with a reflection slow wave helix in section 5.1.3. The basic function of the absorption cell is to concentrate the microwave magnetic field in the sample which often has a limited size and must be mounted in a sufficiently stable and homogeneous steady magnetic field which satisfies the resonance condition $h\nu = g\beta H$.

(c) Detection

Electron resonance is observed by rectifying the microwaves which have interacted with a sample and after processing the information, it is displayed on a chart recorder, or on an oscilloscope. The microwave detector is the principal source of noise in a practical spectrometer and great care is taken to find the optimum microwave system consistent with sensitivity considerations and to carry out the most efficient noise averaging.

The 100 Kc/s field modulation ~~system~~ system employing described in the next section is commonly used; its advantages ~~being~~ are reasonably high sensitivity (3×10^{11} spin/gauss can be observed with a bandwidth of 1 sec and a microwave power of 1 mW) coupled with simplicity and ease of operation when compared with the more sensitive superheterodyne system. The 100 Kc/s homodyne spectrometer has many of the advantages of both these arrangements (1,3).

An interesting system which has not yet been extensively used is the "marginal oscillator" arrangement described by Payne (5). This spectrometer is a microwave analogue of the r.f. marginal oscillator circuit commonly used in nuclear resonance spectrometers. The system ~~comprises~~ uses a microwave oscillator in the "just oscillating" condition, the path of feedback containing the absorption cell. A suitable microwave device is a low noise travelling wave tube or a klyston oscillator operating on the edge of one of its oscillation modes. In such a system, the level of oscillation is detected to

observe the resonance in a sample. The overall sensitivity of this instrument, as it was used by Payne, is similar to that of conventional spectrometers, for the optimum level of oscillation.

Silicon microwave diodes are usually preferred to bolometers as microwave detectors ~~owing to~~ because of their greater robustness and their ability to withstand higher microwave powers. ~~The overall sensitivity~~ with each detector operating under its optimum conditions the overall sensitivity is usually comparable. Recently Schmidt and Solomon have described the use of a bolometer directly coupled to the microwave system by a resonant sample (6).

As the noise spectrum of the detector is "white" over a limited range, the signal to noise ratio for a given sample can be improved by reducing the overall bandwidth of the system. This is possible in a field modulation system by reducing the ~~field~~ modulation amplitude to a value rather less than the line width and detecting the first derivative of the resonance at the ~~field~~ modulation frequency. The bandwidth of the detecting system may now be drastically reduced without distorting the lineshape. The signal is amplified to a level of a few volts and is then compared with the original field modulation frequency in a phase sensitive detector (P.S.D.) before finally recording the signal on a chart recorder. The bandwidth of the detecting system is controlled by a time constant (usually an RC network) between the P.S.D. and the recorder. It is usually found that there is little advantage in using a time constant

facing page 112

figure 5.1

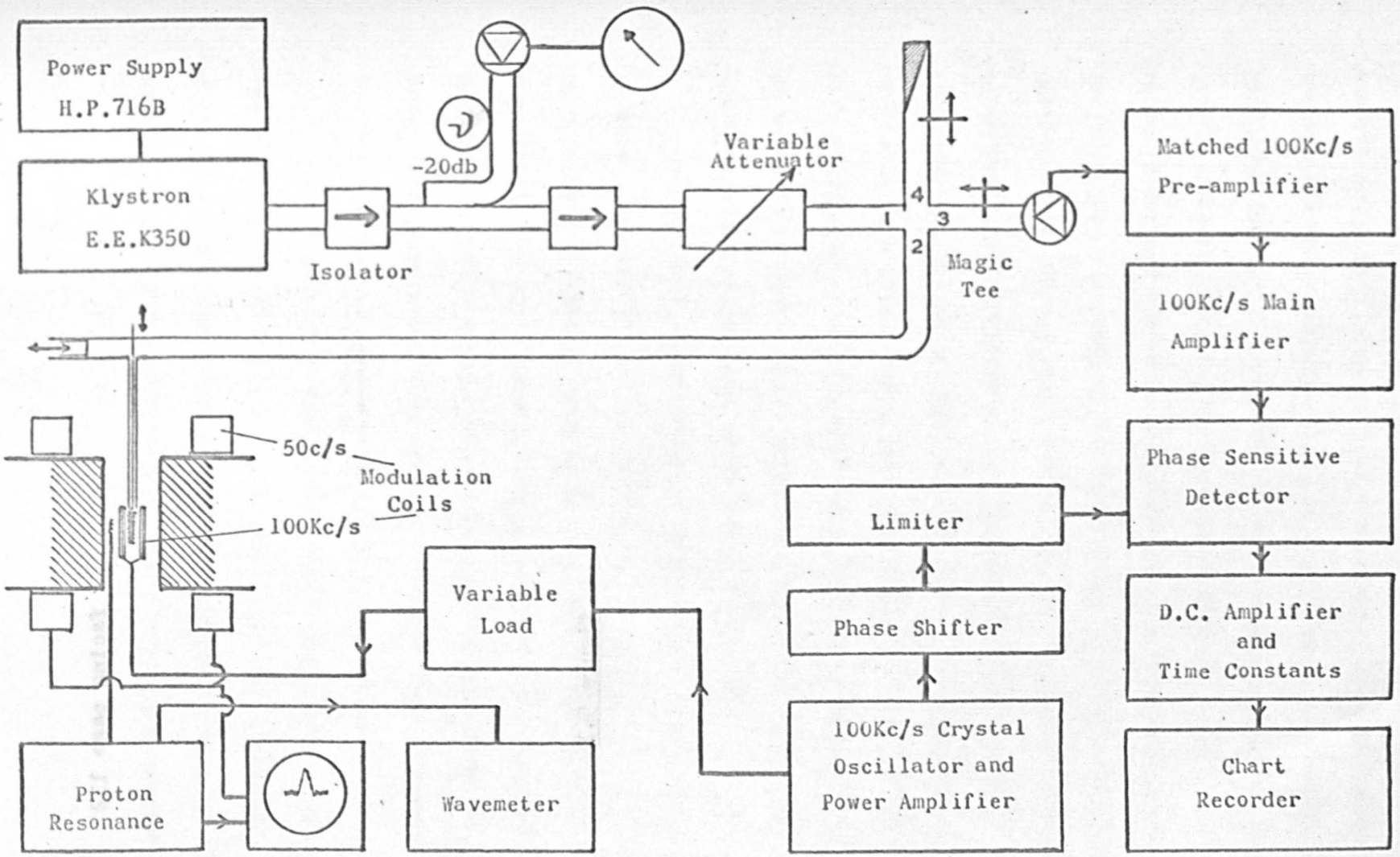

Figure 5.1

Layout of E.S.R. Spectrometer

of greater than 30 seconds due to d.c. instabilities. To obtain further improvements, or else when studying transient phenomena, repetitive sampling systems are better (7).

5.1.2 The Electron Resonance Spectrometer

The electron resonance apparatus used in all the experiments described in this thesis is a fairly conventional X-band system employing 100 kc/s field modulation ~~X-band system~~. The spectrometer which has been built will only be briefly described and the absorption cell, a helix, is described in the next section.

The basic layout of the paramagnetic resonance apparatus is shown in Figure 5.1. The English Electric K350 klystron is immersed in an oil bath and is tuned to operate at 9.18 Gc/s. This klystron produces about 2 watts of microwave power when operated on its highest power mode, with the disadvantage that its electronic tuning range is limited to about 8 Mc/s and mechanical tuning of the two cavities is an involved procedure taking about 8 hours.

The klystron power supply used in the early part of the experiments was augmented by a modified Pound automatic frequency control system (A.F.C.) (8). Subsequently, when using a Hewlett-Packard Type 716B supply, the klystron A.F.C. system was found to be unnecessary due to the excellent inherent stability of the K350 klystron and the supply. After an initial warm up period, it is not possible to detect any slow drift of the klystron frequency. To obtain further useful stabilization it would be necessary to use

a locking system with a response time of faster than 5×10^{-5} secs.; klystron frequency noise at about 100 kc/s is easily detected when the phase of the bridge is set to detect dispersion (i.e. is "frequency sensitive") (1).

The microwave bridge is balanced by adjusting the helix matching (5.1.3 (d)) and crystal biasing is obtained by introducing a suitably phased mis-match (slide-screw tuner) into the balance arm of the magic-tee. The silicon diode (A.E.I. CS10B) detector crystal is matched using a tuned transformer wound on a Mullard "Vinkor" pot-core assembly, into the cascode preamplifier (a pair of STC 3A/167M triode valves). The main signal amplifier has a Q factor of about 300 which is sufficient to allow video display of resonances on an oscilloscope when the magnetic field is modulated at 50 c/s as well as 100 Kc/s. The phase sensitive detector ~~comprises~~ consists of a carefully matched diode bridge using four OA202 silicon diodes immersed in an oil bath.

Reference switching is taken from the output of the crystal controlled 100 Kc/s oscillator and power amplifier. This system can provide up to 30 gauss, peak to peak modulation at the sample; the modulation coils are attached to the outside of the low temperature dewar as there is virtually no attenuation in the thin silvering. Time constants of between 0.5 and 30 seconds can be switched into the d.c. amplifier which feeds an Evershed moving coil pen recorder. The recorder limits the fastest response of the spectrometer to about

0.5 secs full scale (2.5").

A 7" Newport Type E electromagnet is used and ~~it has been~~ set up to give a homogeneity of about 2 parts in 10^5 over a cylinder about 2 cm. in diameter across the full 5.5 cm. gap of the magnet. The magnet is supplied from a Newport Type D power supply equipped with both a mechanical and an electronic sweep unit. The maximum sensitivity of the spectrometer with a 10 sec. bandwidth and measured at full klystron power (≈ 1 watt at the helix) is about 7×10^{10} spins/gauss linewidth for a 1 : 1 signal to noise ratio, which is equivalent to about 7×10^{12} spins/gauss for 1mw at the helix and a bandwidth of 1 sec. The measurement was made at room temperature using a standard carbon sample.

5.1.3 The Helix

A helix has been used in all the experiments described. The more conventional resonant cavity arrangement could equally well have been employed but the great simplicity of the system has made the use of a helix worth while. The arrangement that is described below has a number of advantages over the cavity system which would be necessary for the same experiment. The most important advantages are the ease with which samples can be irradiated at all temperatures and the simplicity ~~attached to using~~ with which 100 Kc/s field modulation of fairly large amplitude (30 gauss) can be used. It is also possible to alter the orientation axis of crystals without warming from liquid nitrogen temperature.

There are no problems concerning matching of the helix at different temperatures (it has been used at 300°K, 77°K and 20°K) and the compactness of the coaxial "probe" is such that low temperature dewars which would normally be used with Q-band cavities can be used; the heat loss in the German Silver coaxial line is much less than along a comparable X-band waveguide arrangement. The broadband nature of the structure has allowed the powerful K350 klystron to be used. (An equally stable reflex klystron was not available for this spectrometer when these experiments were initiated). The extra power available from this klystron approximately compensates for the possibly lower "Q factor" of the helix. It has been possible to orient single crystal samples by simply rotating the central conductor of the coaxial line after the crystal had been mounted with a predetermined axis parallel to the central conductor and normal to the steady magnetic field. In this way, it has not been necessary to rotate the magnet about this axis. Perhaps the greatest advantage in using a helix is the ease with which the system could be modified to carry out double resonance experiments; if these were required, the present arrangement could easily be altered for this purpose.

The principal disadvantages are probably associated with general sensitivity, particularly in some single crystal work when the ~~orientation~~ possibly irregular shape of the crystal cannot be fitted easily into a helix of narrow diameter and given axial direction. Silver chloride

facing page 116

figure 5.2

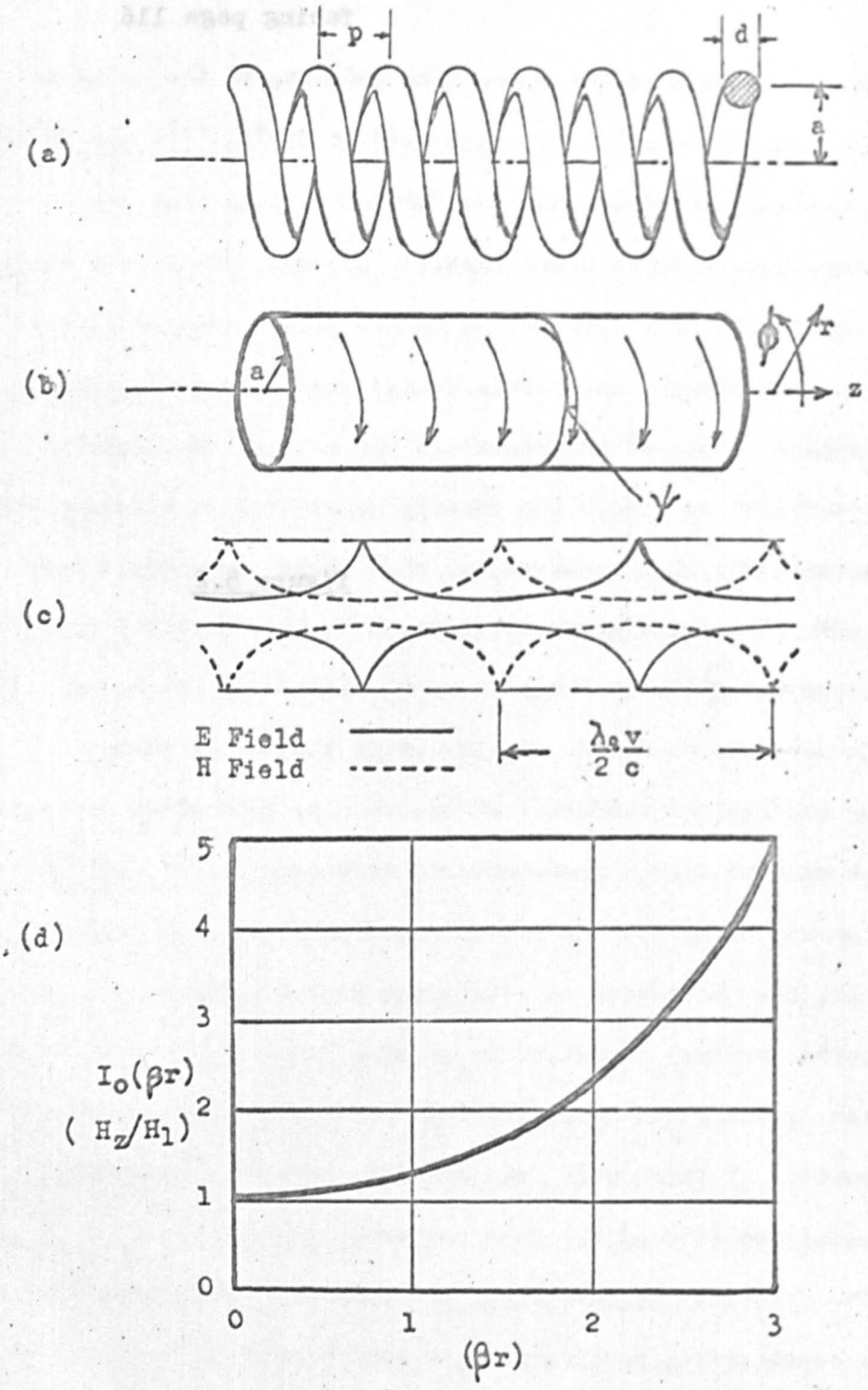

Figure 5.2

(a) Actual Helix (b) Conducting Sheet (c) Instantaneous Field across Helix Section (d) Variation of H_z with (βr)

crystals have been cut so as to give the maximum filling factor in the helix and as well as can be judged, the sensitivity of the spectrometer is not markedly lower than that obtained if a typical reflex klystron had been used with a cavity (see 5.1.3c and d)). It has not been possible to use aqueous samples due to inadequacies in the matching system. Suitable matching arrangements can nevertheless be devised (9).

The important parameters describing the helix and its matching into the microwave system have been determined empirically. The matching does not present a serious problem as the spectrometer has been operated at a single frequency.

The sensitivity depends considerably on the axial microwave magnetic field (H_1) in the helix, for a given incident microwave power (P) and on the variation of H_1 with the parameters describing the geometry of the helix.

(a) A Simple Description of the Fields

The field modes in a helix have been studied in some detail by Pierce (10) for travelling wave tube theory and Webb has described some of the application to e.s.r. (11). It would be an extremely complex problem to find the field distribution in a real helix (Figure 5.2 a) but Pierce has solved Maxwells' equations for a ~~helically conducting~~ cylindrical sheet of the same radius (a) and pitch (ψ) as the helix (Figure 5.2 b), which is constrained to conduct in a helical direction by restricting the boundary conditions.

The helix is a microwave delay line; the waves are constrained to travel in the direction of the wire with a phase velocity (c) along the spiral. The phase velocity, v, of the travelling waves along the z-axis of the helix ~~will be~~ is much less, depending on ψ and the magnitude of $2\pi a$ compared with the free space wavelength $\lambda_0 = 2\pi/\beta_0$. Pierce shows that, for slow waves,

$$v/c = \text{Tan}\,\psi \qquad 5.1\,a$$

(when $\beta_0 a \text{Cot}\,\psi > 1.5$) with no dispersion ($v_g = v$). If the wave travelled in the direction of conduction, with the speed of light then $v/c = \text{Sin}\,\psi$, which is essentially the same as 5.1a for small pitch angles ψ giving

$$v/c \approx 1/2\pi na \qquad 5.1\,b$$

where n is the number of turns per unit length ($1/p$).

Thus, for $\beta_0 a \text{Cot}\,\psi > 1.5$ and $\text{Cot}\,\psi \gg 1$ the phase velocity is ~~just~~ that corresponding to propagation along the sheet in the (helical) direction of conduction with the speed of light and hence the velocity of propagation in the axial direction is at a much reduced speed. For helices of smaller radius compared with the wavelength ($\beta a < 1$, say) the speed is greater. The field distribution in the helix is shown in Figure 5.2c, the radial component is too small to be of interest and Pierce finds

$$H_z \approx H_1 \, I_0(\beta r) \, \exp.j(\omega t - \beta z) \qquad 5.2$$

in the helix for the conditions described above. $I_0(\beta r)$ is the (of zero-order modified Bessel function) of argument (βr), and H_1 is the maximum value of H_z on the axis of the helix.

From equation 5.1a, $\beta_0 \mathrm{Cot}\,\psi \approx \beta$ and for $\beta a > 1.5$ the function $I_0(\beta r)$ is smaller at the centre for increasing radius (Figure 5.2d). For $\beta a < 1$, $I_0(\beta a)$ is close to unity and the field distribution is virtually constant across the cross section of the helix.

Of interest in a magnetic resonance experiment is the field H_1 within a sample (more correctly, one of the circularly polarized components), the coupling between the microwave field and the sample is a maximum in the region $1 \leq \beta a \leq 1.5$ (11) and it is within this range that the best helices are made.

Pierce compares the performance of real wire helices with the conducting sheet. His results show that H_z^2 on the inner surface of the wire is about 0.75 of H_z^2 on the surface of the sheet for about 4 turns per wavelength and about 0.6 for 2 turns per wavelength ($d/p = 0.5$ where d is the wire diameter and p the pitch, although the ratio is better smaller than larger). This reduction in H_z^2 does not fully occur as Pierce calculates it for a simplified case; the helix is slit normal to the direction of conduction and it is ~~developed~~ spread out, so that the influence of the other side of the helix is not taken into account. The field within a real helix is thus not substantially different from the sheath helix although useful volume is effectively lost as the finite size of the wire reduces the usable diameter of the helix. The total radiation field is divided so that the energy propagated inside the helix is about 0.7 that propagated

facing page 119

figure 5.3

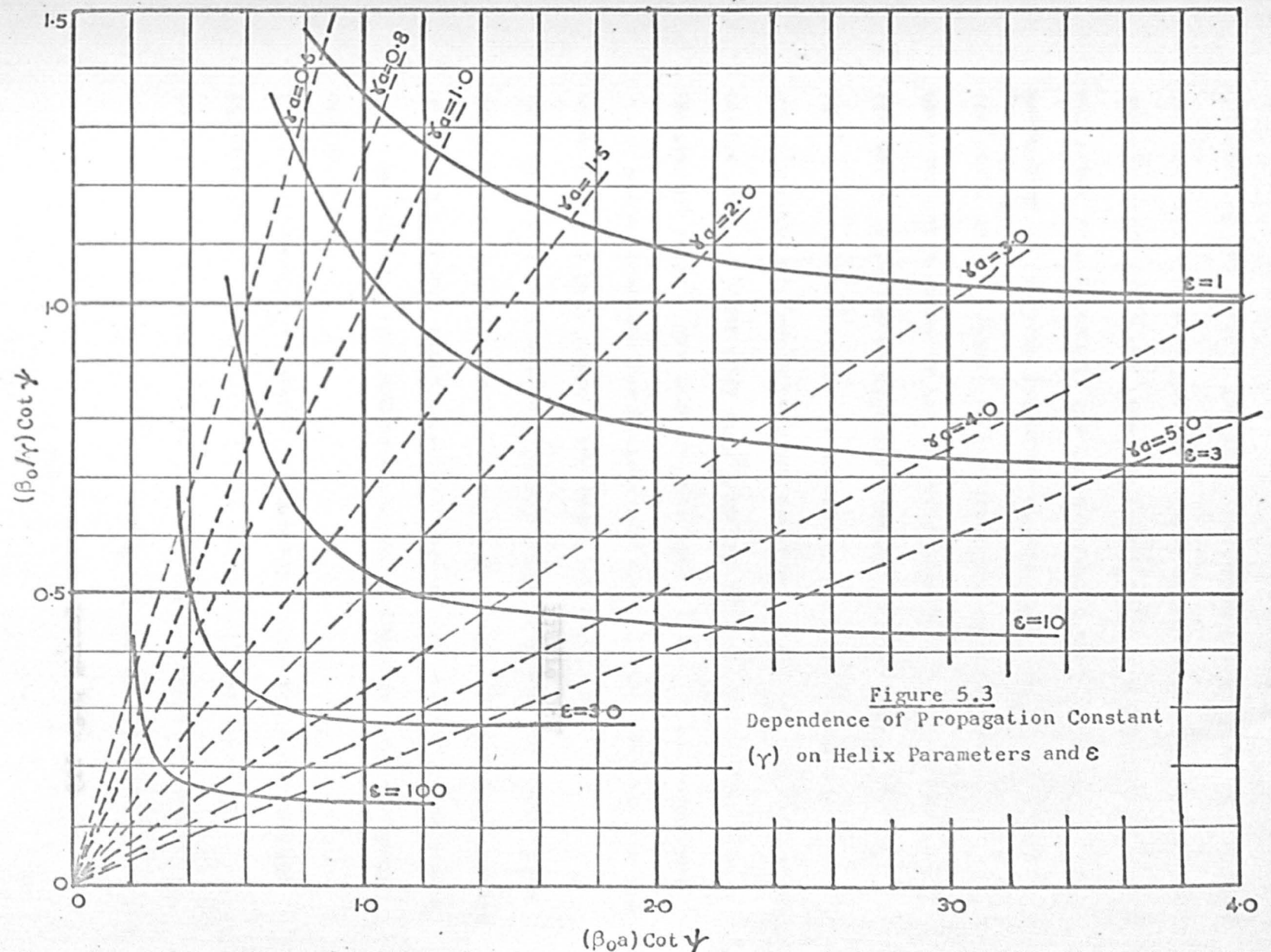

Figure 5.3
Dependence of Propagation Constant (γ) on Helix Parameters and ε

outside (12), the ~~distinction~~ boundary between outside and inside being to a first approximation at the mean radius, a.

(b) The Effect of a Dielectric

The analysis which has been used above takes no account of the effect of dielectric materials which must play an important part in the operating characteristics. The microwave electric field as well as the magnetic field travels through a sample. In silver halide crystals, this will be of primary importance as the microwave dielectric constant is about 10. In this section, it is shown how the design parameters of the helix depend on the dielectric filling it.

It is quite straightforward to calculate the effect of filling the sheath helix with dielectric. Pierce's field equations inside and outside the helix are given in Appendix 1; they are altered to include the effect of a dielectric and are given in terms of the coefficient H_1. The propagation constant is now given by the equation A1.13.

$$(\gamma a)^2 \frac{I_o(\gamma a)\ K_o(\gamma a)}{I_1(\gamma a)\ K_1(\gamma a)} \cdot A = (\beta_o a \cot \psi)^2 \qquad 5.3$$

where $A = \dfrac{I_1 K_o + I_o K_1}{\epsilon_1 I_1 K_o + \epsilon_2 I_o K_1}$; $\gamma^2 = \beta^2 - \beta_o^2$;

ϵ_1 is the dielectric constant of the material filling the helix and ϵ_2 describes a dielectric outside extending to infinity. The case A = 1 is equation 22 of Pierce's Appendix II (10). Figure 5.3 shows a series of curves for different values of $\epsilon = \epsilon_1$ ($\epsilon_2 = 1$) which

facing page 120

figure 5.4

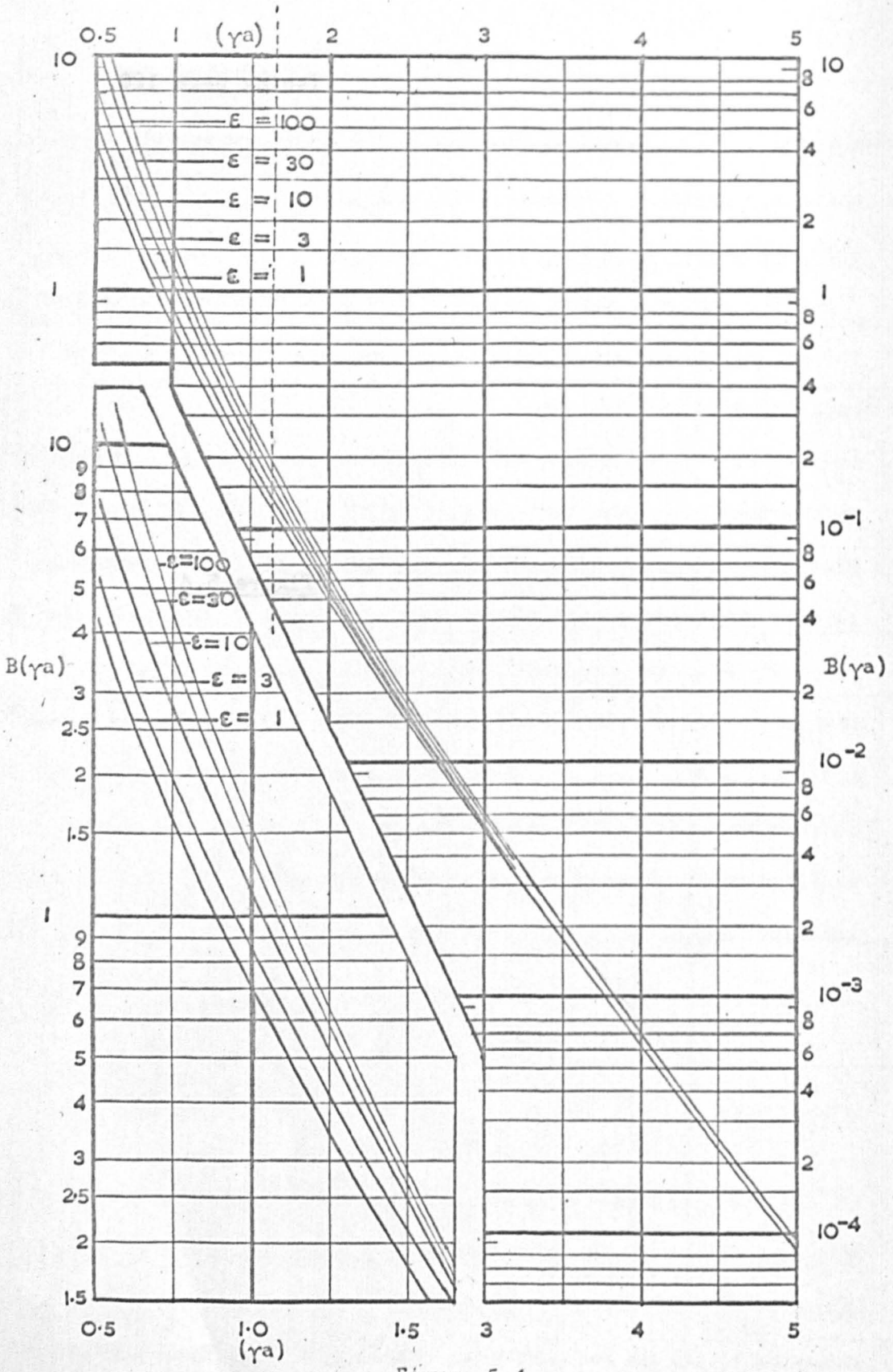

Figure 5.4

Dependence of B(γa) on (γa) and the Dielectric filling the Helix (ε)

allows one to find the radial propagation constant γ, and hence β for any value of the parameter $\beta_o a \cot\psi$. For tightly wound helices where v is small compared with c, $\gamma \approx \beta$.

It can be seen from Figure 5.3 that the travelling wave is slowed by about a further factor of 2.5 when the helix is filled with a sample of silver chloride. In a real helix, due to the reduced filling factor, this slowing will not quite be attained. The condition $1.0 \leq \beta a \leq 1.5$ would no longer hold and the field distribution across the sample would no longer have the optimum configuration. Retaining a given value of $\beta a \approx \gamma a$ and of a, the pitch of the helix should be increased by an amount Δp. If a_o is the mean radius of the sample, to a first approximation, the increase Δp will be multiplied by a factor $\frac{a_o}{a}$, remembering that the spacing between turns should be approximately the thickness of the wire.

The relationship between the power flow along the helix (P) and the maximum magnetic field on the axis, (H_1) is given in Appendix I (equations AI.15, 16) as

$$P = 600\, H_1^2\, \frac{\beta\, \beta_o}{\gamma^4}\, B^{-1}(\gamma a) \qquad 5.4$$

where $B(\gamma a)$ is a function of ϵ_1, ϵ_2 and γa.

$\frac{H_1^2}{P}$ is a parameter of importance in considering the sensitivity of the helix. This function is plotted against γa for the case $\epsilon_2 = 1$, $\epsilon_1 = \epsilon$ with values of ϵ between 1 and 100, in Figure 5.4. It can be seen that, for a given value of γa, $B(\gamma a)$ is

facing page 121

figure 5.5

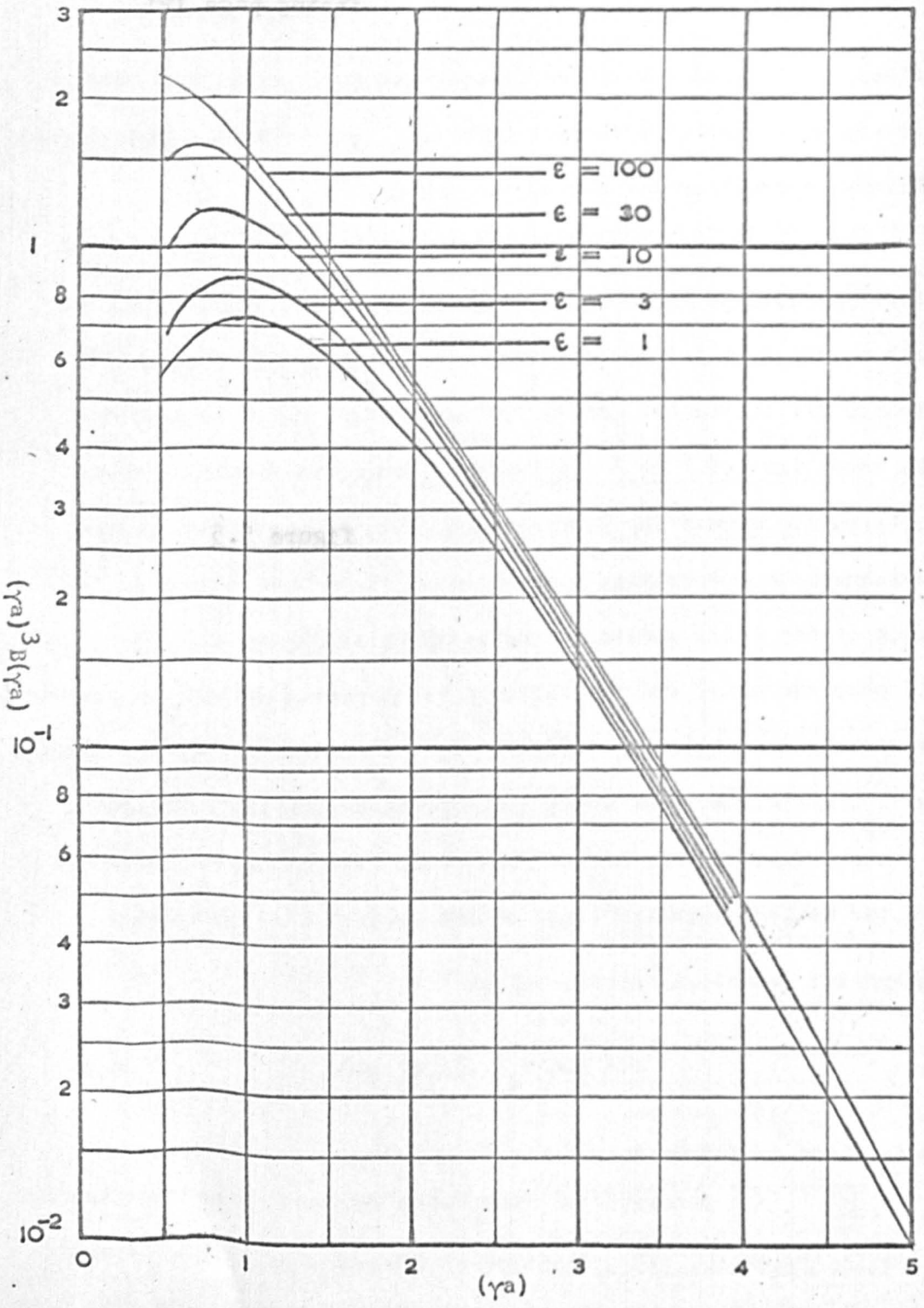

Figure 5.5

Dependence of $(\gamma a)^3 B(\gamma a)$ on (γa) and on ε

fairly insensitive to the effect of the dielectric, but it should be noted that a helix with a large γa has a very small value of $B(\gamma a)$. If a given helix is of interest, (i.e. given a), the function $(\gamma a)^3 B(\gamma a) \approx (\gamma^4 a^3/\beta) B(\gamma a)$ is of more value. (This function is plotted in Figure 5.5). As an example, if an "optimum" helix, i.e. $1.0 \leq \beta a \leq 1.5$ is filled with a dielectric without altering any of the helix parameters, $\frac{H_1^2}{P} \propto \frac{\gamma^4}{\beta} B(\gamma a) \approx \gamma^3 B(\gamma a)$ is reduced by between 2.5 and 3.0 times by filling the helix with a dielectric with $\epsilon = 10$. An increase in sensitivity cannot be expected if the pitch is increased without increasing the wire diameter; if both are increased, the filling factor is reduced. When the sample size is not limited, $\frac{2\pi}{P}\int_0^a H_z^2 r\, dr \approx (\pi a^2 H_1^2/P)$ should be considered, as the total field across the sample is more important than the maximum field density.

(c) Operating Conditions

The discussion above has been limited to a travelling wave flowing along a helix of indefinite length. This condition would be appropriate to a transmission spectrometer, however in the reflection configuration, if all the microwave power was dissipated along a sufficiently long matched helix, the sample absorption would not be detected. If, however, a standing wave is set up by the mismatch at the end of the helix, resonance absorption will be observed. The matching condition is precisely the same as that for a critically coupled cavity and a standing wave pattern is set

facing page 122

figure 5.6

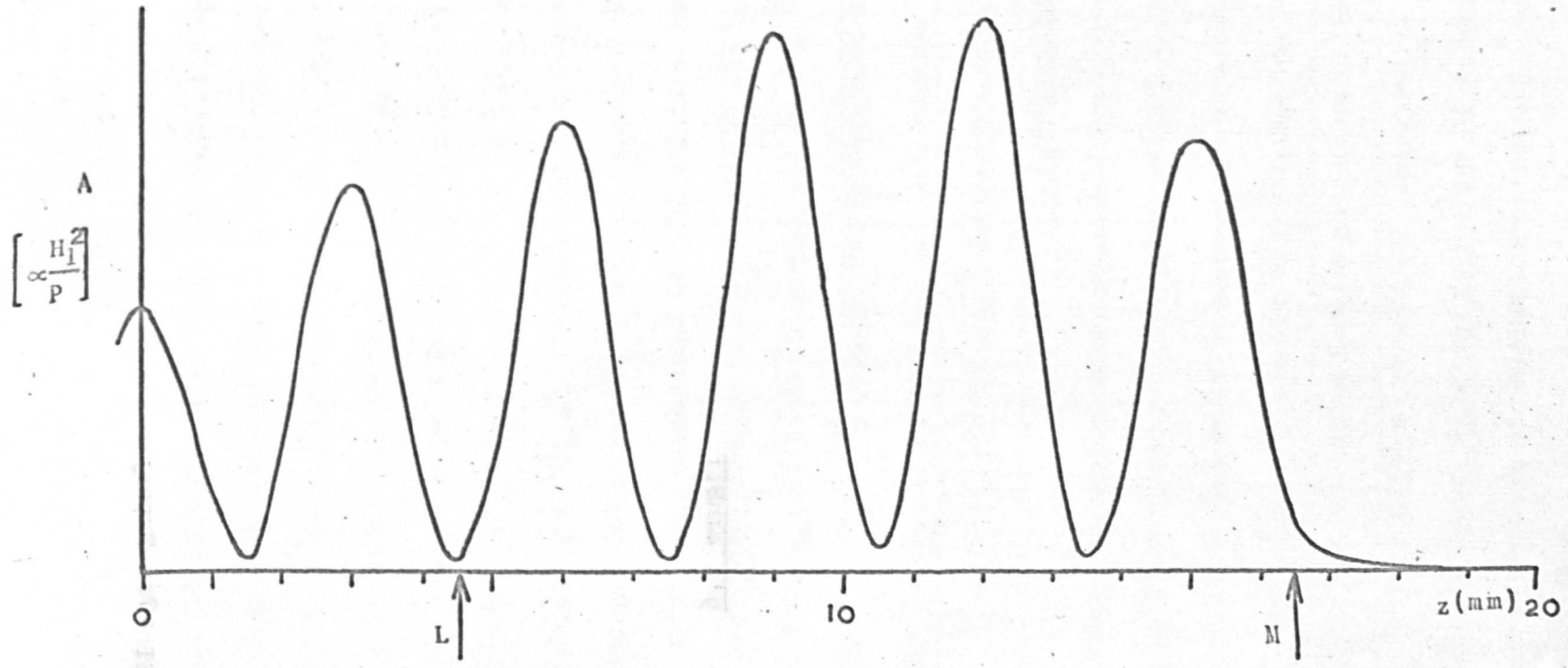

Figure 5.6

Intensity of the Standing Wave Pattern along the axis of the Helix.
The point L is the end of the coaxial line and M is the end of the Helix.

up along the helix with the matching of the helix amounting to the adjustment of its coupling to the waveguide. This standing wave arrangement is essentially a narrow-band arrangement being described by a suitable Q-factor although the adjustment for different operating frequencies is rather more straightforward than with a cavity.

It has been possible to measure the field distribution by using a brass micrometer device to drive a silica fibre with a very small quantity of DPPH, without any sideways or twisting movement, up through the helix so that it accurately remained on the axis of the helix. The fibre, which was about 0.2mm in diameter, did not seriously affect the balance of the bridge, and slight off-balance was made negligible by a rather larger unbalance introduced elsewhere in the bridge. The magnitude (A) of the DPPH resonance was observed as a function of its position (z) along the axis of the helix. The result of this is shown in Figure 5.6, which is of the form expected for a standing wave pattern. If the power dissipation in the helix was such that the wave mode contained an appreciable amount of travelling character, all of the minima in Figure 5.6 would not fall to zero (the magnitude of the minima actually represent the resolution due to the finite size of the piece of DPPH). The minima may also be non-zero away from the helix axis because of the finite thickness of the helix wire.

The actual helix used to obtain the pattern had a mean radius (a) of 1.14mm. and pitch (p) of 1.07mm. Substituting these values into equation 5.1 (b can be used in this case) gives $\frac{\lambda}{c} = \frac{\lambda}{\lambda_0} \approx 0.15$ so that the helix wavelength (λ) is calculated to be 5.0mm. for λ_0 = 3.3 cms. This compares fairly well with the measured wavelength of 6.0mm. (see Figure 5.6), considering the approximations which have been made. The agreement could be improved by suitably redefining "mean radius". If the inside surface of the helix is chosen to describe the radius a', λ is calculated as 6.4mm.

The Q-factor which describes the standing waves in the helix can be used in the normal analysis of resonant cavity e.s.r. spectrometers (1 to 4). The condition for optimum power matching (i.e. bridge balanced) will demand that the actual Q (Q_L) will be a half of the unloaded Q. It would be possible to calculate the helix Q factor from the expected loss in the helix wire, but this ideal Q will not be realistic as the microwave field is allowed to interact with geometrically complex surroundings and with samples which do not necessarily fill the helix. The bandwidth of the helix and its matching system has been measured by observing the response of the matched bridge when the klystron frequency is modulated. This bandwidth is typically equivalent to a Q-factor of about 1000, but it must be noted that there may be a contribution to this from the matching system and Q_L for the actual helix may be rather lower.

In the usual formulae for spectrometer sensitivities when operating in the linear range of the detection crystal, the detected voltage (ΔV_L) is given by (1)

$$\Delta V_L = k P^{\frac{1}{2}} Q_L \chi'' \eta \qquad 5.5$$

where k is the proportionality constant depending on the configuration among other things. χ'' is the paramagnetic susceptibility (given for example by Bloch's equations 3.12), P is the incident microwave power and η is the filling factor of the helix, given by

$$\eta = \frac{\int_{sample} H^2 \, dv}{\int_{field} H^2 dv} \qquad 5.6$$

This is simple to assess for a sample which is long compared with the helix wavelength. If the sample fills the helix, and noting that the energy associated with the radiation field inside the helix is 0.7 of that outside (see end of section 5.1.3a),

$$\eta = 0.2 \times (1 - \frac{d}{2a})^2 / (1 - \frac{\pi d}{16a})^2 \qquad 5.7$$

where d is the wire diameter and a the mean radius. The standing wave mode indicates that only half of the sample is actually in the microwave field. For the specific helix described above, $\eta \approx 0.17$ and for a typical cavity $\eta \approx 0.04$, say.

To compare a resonant cavity with a helix used in the same configuration (e.g. bridge with reflection matching), the important

facing page 125

figure 5.7a

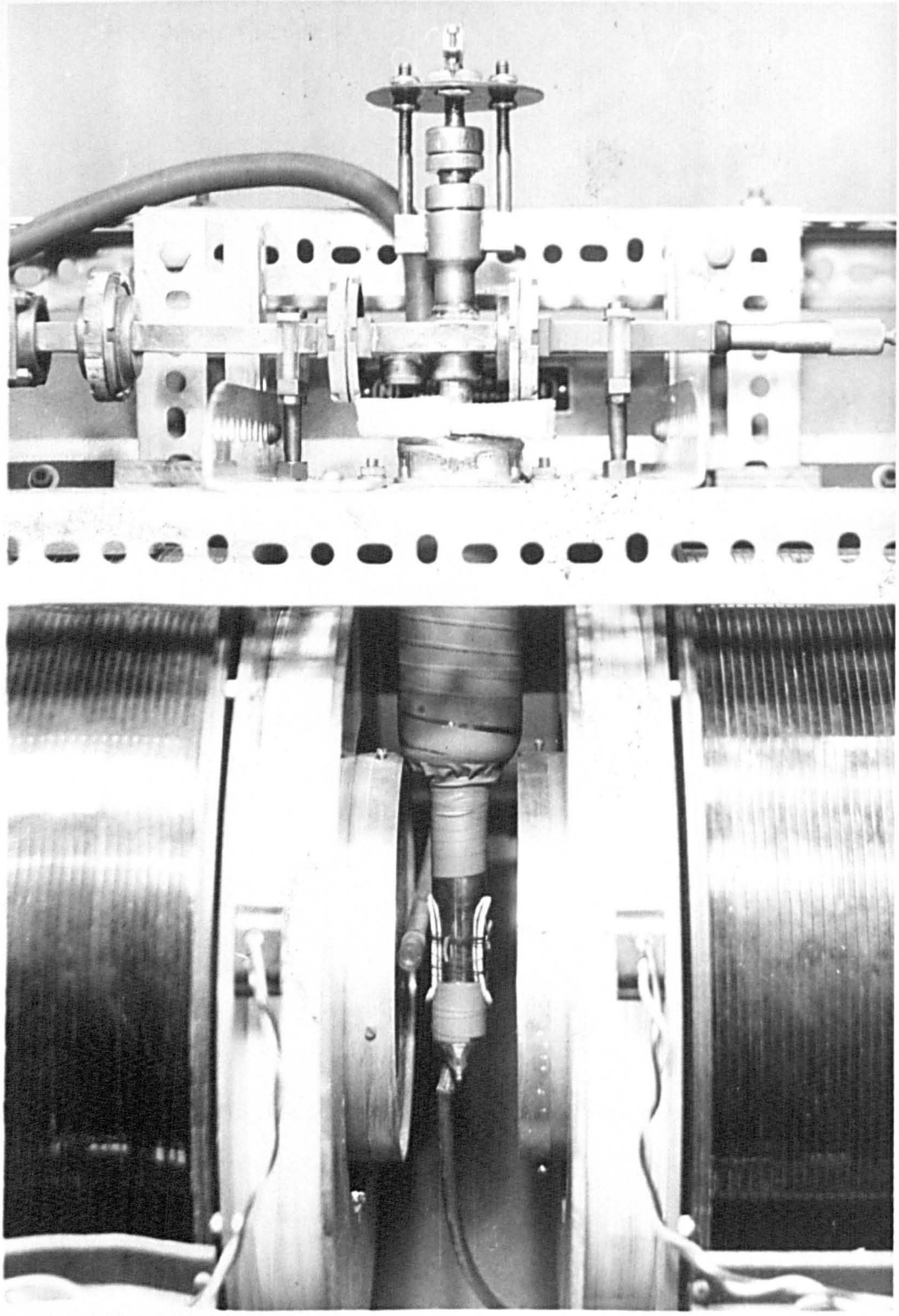

Figure 5.7a Helix Matching Unit in Position in Magnet: showing Low Temperature Dewar, Modulation Coils and Proton Resonance Probe.

facing page 125

figure 5.7b

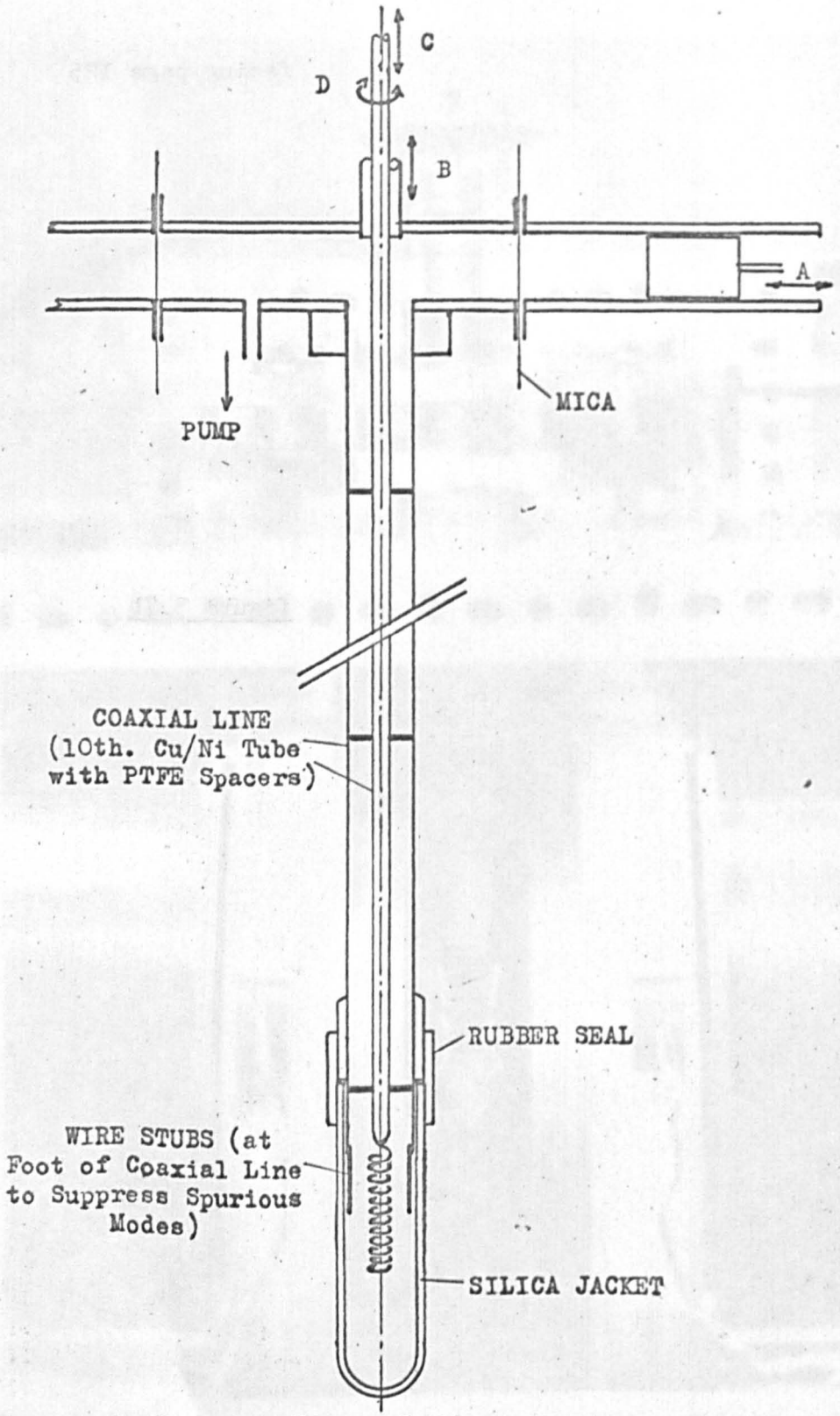

Figure 5.7 b

Waveguide/Helix Matching Unit (to scale)

parameter from equation 5.5 is $Q_L\eta$. For a typical cavity ($Q_L \approx 4000$, say) this may be in the region of 160 and for a helix, taking the observed Q for Q_L, $Q_L\eta$ = 170. The helix is thus comparable with a cavity as the absorption cell in a spectrometer. This is in agreement with the overall sensitivity quoted in section 5.1.2, which is similar to that attained with an otherwise similar cavity spectrometer operating under the same conditions of power, time constant etc. The additional power available from the K350 klystron which is not generally suitable for a cavity instrument constitutes a useful further improvement in sensitivity.

(d) Helix Matching

The apparatus used for matching the helix into the waveguide is shown in Figures 5 .7a and 7b. The waveguide/coaxial transformer is adjusted using a variable short A and stub B. (The latter is not essential but often proves to be helpful). The coaxial line is made from copper plated copper/nickel tubing with p.t.f.e. spacers. The helix is matched to the coaxial line by altering the length of the central conductor - i.e. by adjusting C. As crystal orientation is altered by rotating the central conductor, it is not possible to attach the lower end of the helix to the outer conductor. This can cause spurious modes to be excited outside the coaxial line, but this has been overcome by attaching three ~~of~~ four wire stubs about 1/4" long to the bottom of the outer conductor.

The arrangement is sealed for operation at low temperatures using a silica jacket around the helix, p.t.f.e. seals on the adjustments B and C and mica windows across the rectangular waveguide.

Crystals must be firmly wedged in the helix to avoid severe microphonics ("bumping") when the assembly is immersed in liquid nitrogen. Lens tissue is an ideal material for this wedging as it does not give rise to e.s.r. signals..

If thin wire is used to make the helix, microphonics would be a problem if support was not provided. The function of the matching system is to match the waveguide to the coaxial system so that a travelling wave is sent along the coaxial line, and so that any wave reflected from the bottom of the coaxial line is fully transmitted back through the waveguide/coaxial matching (i). The coaxial/helix matching, on the other hand, couples the power into the resonant helix (ii). It is not possible to adjust the apparatus of Figure 5.7 to satisfy the criteria (i) and (ii) separately, so it is not certain if this matching system is totally satisfactory.

The point M on Figure 5.6 coincides with the end of the helix (it is simply cut off at the end with no modification to assist reflection; this does not appear to be very important). L corresponds to the end of the coaxial line; this helix was matched so that the transition was actually within the coaxial

line, but this is not very important. It is interesting to note that L corresponds to a minimum in H_1^2. The apparent reduction in H_1^2 within the helix is due to screening of the 100 Kc/s modulation.

Further investigation of helix matching conditions could prove valuable in assessing the optimum sensitivity.

5.2 Techniques of Measurement and Irradiation

All e.s.r. spectra have been measured by reference to a proton resonance unit (Newport type P Mk II) locked to a heterodyne wavemeter (U.S. Navy Type CKB 74028). Pips are put onto the e.s.r. trace as the magnetic field is swept, at intervals determined by the wavemeter. The proton resonance line-width is about 70 milli-gauss and this is about the accuracy of the position of each pip. These markers are obtained by discharging a capacitor onto the chart pen.

For g-value measurements, and measurements of the klystron frequency, a small quantity of the free radical DPPH (diphenyl-picrylhydrazyl) "g-marker" has been attached to the crystal under observation.

Crystals have always been irradiated while mounted in the helix. The crystal temperature has been adjusted by precooling methylated spirit (freezing point $\approx -110^{\circ}C$) or acetone (freezing point $-95^{\circ}C$) with liquid nitrogen and immersing the lower part of the helix matching assembly in the coolant. Irradiation has also been carried out at liquid nitrogen temperatures. The temperature

of the coolant has been measured in a number of ways; namely, by an alcohol or pentane thermometer or by a copper/constantan thermocouple. The latter was found to be the most satisfactory.

Both a high pressure mercury arc source (Mazda Type ME/D 250W) and a high pressure xenon arc source (Seimens Type XC 500W) have been used as radiation sources. The sources were either used unfiltered or with one of the the following filters: a glass plate, opaque at less than 3,000 Å; a Kodak Wratten Type 47 B Gelatine Filter passing 4,000 to 5,000 Å; a silver chloride filter at the same temperature as the crystal under irradiation. The AgCl filter is of particular value when the crystal surface rapidly becomes blackened, stopping further volume irradiation. It is important that the temperature should be near to that of the specimen for optimum irradiation due to the large variation in shape of the u.v. and optical fundamental absorption spectrum with temperature (Section 2.3.2).

5.3 Optical Measurements

All optical absorption measurements have been carried out on a Unicam SP 700 Dual Beam Spectrophotometer. The reference beam has been used without any reference crystal so that the output of the instrument is a direct measurement of the total absorption spectrum of the crystal. The absorption spectra have been observed at room temperature and at 77°K and an absorption cell has been constructed for operation at low temperatures. The polished crystal

facing page 129

figure 5.8

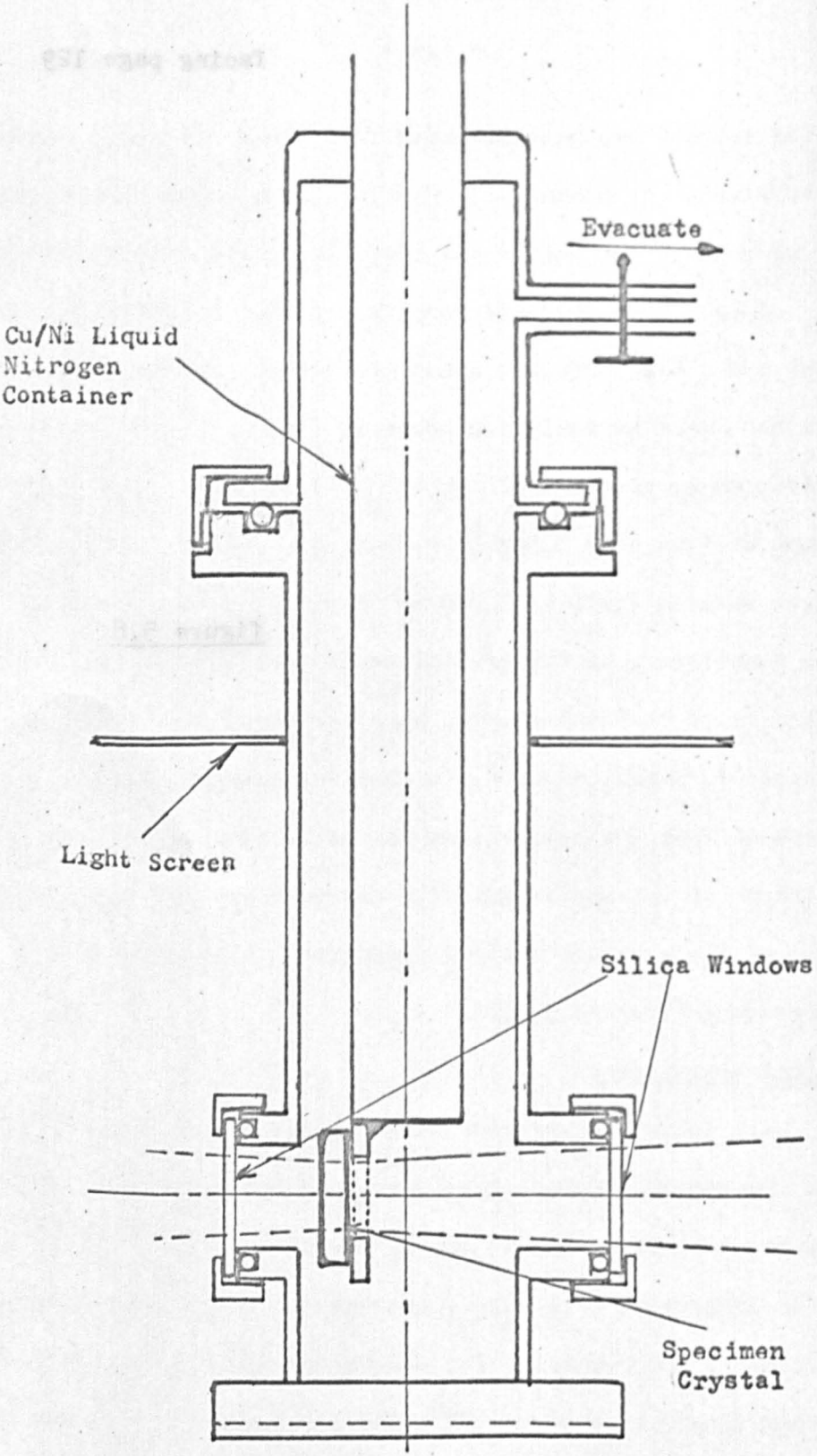

Figure 5.8

Diagram of Cell used in Low Temperature Experiments
(approximately to scale)

specimens were mounted in an evacuated dewar assembly with two silica windows to pass the light beam. Figure 5.8 shows this diagrammatically.

This chapter has been largely devoted to describing the use of a helix as a spectrometer absorption cell as there is little published work on this subject. Webb's application of Pierce's theory to an e.s.r. helix cell has been briefly described and ~~this is~~ extended to include the effect of a dielectric in the helix. Filling a helix with a dielectric only has a relatively small effect on the fields in the helix. The matching conditions are described qualitatively and more detailed information on this subject would be very useful.

The next chapter describes the preparation of the samples which have been used.

CHAPTER V - REFERENCES

1. G. Feher, Bell. Syst. Tech. J., 36, 449 (1957).

2. D.J.E. Ingram, "Free Radicals", Butterworths (1958).

3. H.A. Buckmaster and J.C. Dering, Can. J. Phys., 43, 1088 (1965); also J.C. Dering, Thesis, University of Alberta, Calgary (1964).

4. T.H. Wilmshurst, W.A. Gambling and D.J.E. Ingram, J. Elect. Control, 13, 339 (1962).

5. J.B. Payne, IEEE Trans. MTT, 12, 48 (1964).

6. J. Schmidt and I. Solomon, J.Appl. Phys., to be published.

7. A.J. Parker, D.C. Laine and D.J.E. Ingram, J. Sci. Instr., to be published.

8. R.V. Pound, Rev. Sci. Instr., 17, 490 (1946).

9. R.E. Richards and J.W. White, Proc. Roy. Soc., A 269, 287 (1962).

10. J.R. Pierce, Bell Syst. Tech. J., 29, 1 (1950), also published as "Travelling Wave Tubes", Van Nostrand (1950).

11. R.H. Webb, Rev. Sci. Instr., 33, 732 (1962).

12. J.R. Chamberlain, unpublished results.

CHAPTER VI

THE PREPARATION OF SILVER CHLORIDE

6.1 Introduction

Considerable difficulties were encountered in attempting to reproduce the results obtained in early experiments with silver chloride and bromide. It appeared that this was in part due to the low purity of the material being used and in part due to lack of experience in handling silver chloride, which has a number of unusual and awkward practical properties.

It was decided that the best course would be to follow the information available from workers (1 to 6) who are responsible for many of the results described in Chapter II. The techniques which are described in this chapter are derived from these references and the more difficult parts of the preparation are emphasised. Apparatus has been built to zone-refine silver chloride and bromide, particularly because the study of nominally pure crystals can, as is clear from Chapter II, be seriously disturbed by unknown impurities. All silver chloride which has been produced has been zone-refined, and the same mechanism has been used for crystal growing.

The procedure described is essentially the same for making silver bromide.

6.2 Chemical Preparation

Silver chloride is precipitated as a fine powder when silver nitrate and hydrochloric acid are mixed. Silver nitrate of spectro-

scopic purity has been used without further purification.* The reagent grade acid was fractionally distilled to give a constant boiling mixture and then re-distilled in a Fenski type of fractionating column. At all stages, doubly distilled and usually deionised water has been used. A normality for both solutions of weaker than N/5 should be used to give a fine precipitate. (With more concentrated solutions, when the precipitate is nearly dried, it tends to stick together in lumps making complete drying difficult). The solution in which the precipitation is carried out should contain an excess of acid and should be at a temperature of about 70°C.

The actual precipitation of AgCl has followed the conditions mentioned above. In order to produce a useful quantity of silver chloride, many litres of liquid must be handled. A well aged borosilicate flask (5 litre) was used, allowing the silver nitrate and hydrochloric acid to enter at about 50ml./min. into the already acid (N/10, say) contents of the flask with continuous stirring.

When precipitation is complete, the AgCl quickly settles and most of the liquid can be drained off. The AgCl is repeatedly washed, say ten times, stirring it up well with the water. (In the earlier washes this can be mildly acid, N/100 HCl).

---

* Eastman-Kodak Special Product Silver Nitrate X-491

Drying was achieved by first of all washing the AgCl into a sintered glass funnel (porosity 4), and then after filtering, the AgCl was slowly pumped dry. This was carried out by initially using a backing pump and finally, after about two days, using a diffusion pump and warming the AgCl up to about 150°C. Following this procedure, it is possible to prepare a reasonably free running powder.

Some of the silver chloride which has been used was bought as a powder to avoid the initial precipitation procedure.* This material was not nearly so finely divided and it could not be dried further. It probably contains about the same amount of transition metals - a few parts per million of the important impurities such as iron and copper.

The next step in preparation is the melting and "pinholing" of the AgCl. This is the most awkward part of the procedure partly because silver chloride can stick to its surrounding tube on solidification, causing the silica to shatter. The latter problem has largely been avoided by always melting the AgCl in an atmosphere of chlorine. (Silver oxide and silver are largely responsible for the sticking).

6.3 Melting

As the melting point of silver chloride is at 450°C, it was found necessary to melt it in a silica container. It was clear from

---

* Johnson-Matthey "Specpure" Silver Chloride JM-58.

facing page 134

figure 6.1

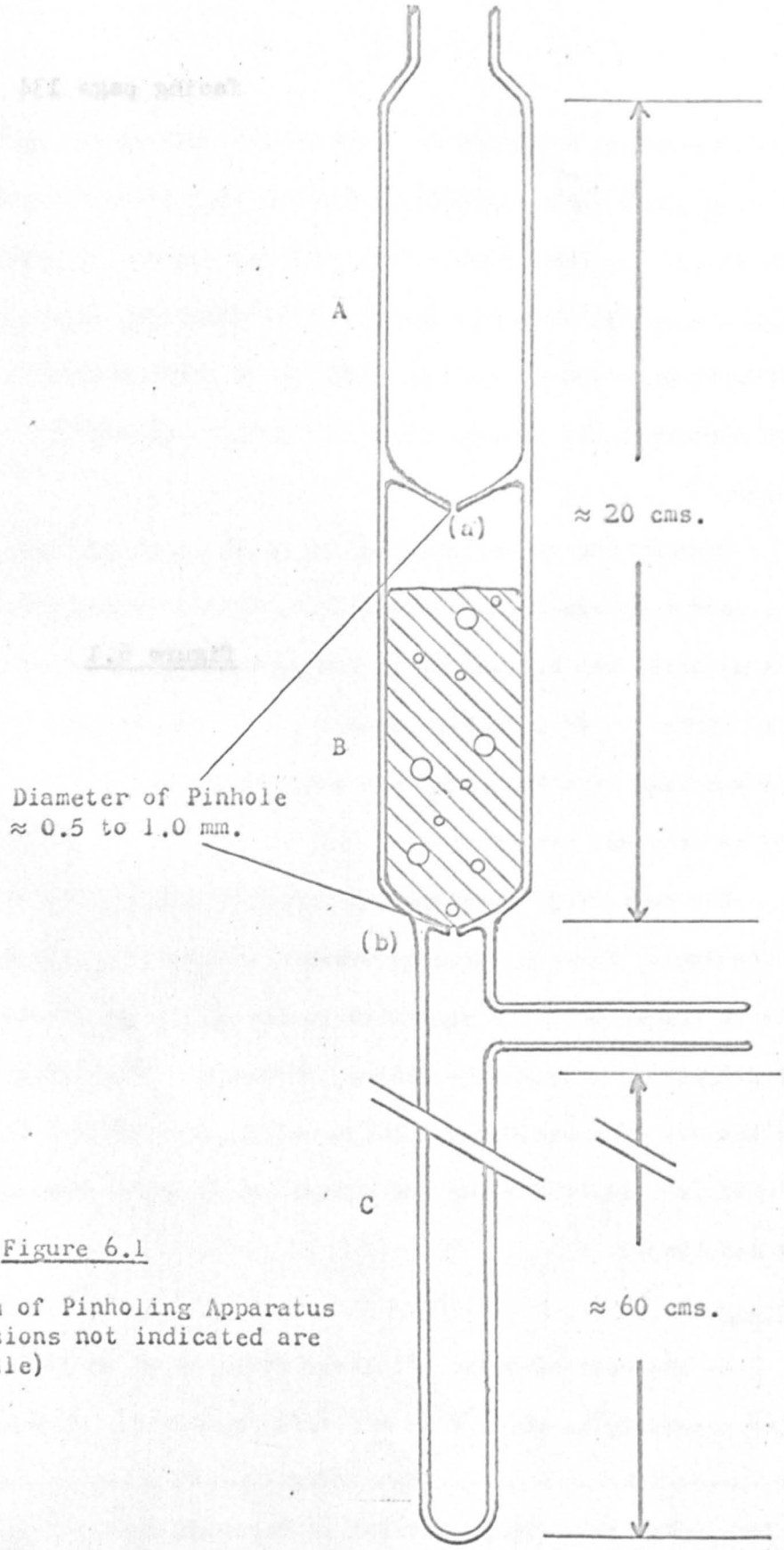

Figure 6.1

Diagram of Pinholing Apparatus
(dimensions not indicated are
to scale)

an early attempt that borosilicate (Pyrex) glass is very "dirty" at such temperatures. An additional advantage in using silica is its much greater mechanical strength.

The "pinholing" apparatus was a simplified version of that originally described by Mitchell (1) and is shown in Figure 6.1. Ordinary quality (Thermal Syndicate) silica tubing has been used and typical dimensions are indicated. (The bore of the lower tube is of importance as will be seen in the next section.)

The upper compartment A is first of all packed with the AgCl powder and an atmosphere of chlorine is substituted. The silver chloride is now melted using a gas torch with a large flame, which is more convenient and flexible than a furnace as it allows the state of the contents to be examined. When all the AgCl has been melted, it can be run through the "pinhole" (a) to solidify immediately in compartment B. A black debris is left behind on the wall of compartment A. This is mainly silver and silver oxide and the pinholing constitutes a very useful part of the purification.

When the AgCl, now in B, has been remelted* and chlorine gas has been bubbled through it for about 30 minutes, it is finally

---

* It may be worth bubbling oxygen through the AgCl at this stage or at the corresponding stage in A, in an attempt to oxidize any iron impurity. The oxide is virtually insoluble in AgCl and would be left behind on the wall.

facing page 135

figure 6.2

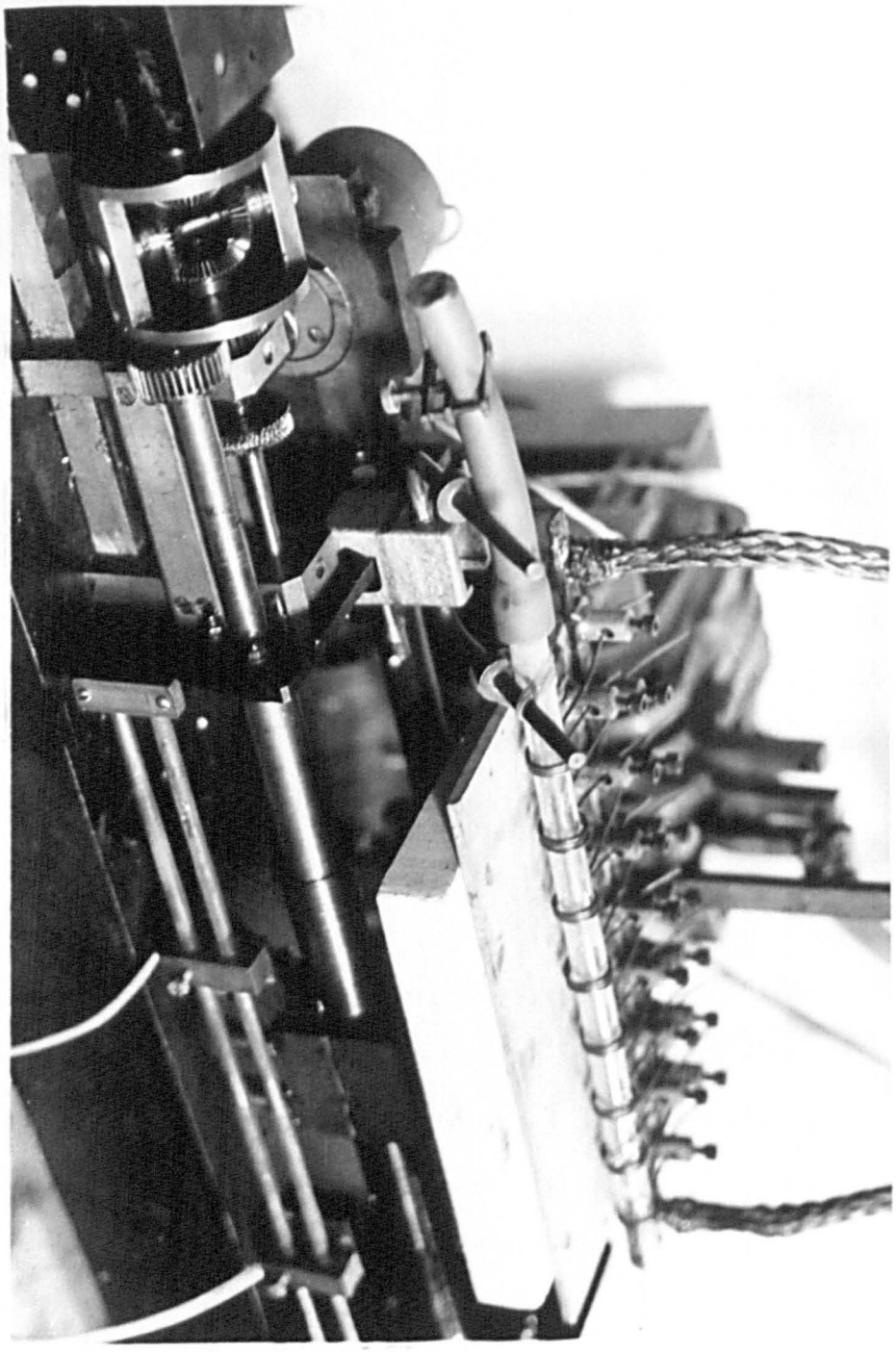

Figure 6.2

Zone-Refiner.

pinholed into C. A very small amount of impurity is left on the wall of B.

As the AgCl pours into C it must be kept molten and only allowed to solidify slowly from the bottom.* This cast cylinder of silver chloride is now ready for zone-refining after extraction from the silica tubing.

The process described in this section removes virtually all insoluble impurities (most of them are introduced in the precipitation) The zone-refining described in the next section reduces the concentration of soluble impurities such as transition metal ions.

6.4 Zone-Refining

The principles of zone-refining are well known and are described in Pfann's book (7). The application of this technique to the purification of silver chloride is described in reference 4.

The apparatus shown in Figure 6.2 was built to allow vertical as well as horizontal zone-refining. The latter must be used for the silver halides. It was used very successfully in a vertical position to zone-refine naphthalene and similar chemicals as the conditions for refining such compounds with complex structures are not nearly as strict as for refining simple lattices such as AgCl.

---

* Remelting of the AgCl at this stage would almost certainly cause the tube to shatter as AgCl expands substantially before it melts and by a few percent on melting.

The distribution coefficients were measured by Moser, Burnham and Tippins (4) for a number of important impurities in AgCl and these are shown in Table 6.1. The distribution coefficient is the ratio of the solubility of an impurity in the host when liquid, to the solubility in the solid.

Table 6.1

Halide	Impurity	Atmosphere	Distribution Coefficient
AgCl	Cu	Cl_2 or vacuum	0.4 - 0.6
AgCl	Pb	Cl_2 or vacuum	0.4
AgCl	Ni	Cl_2 or vacuum	1.4
AgCl	Fe	Cl_2	≈0.7
AgCl	Fe, Mn, Cd	Vacuum	> 1
AgCl	Sn, Al, Sr	Vacuum	< 1
AgBr	Cu	Vacuum	< 1
AgBr	Fe, Ni, Mn	Vacuum	> 1

In the case of crystal structures made up of large molecules this coefficient is usually much greater than unity which means that refining is simply and effectively achieved. As can be seen from the table above, this is not true in materials such as silver chloride, but as long as a large number of "zone passes" with short molten zones can be passed through a sample, very useful purification can be obtained. The case of iron with refining under chlorine, is

of particular interest as the iron is more soluble in the solid; this is presumably due to the presence of the stable $(FeCl_4)^-$ complex, which fits well in the lattice. It is not possible to remove iron very effectively by zone-refining, even in a practical "ultimate" distribution and it is for this reason that it must be taken account of in many experiments with nominally pure AgCl.

Silver chloride must be zone-refined horizontally because of the expansion and sticking problems. It is necessary to tilt the refiner to avoid transport after many passes due to the expansion when one end is melted and the contraction when the zone leaves the other end. The necessary angle of tilt depends on the expansion and on the surface tension of the liquid and is found empirically to be about 6^o to the horizontal.

The details of the actual refining are as follows. About 9 inches of the 9mm AgCl bar prepared as described in the last section is placed in a well cleaned 1cm. bore silica tube. This tube has one end closed, with a further piece of silica attached at this end as a support. The silver chloride is melted to fill about 80% of the cross section of the tube, care being taken to restrict the unsupported end of the AgCl by tipping the tube. It is essential that the AgCl should be allowed to freeze rapidly as the remelting prior to zone-refining can easily shatter the tube.

The eight heaters are each made from three turns of 0.062" diameter "0" grade nickel wire, supported simply by the terminals.

The heaters are mounted in parallel, drawing about 300 amps at 2 volts from a welding transofrmer. The input to the transformer is fed from a "Variac" and the end heaters in particular are shielded from draughts by a box of asbestos paper. The heaters are 1¼ inches apart and a zone length of 3/16" to ½" can be maintained at refining speeds of up to 1.5" per hour. The heater carriage is driven on a lead-screw, from a reduction gear-box followed by a differential gearbox. The initial drive is taken from a "Velodyne" type 74 motor-generator. The generator provides a d.c. output proportional to its shaft speed and after comparison with a reference voltage, this output is fed through a servo-circuit to control the motor armature current. By this means, a stable, reproducible and continuously variable range of output speeds between 50 and 11,000 r.p.m. is available by varying the reference voltage. This range is of great use as zone-refining has been possible at speeds of up to 3"/hour. Using a different furnace crystals have been grown at 0.05"/hour (more usually 2mm.(0.08")/hour).

Usually 80 to 100 zones have been passed along the silver chloride bar. Great care must be taken to avoid the AgCl "bridging" the full section of the tube. This is especially important at the starting end as remelting would almost certainly shatter the tube. This number of zone-passes should be sufficient for a nearly optimum impurity distribution.

facing page 139

figure 6.3

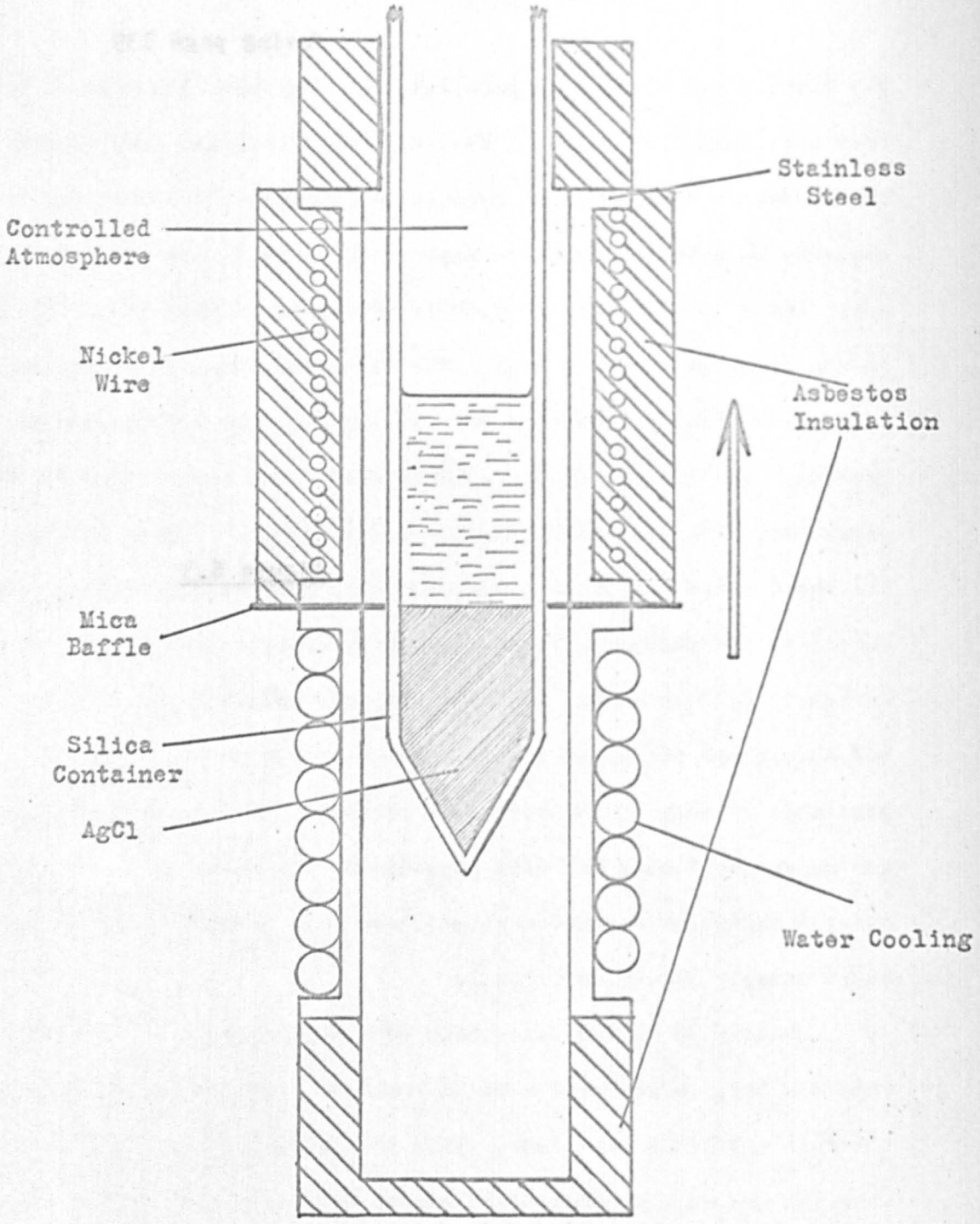

Figure 6.3

Diagram of Bridgman-Stockbarger Furnace
(twice actual size)

After zone-refining, both ends of the AgCl show some colouring. The zone starting end is yellowish brown (typical of iron) and the finishing end, after some irradiation, is a blue colour typical of silver colloid. This indicates the presence of copper among other things (2.4.5a). The central portion is not at all photosensitive and about 33 to 50% of the total bar has been selected for further use.

It has not been possible to have the purity of the silver chloride spectroscopically analysed but it is reasonable to assume that there is less than 1 part in 10^7 of all impurities. The sensitivity of the e.s.r. spectrometer is such as to be able to detect certainly less that 1 part in 10^6 of certain specified impurities (e.g. Fe^{3+}, Cu^{2+}, Mn^{2+}). The limit may be as low as 1 part in 10^7 for cubic Fe^{3+}. It is important to grow crystals in high purity quartz containers as is explained in the next section.

6.5 Crystal Doping and Growing

The crystals used in all the experiments were grown in a silica tube, drawn out to a point, as container and using the Bridgman-Stockbarger technique. The arrangement is shown in Figure 6.3. The upper furnace was set nominally at 500°C and the lower was water cooled. The temperature of the solidified material was much higher than this, about 350°C. This could be seen from the yellowish colour of the crystal which is a result of the extension of the long-wave tail of the fundamental u.v. absorption well into

the optical region at high temperatures. Using this procedure, quite good single crystals have been grown, usually under a pressure of about 20cm Hg of chlorine.

Doping of most crystals has been carried out by adding about 1 to 2 parts in 10^4 molar, of the impurity as the anhydrous metal chloride before melting the silver chloride. Ferric chloride was separated from the hydrated form by fractional sublimation, and both ferrous chloride and auric chloride were prepared by pumping and heating the hydrated ferrous chloride and chloroauric acid respectively. The effect of water attached to the iron chlorides is that they oxidize when melted with the silver chloride, but with care this can be avoided.

Crystals with 1 part in 10^5 of impurity were doped by mixing 10% of a previously doped 1 : 10^4 crystal with pure silver chloride.

About 1 ppm of iron was found to be present in gold doped and nominally pure crystals. The source of this was eventually found to be the silica tubing used in the furnace. High purity quartz tubing was subsequently used and this gave no trouble. On one occasion a "pure" crystal was grown in a tube that had previously been used to grow a gold doped crystal. The pure crystal showed the characteristics of a gold doped crystal. For this reason all tubing has been used once only.

All zone-refining has been carried out using ordinary quality tubing with no apparent introduction of impurity. This must be a

result of "ageing" of the silica in the early stages of the refining and the subsequent extraction of the introduced impurity later in the process. Clearly, in the future high purity tubing must be used for zone-refining as well as for crystal growing, as the final purity must be affected.

6.6 Crystal Cutting and Handling

Handling crystals of the silver halides introduces many problems. Dislocations are remarkably unstable and it is probably nearly impossible to cut the crystal without causing severe mechanical damage. (Bending a crystal of silver chloride requires little effort and ~~the effect~~ this bending is quite plastic until it hardens and can then be broken).

In general, crystals have been cut using a fine stainless steel saw lubricated with xylene. About 0.5mm. is then removed from the cut surface using a very fine "wet and dry" carborundum paper (600 grade) with distilled water as lubricant and finally the crystals are etched in a 3N hypo (sodium thiosulphate) solution to remove a further 0.5mm. Provided the initial surface of the crystal is clean and free from grease, and the hypo is continuously agitated, this method is satisfactory for crystal preparation. Other workers have found it necessary to use cyanide solutions to etch samples for optical work, but polishing in hypo has been quite satisfactory.

6.7 Methods of Crystal Orientation

Silver halides are mechanically very isotropic. They do not cleave and because of the cubic structure, do not exhibit any

directional properties as far as distortion or polarization are concerned. A few seconds etch in hypo produces etch pits on the crystal surface but it has been much simpler to find the crystal orientation to a first approximation by growing epitaxial NaCl crystals on the surface. After this stage, two methods have been used for more detailed information regarding the crystal axes.

(a) Crystals have been mounted in the oscillating camera of a X-ray goniometer*, a back-reflection method being used, and it was found possible to cut the crystal to within one degree of the measured axes, the final adjustment being possible in the e.s.r. spectrometer by inclining the helix and dewar by as much as 3^{o} to the magnetic field.

(b) In iron doped crystals, the relatively simple anisotropic fine structure of the $(FeCl_4)^-$ spectrum was latterly used to find the crystal axes. Adjustments normal to the axis of the coaxial line leading to the helix were made by bending the helix by up to 30^{o} from normal to the field direction. Where it has been possible, this procedure has been used, as it is much more straightforward than the X-ray method.

All crystals have been cut so that they are rotated about a crystallographic (110) axis, the field direction lies in the plane normal to this axis and allows the observation of spectra along

---

* Philips Type PW 1009/25 Generator with a Nonius-Weissenberg camera

(100), (110) and (111) axes, without disturbing the crystal.

It has been found that wandering of the crystal axis can cause appreciable problems. It has been possible to estimate this wander to be as much as 5^{o} in some iron doped crystals, by examining the loss of spectral resolution in certain directions. It has usually been found possible to find crystals with the axis defined to better than 1^{o}. Examining the anisotropy of spectral resolution of the $(FeCl_4)^-$ spectrum it is possible to distinguish between a lot of small variations in crystal axis and a small degree of "twinning".

The reason for the failure to orient the gold doped crystals is probably a result of the superposition of a number of spectra from sub-crystals with a few degrees variation in axis.

CHAPTER VI - REFERENCES

1. P.V.Mc D. Clark and J.W. Mitchell, J. Photo. Sci., 4, 1 (1956).

2. N.R. Nail, F. Moser, P.E. Goddard and F. Urbach, Rev. Sci. Instr., 28, 275 (1957).

3. F.C. Brown, J. Phys. Chem. Solids, 4, 206 (1958).

4. F. Moser, D.C. Burnham and H.H. Tippins, J. Appl. Phys., 32, 48 (1961).

5. L. Slifkin, private discussion.

6. F.C. Brown, private discussion.

7. W. Pfann, "Zone Melting", Wiley (1958).

CHAPTER VII

RESULTS OF E.S.R. STUDIES IN SILVER CHLORIDE

The measurements which are described in this thesis are principally concerned with the properties of iron as an impurity in silver chloride. A brief description will also be given of some observations on crystals of AgCl:Au and AgCl:Mn.

Attempts to observe e.s.r. signals in pure, undoped silver chloride or bromide have been unsuccessful; in general, these experiments set out to find if a high temperature oxidizing or reducing anneal followed by slow cooling or quenching could produce paramagnetic centres. The irradiation of crystals with different histories at temperatures between $300^{\circ}K$ and $77^{\circ}K$ was also investigated. The only signals which have been observed are due to small traces of Fe^{3+} or Cu^{2+} impurity under conditions when these would be the expected valencies. The sensitivity of the spectrometer is difficult to calibrate when using a helix with silver chloride crystals because of their large dielectric constant. Less than 1 ppm of Fe^{3+} or Cu^{2+} should be very easily detectable. If the amount of iron present in doped crystals has been correctly estimated, the limit of detection for Fe^{3+} is probably in the region of 0.1 ppm.

facing page 146

figure 7.1

7.1 E.S.R. Spectra of Fe^{3+} in Silver Chloride

(a) Cubic $(FeCl_4)^-$ Complex

The cubic spectrum of trivalent iron in silver chloride which has been mentioned in section 2.4.5(b) has been produced under different conditions which are described in 7.2. The analysis of this spectrum has been published by Hayes, Pilbrow and Slifkin (1) and the parameters describing it are given in table 2.3. The parameters fit a spin Hamiltonian of the form

$$\mathcal{H}_s = g\beta \underline{H}.\underline{S} + \frac{a}{6}(S_\xi^4 + S_\eta^4 + S_\zeta^4 - \frac{1}{5}S(S+1)(3S^2+3S-1) + \sum_n [AS_zI_z^n + B(S_xI_x^n + S_yI_y^n) + P(I_z^{n\,2} - \frac{1}{3}I^n(I^n+1)) - g\beta_N \underline{H}.\underline{I}^n] \qquad 7.1$$

which is a combination of the terms 4.16, 17 and 19. ξ, η and ζ are the cube axes which coincide with the crystallographic <100> axes. Measurement of the g and a parameters at 20°K and at 77°K yielded the following values:

$$g = 2.0158 \pm 0.001; \qquad a = 75.2 \pm 0.7 \times 10^{-4}\,cm^{-1}$$

The $H_{1,5}$ [$|\mp 3/2\rangle \rightleftarrows |\pm 5/2\rangle$] and $H_{4,2}$[$|\mp \tfrac{1}{2}\rangle \leftrightarrows |\mp 3/2\rangle$] transitions are well resolved along the <100> cubic axes but only partially resolved along a <111> axis of the cube. Otherwise the two pairs of fine structure lines coincide sufficiently to produce a pair of distorted lines. Figure 7.1 shows the <100> and <111> spectra with the partially resolved extrahyperfine structure on the

$H_3[\ |-\tfrac{1}{2}\rangle \rightarrow |+\tfrac{1}{2}\rangle]$ transition. The angular variation of the fine structure is as would be expected for the cubic term. (The expression for the a term specified relative to the magnetic field (z) axis is given in Appendix II, also references 2 and 3).

A detailed analysis of the partially resolved extrahyperfine structure on the $|-\tfrac{1}{2}\rangle \rightarrow |+\tfrac{1}{2}\rangle$ transition was not carried out owing to the publication of Hayes' results. Garth's much more accurate ENDOR results should provide a more reliable set of parameters (4). A careful check was made to ascertain that the extrahyperfine structure corresponded with that of Hayes' results. It was not possible to detect any difference between the spectra so it is safe to conclude that they originate from the same centre.

One interesting characteristic of the resonance which has not been mentioned in any of the publications (1,4, 5) is that the degree of hyperfine resolution of the central line is slightly anisotropic, the resolution being poorer on the low field side. The resolution of the spectrum is ~~very susceptible to~~ reduced by saturation broadening; at 77^{o}K the microwave power at the helix must be below about -5db (approximately 1 watt at the helix is 0db) and at 20^{o}K below about -25db.

The overall resolution of the fine and hyperfine e.s.r. spectrum has been found to be very dependent on the particular crystal and it has proved very useful to examine the spectra carefully

as this provides information regarding the degree of crystal perfection (section 6.7) The best crystals show considerably better resolution than the published results (1, 4, 5).

This spectrum will be referred to as spectrum A.

(b) The Trigonal $(FeCl_4)^-$ Complex

In the investigations into the formation of spectrum A during irradiation, a new trivalent iron spectrum has been observed. This spectrum (B) is produced by irradiating certain crystals at about - 105°C and is unstable above - 75°C. The specific thermal characteristics are described in 7.2.

The best resolved version of spectrum B has a background of spectrum A and there is also another spectrum (C) superimposed which it has not yet been possible to analyse. Despite serious attempts to include ~~it~~ C in an analysis of B, it has not been possible to take it into account. Typically, the splittings of C are in the region of three times greater than B and what is possibly the central line is proportionately more anisotropic. The overall intensity is probably between five and ten times below that of B, and the behaviour of the spectrum C within a region of up to about 650 gauss on each side of g = 2, depending on the orientation, is obscured by up to 14 lines of B, and 5 of A. In the discussion of the origin of B in the following chapter, it is pointed out that some other distorted complexes may exist under conditions favourable to the formation of B.

Two properties of C are worth noting: the line widths of the absorption are comparable with A and B and the spectrum is approximately distributed about g = 2, which might imply that it is basically a high spin Fe^{3+} resonance. The saturation may be slightly greater under similar conditions. Spectrum C has only been seen in one crystal, but this was considerably more perfect than the others in which B was examined; the larger splittings of C will make the spectrum more susceptible to line broadening by variations in the crystal axes and it is thus not certain that C did not exist in the other crystals.

It has been possible to fit spectrum B to a first order using a spin Hamiltonian $\mathcal{H}_s$ given by

$$\begin{aligned}\mathcal{H}_s = g\beta\, \underline{H}.\underline{S} + \frac{a}{6}\left[S_\xi^4 + S_\eta^4 + S_\zeta^4 - \frac{1}{5}S(S+1)(3S^2+3S-1)\right] \\ + D\left(S_1^2 - \frac{1}{3}S(S+1)\right) + \frac{F}{180}\left(35S_1^4 - 30\,S(S+1)S_1^2\right. \\ \left. + 25S_1^2 - 6S(S+1) + 3S^2(S+1)^2\right) \qquad 7.2\end{aligned}$$

where the axis (1) is the axis of distortion and the term in F takes account of possible fourth order effects from the distortion. The maximum splitting from g = 2 is along a <111> axis and is in the region of 650 gauss, so that an examination of $\mathcal{H}_s$ for various directions of magnetic field and distortion to the cube axis implies to first order that the most important term is $g\beta\underline{H}.\underline{S}$ which should be diagonalized and that the other terms should be specified relative to the $\underline{H}$ axis where $H \parallel z$. The result of this transformation is given in Appendix II.

facing page 150

figure 7.2

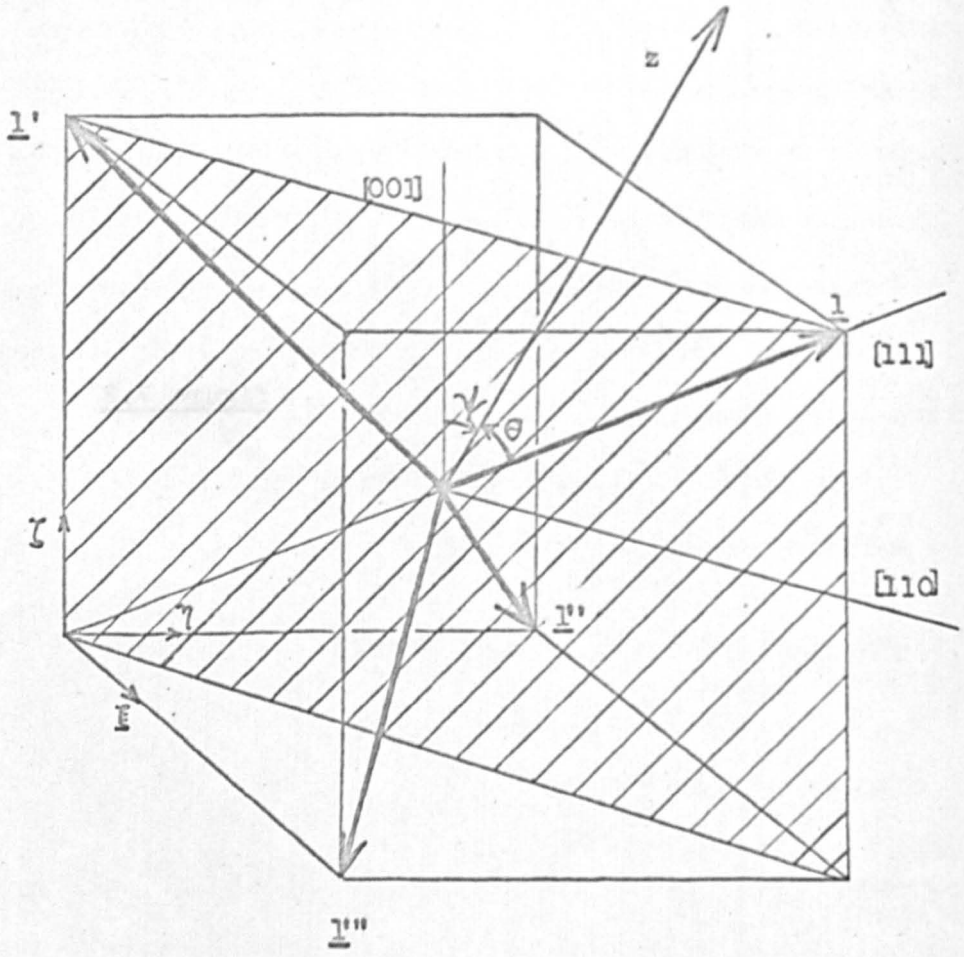

Figure 7.2

Cubic and Trigonal Coordinates

For any given orientation of a complex, five transitions are observed at the magnetic fields:

$$H_{1,5} : \left|\pm\tfrac{3}{2}\right> \rightleftarrows \left|\pm\tfrac{5}{2}\right>; \quad H_{2,4} : \left|\pm\tfrac{1}{2}\right> \rightleftarrows \left|\pm\tfrac{3}{2}\right>; \quad H_3 = \left|-\tfrac{1}{2}\right> \rightarrow \left|+\tfrac{1}{2}\right>$$

The angular variation and the "off-diagonal" corrections to these are necessary to examine the detailed fitting of the spectrum B. The equations which are given for the splittings reduce to those quoted by various authors for specific cases (e.g. references 2 to 5 of Appendix II).

The possible relationships between the $\underline{1}$ axis and the cube axes ξ, η, ζ have been studied in detail and only one possibility has been found which shows any agreement with the experimental data. This is with the cubic axes coinciding with the crystallographic axes and the trigonal (or tetragonal) axis coinciding with a crystallographic <111> axis. This arrangement is shown in Figure 7.2. There are four possible orientations of the trigonal axis within the cube, and as the AgCl crystal has cubic symmetry (NaCl structure), all of these must be equally possible. For an arbitrary orientation of the magnetic field relative to the axes, there will in general be four separate spectra of five lines each. By restricting the magnetic field to a crystallographic {110} plane (shaded in Figure 7.2) the $\underline{1}''$ and $\underline{1}'''$ axes are equivalent and so the spectra associated with distortions along these axes coincide.

facing page 151

figure 7.3a

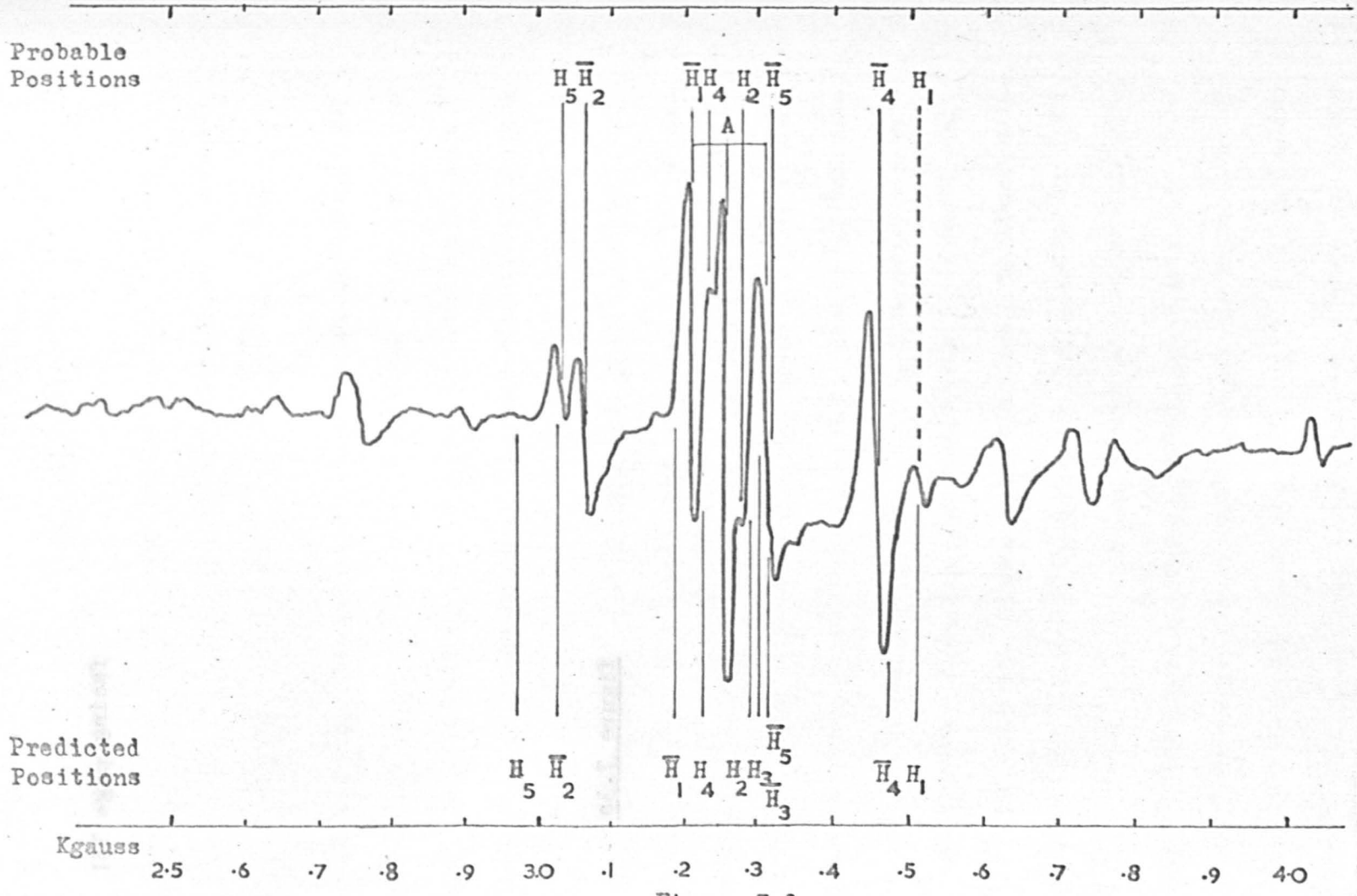

Figure 7.3a

Trigonal $(FeCl_4)^-$ Spectrum H∥110, 20°K. Lines not assigned belong to spectrum C.

facing page 151

figure 7.3b

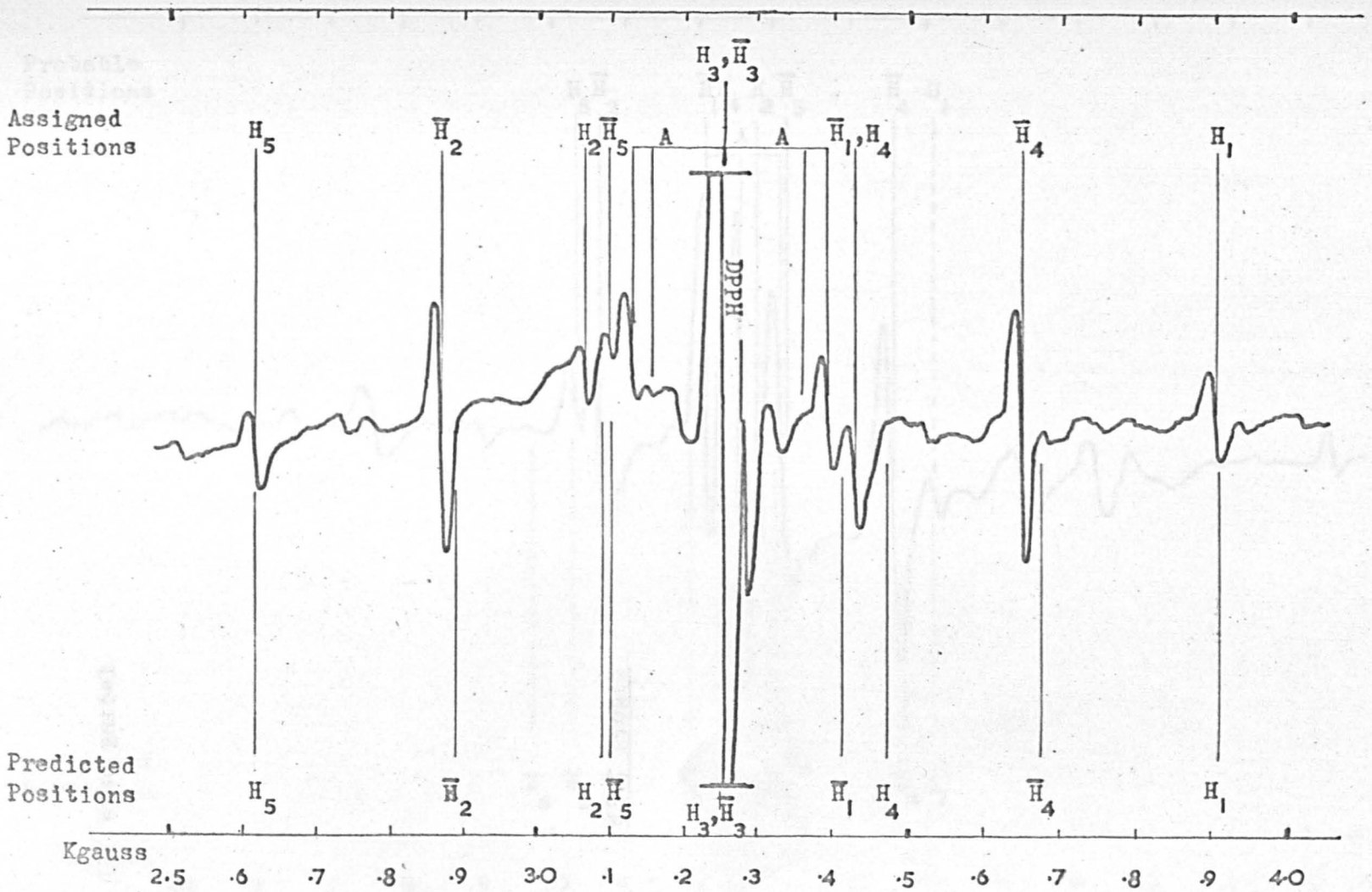

Figure 7.3b

Trigonal $(FeCl_4)^-$ Spectrum H‖111, 20°K. Lines not assigned belong to spectrum C.

Considering the three high symmetry directions in this $(\bar{1}10)$ plane, when z is parallel to ζ, [001] all distortions are indistinguishable and there should be a single spectrum. In practice the crystals have either not been sufficiently perfect or have been incorrectly aligned as the spectrum has not been simply resolved. This is not surprising as an examination of the angular variations shows the coincidence of the spectra from near-equivalent sites to be very sensitive to orientation. For $H \| [110]$ the axes $\underline{1}$ and $\underline{1}'$ are indistinguishable, but detailed assignment of the lines (Figure 7.3(a)) has only followed a detailed assignment of the $H \| [111]$ spectrum. When H is parallel to $\underline{1}$ ([111]) the $\underline{1}'$, $\underline{1}''$ and $\underline{1}'''$ axes are all equivalent and it has been possible to fit the spin Hamiltonian 7.2 to this spectrum (Figure 7.3(b)) by measuring the splittings $W_{1,5} = H_1 - H_5$ and $W_{2,4} = H_2 - H_4$ for both sets of spectra. The following parameters (in units of 10^{-4} cm^{-1}) fit these splittings to within 3 gauss provided the difference in "off-diagonal" terms in AII.7 is taken into account:

$20^{\circ}K$: a = (+) 187.0 $\pm$ 1, D = (-) 81.3 $\pm$ 1; F = (-) 6.3 $\pm$ 1

$77^{\circ}K$: a = (+) 181.0 $\pm$ 2; D = (-) 79.0 $\pm$ 2; F = (-) 4.0 $\pm$ 2

where g is assumed = 2.0063 (see below) and a is assumed positive.

Using these parameters and predicting the splittings for the $H \| \langle 110 \rangle$ spectrum, produces a fit for the splittings $W_{1,5}$ and $W_{2,4}$ for the two spectra to within about 8 gauss. The behaviour and

position of the <100> spectrum mentioned above is also in agreement with this assignment of parameters.

The angular variation of spectrum B has been studied in some detail and again, provided the splittings $W_{1,5}$ and $W_{2,4}$ are measured, splittings can be found to fit the predicted variation for most angles. This is not shown graphically owing to the difficulties associated with separating B from the spectrum C with any degree of certainty.

Care has been taken in the preceeding discussion to restrict the fitting to the difference in field between pairs of lines. If the absolute positions of the lines are studied, there are a series of errors between the measured and the calculated values which are often larger than 20 gauss. These discrepancies can be seen in Figure 7.3 where the assignment of lines has been put above the spectrum and the calculated positions are shown below. The notation used is as follows: for the [111] spectrum (Figure 7.3(b)) with $z \| \underline{1}$, spectra for the distortion $\underline{1}$ are H_1, H_2 etc; for the equivalent distortions $\underline{1}'$, $\underline{1}''$, $\underline{1}'''$, the lines are at $\bar{H}_1$, $\bar{H}_2$ etc. For Figure 7.3(a) ($z \| [110]$), the indistinguishable distortions $\underline{1}$ and $\underline{1}'$ lead to spectra H_1, H_2 etc. and the distortions $\underline{1}''$ and $\underline{1}'''$ give the spectra $\bar{H}_1$, $\bar{H}_2$ etc. Some of the assignments of the [110] spectrum are tentative.

It is not easy to check the relative intensities of the absorption lines. For the [111] spectrum the intensities of the nine

lines should be in the following ratios(6).

$$H_{1,5} : H_{2,4} : \bar{H}_{1,5} : \bar{H}_{2,4} : H_3 + \bar{H}_3 = 5 : 8 : 15 : 24 : 36$$

Apparently the $H_{1,5}$ lines are too intense by a factor of about 2 compared with the $\bar{H}_{2,4}$ lines. This could be because of lines of C superimposed on the $H_{1,5}$ lines or because the $\bar{H}$ lines would be more susceptible to small distortions caused by local defects. Examination of the spectrum under conditions of saturation indicates better agreement and the first explanation might be preferred. The ratios $H_{1,5} : H_{2,4}$ and $\bar{H}_{1,5} : \bar{H}_{2,4}$ are correct to within about 10% which is the best assessment which can be made.

The discrepancies in the fitting of the spin Hamiltonian 7.2 are discussed in Chapter VIII. The inclusion of a rhombic term $E(S_2^2 - S_3^2)$ (AII.1 and 4) is of no value in improving the agreement. Its affect on the $H_{1, 2, ---}$ transitions would be small for $H \| \underline{1}$, but it would cause a further splitting of each of the $\bar{H}$ lines owing to the reduced symmetry; this is not observed. Including the rhombic term in a more general manner does not produce any arrangement which can explain the measured spectrum.

The spin Hamiltonian AII.1 contains all possible terms to fourth order which are even in the components of the spin operators.

The g- value of spectrum B cannot be calculated because the deviations in the spectrum are effectively deviations in the g-value

of individual pairs of lines and it is quite arbitrary which set is chosen to calculate the g-value. In the calculations of the predicted line positions, it was assumed that the $\bar{H}_3 + H_3$ ([111]) line, with its off-diagonal correction gave the g-value. This value is:

$$g = 2.0063 \pm 0.001$$

where the error is due to error in measurement of the H_3 line. The actual g-value is probably substantially different from this. There is no evidence to suggest that the g-value is anisotropic; this would not explain the discrepancies in the results.

(c) Other Spectra

A number of other spectra have been found which are in some way associated with the spectra A and B. It is not possible to offer a reliable explanation of any of them, principally because the conditions under which they are formed are not altogether clear and it is not possible to ~~reliably~~ reliably reproduce the results. On the other hand, in the discussion in the following chapter concerning the formation and decay of A and B, it appears to be possible that other complexes may exist under particular conditions, so it is of value to indicate generally the spectra which sometimes occur.

These spectra can be divided into two categories:

(i) Unstable spectra associated with the rapid warming of crystals which have been irradiated below about $-75^{\circ}C$, (ii) Stable spectra associated with the decay of A at room temperature.

(i) D

In a number of samples, particularly following irradiation at temperatures below -75°C, and rapid warming to about -40°C, a resonance with an isotropic g-value of 4.3 and a very distorted line shape has been found. This spectrum has usually occurred during other experiments and the conditions for formation mentioned above appear to be a common factor, although it has not been possible to reproduce the spectrum by trying to repeat these conditions. The speed of warming and the end temperature may be very important; bearing this in mind a possible explanation is offered in Chapter VIII.

The intensity of the resonance would correspond to about 1 part in 10^5 of the complex for the specimen with the largest signal. Spectrum D quite often occurs with a magnitude not much above the limit of detection during the formation of the $(FeCl_4)^-$ centre (A).

An identical absorption has been observed by Castner et al. (7) for Fe^{3+} in glasses and more recently by a number of other workers (8). It can be explained by assuming a $^6S_{5/2}$ ground state with a spin Hamiltonian in which D = 0 and $E >> g\beta H$ (7). The effect of E is to split the sextet into three doublets with the energies $W = 0, \pm 2\sqrt{7}\,E$ and the magnetic field splits the W = 0 level with an isotropic g-value of 4.286. The other levels are very anisotropic with three principal g-values of 9.678, 0.857 and 0.607. The samples in which a strong 4.3 resonance was observed were not sufficiently well oriented and were probably too imperfect to detect

these transitions. The basically tetrahedral model for this centre which was suggested by Castner fits very well into the silver halide lattice (Chapter VIII).

This spectrum is known as spectrum D.

E

On two occasions, when the spectrum D was allowed to decay by warming the crystal to about $-30^{\circ}C$ for a few minutes, another spectrum (E) has been found. This is also very unstable and warming above about $-20^{\circ}C$, even very briefly, causes the spectrum to disappear. It has not been possible to reproduce this spectrum and measurements have not been made as the crystal orientation in the particular samples was unknown. The absorption was a single line about 100 gauss wide and its g-value varied between about 2.0 and 2.5 depending on the orientation. More information would be needed about the conditions of formation and the parameters for this centre before an explanation could be attempted.

(ii) F

Crystals containing in the region of 1 part in 10^4 molar of iron exhibit a wide isotropic resonance after substantial irradiation at room temperature, or after the spectrum A has been produced and allowed to decay a number of times at room temperature. The g-value of this spectrum is 2.35 ± 0.02 and the linewidth (between points of maximum slope) is about 300 gauss. The spectrum disappears when the crystal is annealed in chlorine at about $400^{\circ}C$, and slowly cooled.

facing page 157

figure 7.4

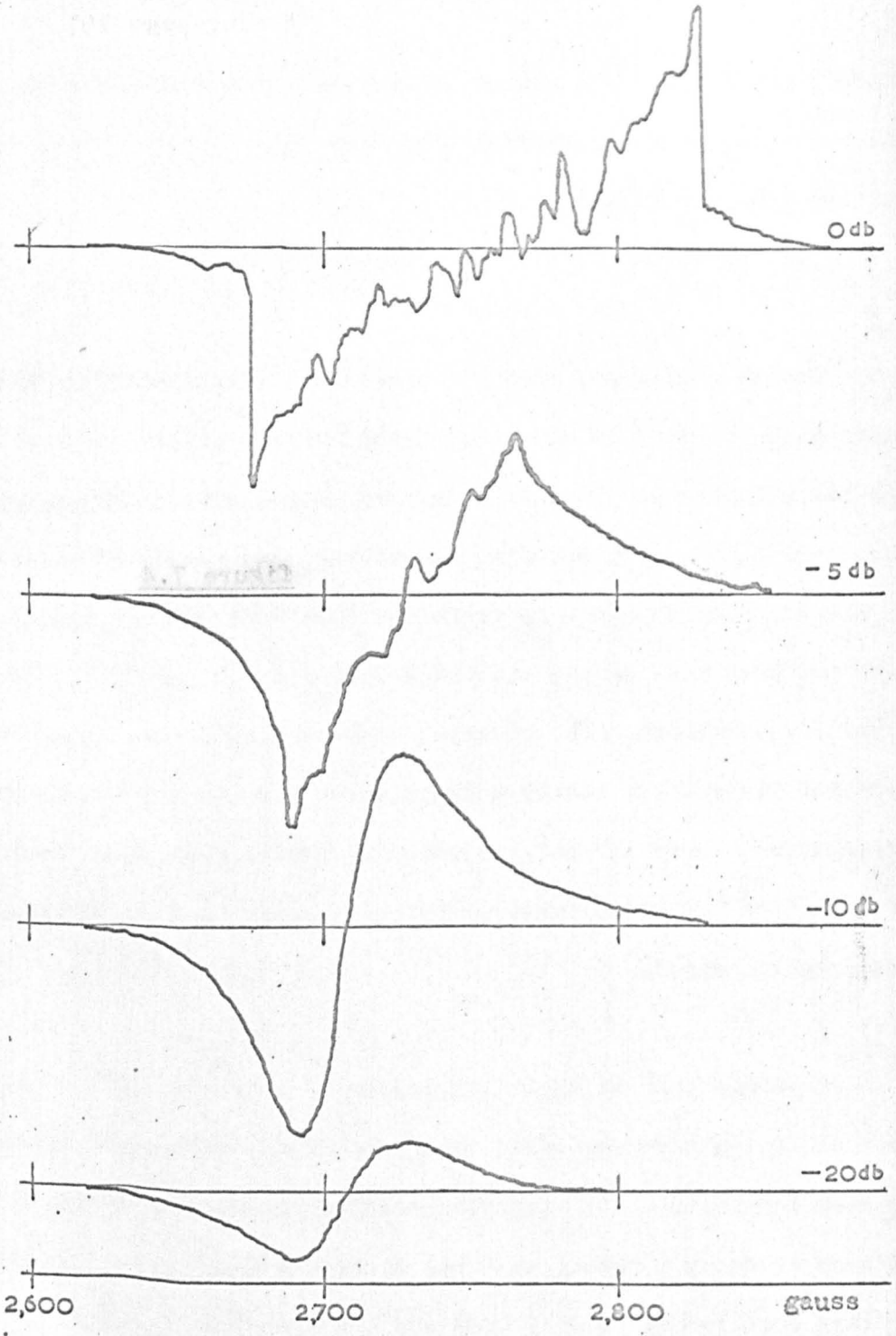

Figure 7.4

Saturation of spectrum G (derivative),
only incident power is varied (ν= 9.19Gc/s.H 110, T = 77°K)

facing page 157

figure 7.5

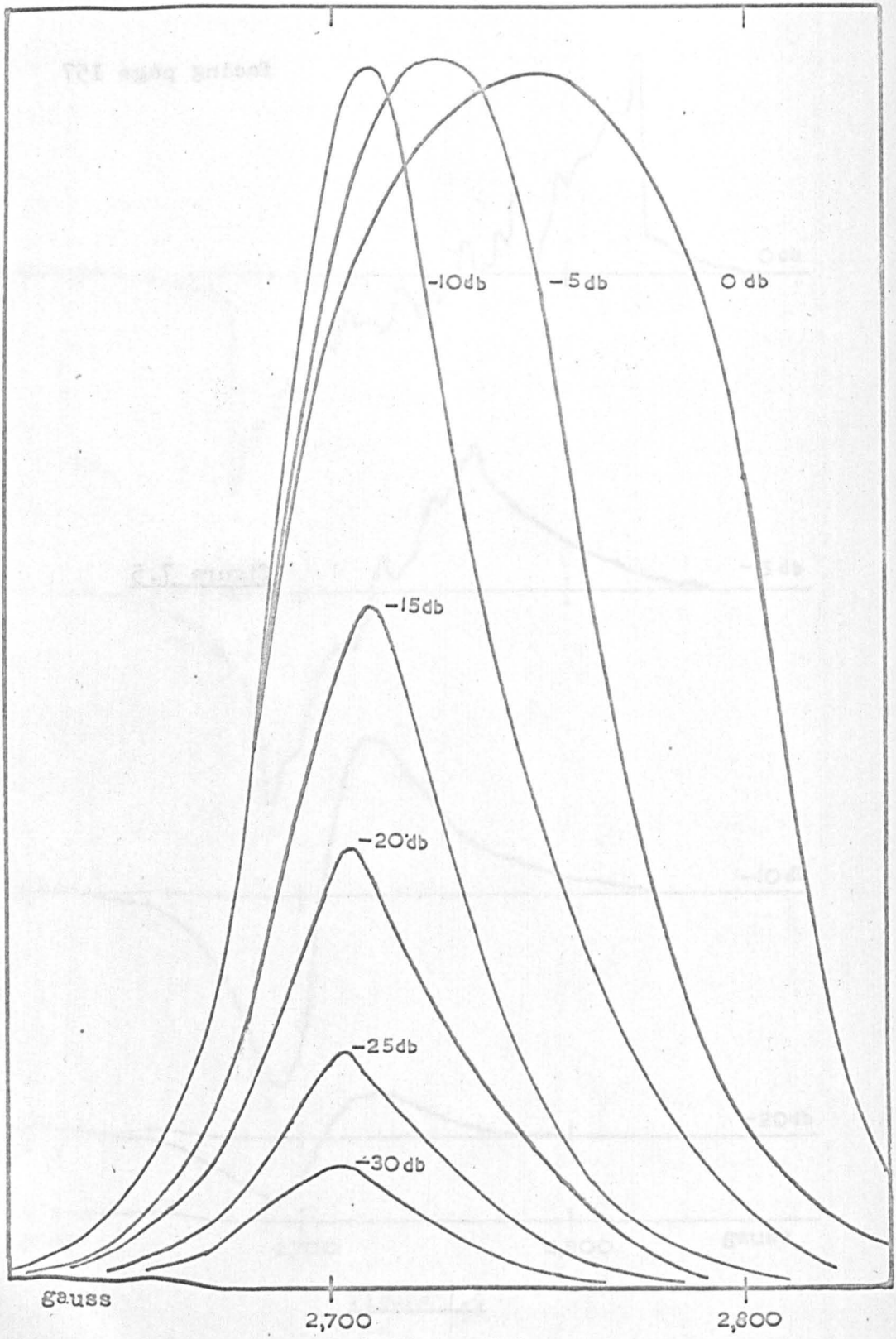

Figure 7.5

Absorption lineshape of spectrum G, only incident microwave power is varied. These curves are the integrated envelopes of the spectra in Figure 7.4, with the structure averaged out.

Annealing in nitrogen or under a vacuum of about 10^{-2}cm.Hg is only partially successful in removing the resonance.

This spectrum (F) is probably due to an Fe^{3+} precipitate in the crystal. It is discussed more fully in Chapter VIII.

G

What appear to be intermediate spectra between A and F are sometimes observed. They are usually rather anisotropic, consisting of a fairly broad line, perhaps with some associated weaker fine structure lines.

One of the spectra with a <110> axis as principal direction and $g_{\parallel} = 2.43$, $g_{\perp} = 2.08$ at 77^{o}K is worthy of special mention. It has a very curious characteristic which it has not been possible to explain. This is associated with the power saturation of the absorption. Figure 7.4 shows the first derivative of the absorption for a number of different incident microwave powers. The gain and sensitivity are otherwise unaltered. The results shown in Figure 7.4 were obtained at 77^{o}K but they are identical ~~to~~ with results at 20^{o}K and 300^{o}K except for a small change in position. Integration of the derivative absorption spectra shows that an individual part of a line is only saturated when it reaches a specific intensity as is shown in Figure 7.5 (the shift in position may be due to "fine structure" on the high field side of the line progressively saturating; measurements at lower temperatures should clarify this point). This is distinctly different from the usual power saturation effect

which is proportional to the transition probability (section 3.3(c)). If the absorption line is assumed to be made up of a number of unresolved (hyperfine) components, and these components are assumed to have the same unusual saturation properties, the extremely large slope on the sides of the individual saturated absorptions will cause a "stepping" of the envelope. It is this effect which is seen in the first derivatives in Figure 7.4. The phenomenon of saturation broadening in this special case leads to an increase in resolution of the components of the line. The unsaturated lineshape is nearly Gaussian.

No attempt has been made to analyse this spectrum but the characteristics described above suggest a possible qualitative explanation which is discussed in Chapter VIII.

This spectrum and a number of apparently similar but less well defined ones which may be more closely related to F are fairly stable at room temperatures. They are destroyed by annealing and also possibly by mechanical damage.

7.2 Thermal Characteristics of the AgCl:Fe^{3+} Spectra

(a) Properties of the Cubic $(FeCl_4)^-$ Centre

The experiments of Hennig (5) and of Hayes, Pilbrow and Slifkin (1) showed that the spectrum A was fairly stable in silver chloride crystals, following quenching from a high temperature anneal (2.4.5(b)) It has been found that this spectrum is obtained by irradiating iron doped silver chloride crystals at temperatures between about $0^{\circ}C$

and -75°C. Both filtered and unfiltered optical and u.v. radiation has been employed (section 5.2) with little apparent difference in effect. (The more energetic radiation produces some darkening of the surfaces of crystals). It is not as important to use well filtered radiation, as has been necessary in the experiments with AgCl:Cu (2.4.5(a)). The formation of A does not appear to be associated with the creation of a latent image in the volume of the crystal (2.6) in contrast to the effect of Cu^+ (2.4.5(a)). This probably explains why u.v. radiation can be more successfully employed. Nevertheless more penetrating longer wavelength radiation should produce a more evenly distributed and probably more intense spectrum, as ultra-violet radiation is heavily attenuated by the crystal (2.3.2.)

Experiments have been carried out on crystals containing two different amounts of iron, namely either about 1 part in 10^5 ~~and~~ or about 1 part in 10^4 molar. Crystals with the former doping which had been grown in an atmosphere of chlorine and carefully annealed (cooling them over a period of about 16 hours) showed a strong $(FeCl_4)^-$ spectrum (A). The intensity of this must be at least equivalent to 50% of the iron in the crystal. This spectrum only decayed after the crystal had been damaged, for example by repeated rapid cooling from room temperature to 77°K. Spectrum A was re-established but with a lower intensity following irradiation. This could again be forced to decay and repeated irradiation suggests that all of the

iron is eventually converted into the form which gives the spectrum F. Annealing the crystals under chlorine re-established spectrum A, but the overall stability was somewhat lower. It is not possible to describe these effects quantitatively as they are apparently very sensitive to crystal handling and history. Re-annealing of the crystals with the lower iron doping followed by fast or slow cooling under vacuum or nitrogen is generally not very successful for re-establishing the state which is the basis for A; growing the crystal under nitrogen would probably be more profitable, but this has not been investigated for these crystals.

Generally, the spectrum A is much less stable in crystals with 1 part in 10^4 of iron. It usually decays in a matter of minutes at about $10^{\circ}C$, although in some crystals, particularly freshly grown ones, the decay may take a few hours. The spectra are always stable over a period of at least some hours at $0^{\circ}C$ and can be stored indefinitely at $77^{\circ}K$. There is no obvious distinction between the effect of annealing followed by slow cooling under chlorine or under vacuum.

The conditions for the formation of the spectra F and G, associated with the decay of A, have been described in 7.1c(ii).

(b) Formation of the Cubic $(FeCl_4)^-$ Centre

The model proposed by Hayes (1) for the spectrum A is that of Fe^{3+} in an interstital site of the AgCl lattice. It is tetrahedrally coordinated to four ligand chlorine ions and the other four tetrahedral

sites which should contain Ag^+ ions are vacant (Figure 8.1). A series of other experiments have shown that this model is correct (2.4.5b) and the results presented in this thesis provide further support for it.

The mechanism for the formation of the $(FeCl_4)^-$ centre by irradiation must be fairly complex because the starting point, as is discussed in Chapters II and VIII, is very probably an Fe^{2+} ion on a silver ion site. A number of steps must be involved in the conversion from one state to the other and it is this process which has been investigated.

Irradiation of iron doped silver chloride crystals at 77^oK has never had any detectable effect on the properties of the crystals which have been studied.

An examination has been made of the effect of illumination on iron doped silver chloride crystals for a range of temperatures between room temperature and -115^oC. Down to about -70^oC (to -75^oC with rather lower efficiency), the spectrum A is produced, as was described in the last section. Between -75^oC and -95^oC irradiation does not produce any spectra, although in one or two particular crystals subsequent warming to -75^oC formed the $(FeCl_4)^-$ centre, perhaps following the release of trapped charge carriers. Below -95^oC, but above about -105^oC, the centre responsible for spectrum B is formed during irradiation. This centre is probably formed more easily if the crystal has been cooled over a period of about an hour,

particularly in the temperature region of -50°C to -90°C. The details of this dependence have not been studied.

The ~~warming~~ thermal characteristics of spectrum B has been investigated by allowing the crystal to warm up in steps of about 3°C over periods of about 5 minutes, re-cooling after each interval to measure the spectrum at 77°K. The spectrum is unaltered up to -75°C where about half of it is converted to A in 5 minutes. The next step of warming to -72°C completed the conversion to A. ~~The total number~~ Approximately all the B centres are changed into A ~~is ≈ 1:1~~, taking account of the intensities of the lines involved. It is safe to conclude that the one centre decayed to form the other.

The possible effect of rapid warming of some crystals irradiated at between -80°C and -105°C is described in 7.1 c(i). Attempts to reproduce spectra D and E in a controlled way by warming crystals containing the centre B from 77°K to -40°C in about 1 minute have always converted B to A.

7.3 Other Experiments

Experiments were carried out preparatory to studying the spectrum of Mn^{2+} in silver chloride.. These experiments were not continued in detail owing to other work which has been described in section 2.4.5c. The spectra which were observed were typical of divalent manganese.

A more detailed study of gold doped silver chloride has been made and early results suggest that under some conditions, a paramagnetic species can exist in the crystal. In general, a search has

been made for paramagnetic centres associated with the effect of radiation on the crystals which appears possible to contain some sensitization mechanism (2.4.5d). Similar experiments have been attempted as those which were carried out on the iron doped crystals. The result of this work was that no paramagnetic centres were observed. The two states of gold which would be likely to occur in AgCl are monovalent Au^{+} and trivalent Au^{3+}. The former is certainly diamagnetic ($5d^{10}$), the latter ($5d^{8}$) may either be diamagnetic or the ground state may be a singlet (non-Kramers) far below any other states.

It was found quite often that freshly grown crystals which were probably only partially annealed (for an hour at 250°C, say) in chlorine, after a nitrogen anneal, or vice-versa, exhibited a weak and very complex spectrum with many lines and a g value of about 2.2. Attempts to find a symmetry axis for the spectrum were unsuccessful but it is now realised that the crystals were not as well aligned as had been thought. Careful X-ray orientation should overcome this difficulty. The spectrum, which is apparently fairly stable at room temperatures but disappears following crystal damage, is possibly associated with Au^{2+}. The degree of bonding between such an ion and its ligands would probably be substantial and lead to a complex spectrum, particularly if the symmetry is lower than cubic. The nuclear spin of gold, $(\frac{3}{2})$, would further complicate the spectrum. If the orientation of this spectrum could be assessed sufficiently

facing page 164

figure 7.6

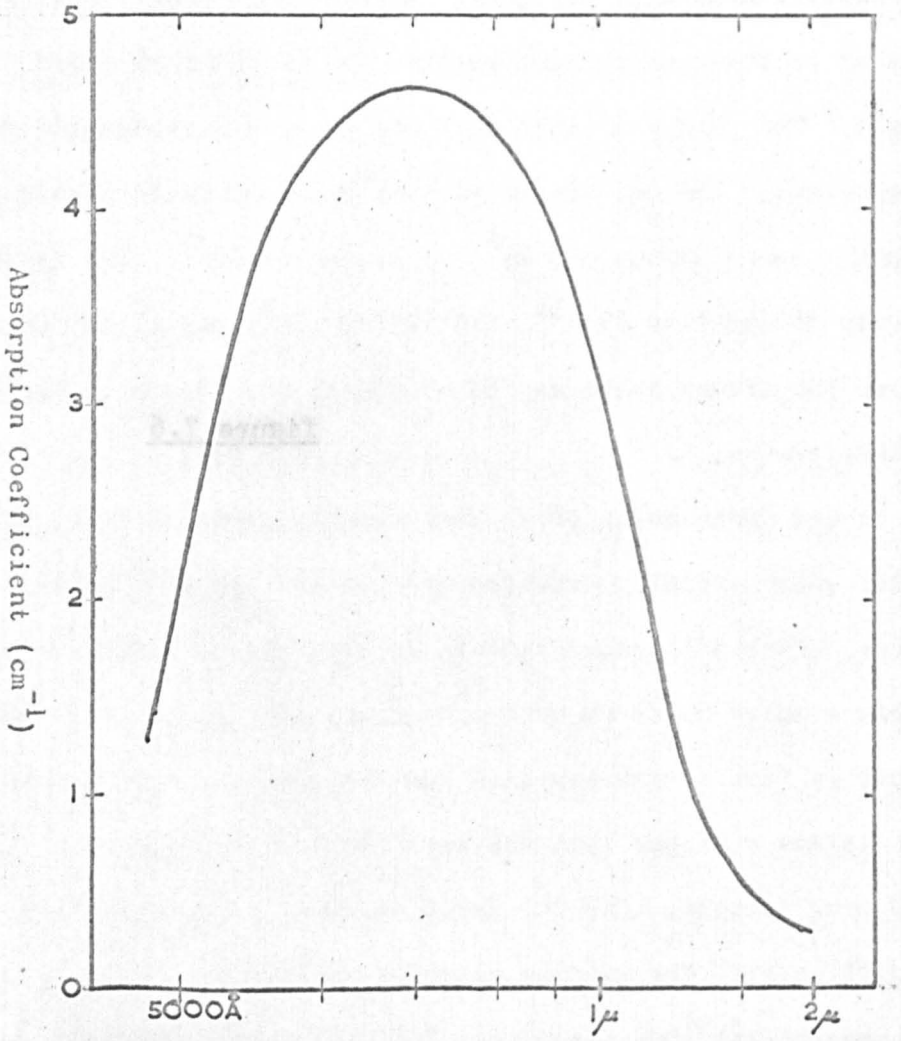

Figure 7.6

Optical Colloid Absorption in an AgCl:Au Crystal (77°K).

accurately, and the conditions for its formation sufficiently confirmed, it would be very interesting to study it in some detail as the reports of e.s.r. of Au^{2+} mentioned in 2.4.5d do not describe this state in single crystals.

Figure 7.6 shows the optical absorption which is obtained in gold doped crystals following irradiation and storage for one year (2.4.5d). This absorption band is included as an example of the colloid spectra described in section 2.4.4. This crystal contained about 0.01% molar of gold, a factor of ten less than Mitchell's (2.4.5d), and the observed effect is an optical absorption rather than scattering, implying that the particle size is rather less than the wavelength of light. Kaiser (9) has attributed a peak at 5,000Å in AgCl to silver colloids and one at 5,800Å to gold colloid in gold doped AgCl. As can be seen from Figure 2.10, this difference is within the range that could be predicted by taking into account sufficient variation in particle size (Figure 2.10 refers to sodium spheres, the position but not the general character of the absorption will be altered by refering to a silver or gold colloid). The great sensitivity of gold doped crystals for the formation of colloids will probably mean that the size and range of shapes will be different from the form of colloids in AgCl without any gold content; for this reason it is difficult to definitely assign the absorption to either gold or silver.

Doremus (10) has calculated from the Mie theory the positions of the absorption bands for silver and gold particles in AgCl as 5,040Å and 5,770Å respectively. These values should be appropriate to spherical particles smaller than 100Å radius. Brown and Waifan (11) have studied colloid absorption in AgCl. Their results show that the various parts of the absorption band have a range of peaks between about 5,000Å to 6,000Å for AgCl (without gold).

The band shown in Figure 7.6 is displaced to longer wavelengths and is much wider than would be expected from the discussion above. The peak is at about 7,000Å, and the band extends from about 5,000Å to 10,000Å. The qualitative discussion given above would imply that the absorption is predominantly due to gold colloids and the great width may imply that some of the particles are quite large (i.e. rather greater than the 400Å radius which is the largest given in Figure 2.10).

The nature of the colloids which form in gold doped crystals is of some interest in the investigations to find if a divalent state of gold is associated with the effect of radiation on gold doped crystals. Such a state may under conditions of irradiation have a short lifetime, but be a necessary step in the sensitizing of the crystal before precipitation can occur. On the other hand, the precipitation may simply be the result of gold in AgCl having a low solubility and a small activation energy for diffusion. The latter process would not appear to be sufficient as some sort of hole trap must be provided to allow the initial sensitization of the crystal (2.6 and 2.4.5a).

CHAPTER VII - REFERENCES

1. W. Hayes, J.R. Pilbrow and L.M. Slifkin, J. Phys. Chem. Solids, 25, 1417 (1964).

2. R.H. Kronig and C.J. Bouwkamp, Physica, 6, 290 (1939).

3. W. Low, "Paramagnetic Resonance in Solids", Solid State Physics Suppl., 2, Academic (1960).

4. J.C. Garth, Phys. Rev., 140, A656, 1965 and M. Satoh and C.P. Slichter, ibid, 144, 259 (1966).

5. K. Hennig, Phys. Stat. Sol., 3, K458, (1963), and 7, 885 (1964).

6. B. Bleaney, Phil. Mag., 42, 441 (1951).

7. T. Castner, G.S. Newell, W.C. Holton and C.P. Slichter, J. Chem. Phys., 32, 668 (1960).

8. W.M. Walsh et al., "Paramagnetic Resonance", Vol. II, p.836, ed. W. Low, Academic (1963); also J. Kirton and R.C. Newman, Phys. Rev. Lett., 15, 244 (1965), disputed by J. Kedzie et al., Phys. Rev. Lett., 15, 632 (1965), Phys. Rev., 138, A918 (1965).

9. W. Kaiser, Z. Physik, 132, 497 (1952).

10. R.H. Doremus, J. Appl. Phys., 35, 3456 (1964).

11. F.C. Brown and N. Waifan, Phys. Rev., 105, 93 (1957).

facing page 167

figure 8.1

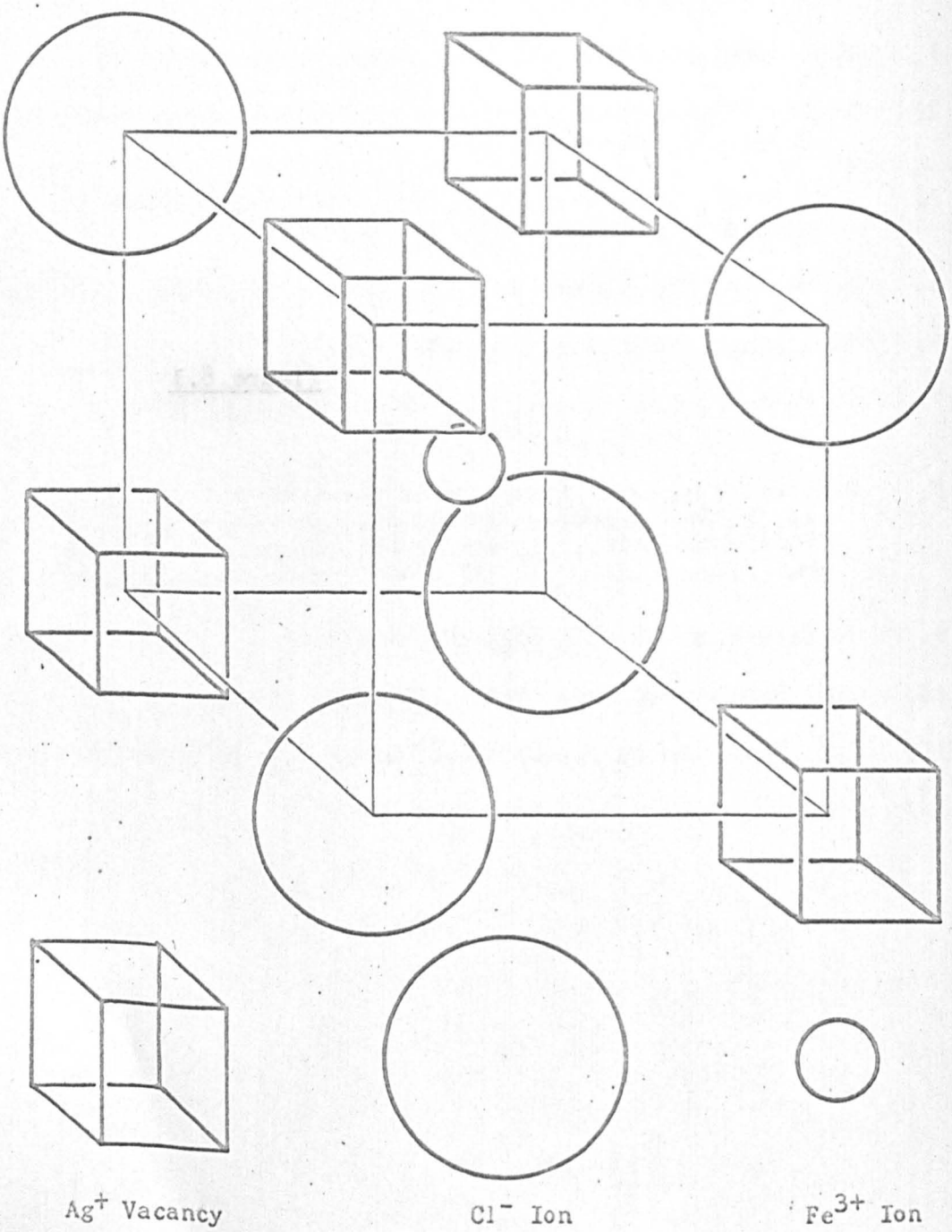

Figure 8.1

Model of Cubic $(FeCl_4)^-$ Centre

CHAPTER VIII

DISCUSSION

8.1 The Cubic $(FeCl_4)^-$ Centre

The spectrum A is identical with that measured by other workers who created it by annealing iron doped silver chloride crystals in an atmosphere of chlorine. They quenched the crystals from about 400°C to room temperature. The model which they have proposed is shown in Figure 8.1*(1); it has been well substantiated. An alternative model proposed by Hennig (reference 5 of Chapter VII) involves the Fe^{3+} ion interacting with the nuclei of eight Ag^+ ions at the corners of the cube and no interaction with the halogen nuclei. Hennig failed to take account of the quadrupole interaction with the halogen nuclei and this model is not considered.

The formation and decay of spectrum A is discussed in section 8.3 but it is worth emphasising at this point its great chemical stability in the silver chloride lattice. There is no evidence to suggest that the complex, once formed, decays to the Fe^{2+} state while still at its original lattice site (at room temperature or below). It is shown in 8.3 that only 0.61e.v. is necessary to

---

* Silver chloride has the NaCl structure with a very similar lattice constant (a = 5.55Å). The model in Figure 8.1 is constructed on the simple cube which is formed by the alternate Ag^+ and Cl^- ions.

excite the last occupant from one of the neighbouring Ag^+ ion sites into an interstitial position. This is compared with the activation energy for formation of a Frenkel defect (1.4e.v.) which at least partially indicates the degree of bonding within the complex. While the $(FeCl_4)^-$ centre has an overall (-e) charge in the lattice, this is distributed over the complex and the occupancy of an Ag^+ site is not very successful in finding the full strength of a more ionic bond. The model proposed in section 8.2 for spectrum B also suggests the same conclusion. These observations are in agreement with those of Hayes and his co-workers and their suggestion that the Fe^{3+} ion is part of an $(FeCl_4)^-$ molecular complex has been adopted. As there could be confusion with the model which is proposed for spectrum B, it is emphasised that this is the cubic centre.

The spin Hamiltonian parameters describing spectrum A are particularly interesting and it is worth making some comment regarding them. The cubic crystal field parameter (a) is of a magnitude and sign which is normal in the S-state Fe^{3+} ion spectra (e.g. see references 20 and 21, Chapter IV). The ligand hyperfine coupling constants indicate an appreciable degree of covalent bonding (1) (specified in terms of the probability of the paramagnetic electrons being found on each ligand ion), the fraction of s bonding is $f_s = 0.86\%$. Only the difference between σ and π bonding is observable from the e.s.r. results and $f_\sigma - f_\pi = 3.4\%$.

Only a vague estimate can be made of the actual magnitudes of f_σ and f_π from the results on octahedrally coordinated Fe^{3+} in $KMgF_3$ in which $f_\sigma - f_\pi = 3.3\%$ (in AgCl, the symmetry is tetrahedral and the ligands are chlorine). Using Nathans' neutron diffraction data, $f_\sigma \approx 5.4\%$ and $f_\pi \approx 2.1\%$, so it may be reasonable to assume that these will be lower limits to the covalencies in $(FeCl_4)^-$ (2, Section 4.4c(ii)).

The g-shift in spectrum A is unusually large ($\Delta g = + 0.013$) for Fe^{3+}, the g-values of the S-state Fe^{3+} ion in a wide range of surroundings typically vary about $\pm$ 0.003 from the free spin value. Other results for tetrahedrally coordinated Fe^{3+} show a positive g-shift but not of this magnitude. Geschwind's measurements in garnet (3) where the Fe^{3+} ion has four tetrahedral ligand oxygen ions with a trigonal distortion, indicate a g-shift of 0.0024.

An attempt has been made to obtain a quantitative understanding for this large effect. The results have so far been fairly unsuccessful, so the calculations will not be presented in detail. It is possible to appreciate those mechanisms which might be important for producing an effect of this magnitude and a description is given of some of the more relevant factors.

The results which are quoted in table 2.3 (p36) for the g-value and the ligand nuclear coupling constants of Fe^{3+} in AgCl and in AgBr (in the latter case the g-shift is + 0.04) imply that the degree of chemical bonding is very important, it must also be

considered a possibility that the larger shift in the bromide is a result of the larger spin-orbit coupling constant of bromine than chlorine ($2{,}400cm^{-1}$, compared with $600cm^{-1}$). In all the calculations which have been carried out, the effect of the spin-orbit coupling on ligand ions amounts to a correction of the central ion spin-orbit coupling. This is a consequence of assuming the admixture of ligand functions is small. Accordingly, it can be assumed that the total cumulative magnitude of central ion contributions to matrix elements will be at least comparable and usually rather greater than the contributions involving ligand functions. As it has not yet been possible to understand the mechanism of the g-shift, the ligand effects are not explicitly included in this discussion although it must be understood that they will play a substantial part. This could be very important if central ion elements cancelled as this would be an "accidental" effect and ligand contributions would not necessarily cancel in the same way.

The molecular orbital calculation of the matrix elements involving ligand functions is quite straightforward but rather long because of the five-electron wavefunctions which must be used. Additional parameters are required some of which are approximately known (the covalency parameters) and some of which would have to be computed (overlap integrals). Taking account of configurational interaction can introduce more parameters so inclusion of these effects is seen as a stage beyond a molecular orbital calculation.

It is known that the crystal field in the $(FeCl_4)^-$ complex is very strong* (but not strong enough to force the Fe^{3+} ion into a low spin state; no low spin tetrahedral Fe^{3+} complexes appear to have been identified). This ~~implicitly~~ implies a substantial degree of covalency which can be usefully included as a parameter by using a diagram of the form given by Tanabe and Sugano (Figure 4.2). The calculation of the magnitude of the crystal field (Δ'/B in Figure 4.2) would be very complex (Section 4.3) but an optical measurement from the ground state of an ion would determine the crystal field, provided the optical transition could be identified.

Attempts to observe the $^6A_1 \longrightarrow {}^4T_1$ transition in the $(FeCl_4)^-$ complex in AgCl at 77^0K using the apparatus described in section 5.3 have not been successful, owing to the inadequate sensitivity of the Unicam SP.700 spectrophotometer and the lack of sufficient centres in the crystal. Accurate knowledge of this transition is vital to any calculation of parameters for an S-state ion, as departures from "free-spin" of the $^6A_1$ state rely on spin-orbit coupling admixing excited $^4T_1$ states with the ground state.

---

* Usually the distinction between medium and strong crystal field for Fe^{3+} complexes is the transition from high to low spin; the discussion that follows relies on techniques which are appropriate to strong rather than medium crystal fields so that the strong description is used here although the spin is still high.

In the absence of a measurement of the $^6A_1 \longrightarrow {}^4T_1$ splitting (Δ) it is of interest that Δ has been measured by Freidman (4) for the tetrachloroferrate ion in association with potassium in ethereal solution and in 16N HCl. He measures this transition at 18,800cm^{-1} and as the $(FeCl_4)^-$ complex is essentially the same (the tetrachloroferrate ion is in the form of a flattened tetrahedron), it seemed worth measuring the g-value of (sodium) tetrachloroferrate. This has been measured by freezing a dilute ethereal solution (4) to 77°K. A single, nearly symmetrical line about 50 gauss wide is observed with a g-value of 2.011 $\pm$ 0.001. If this powder measurement can be accepted as a reasonable assessment of the g-value, it indicates that the process which is causing the g shift (+ 0.009 in this case) is common to both complexes.

In the absence of further information, a first estimate of the optical splitting of $(FeCl_4)^-$ in AgCl is that it is rather less than 18,800cm^{-1}. Figure 4.2 is now applied to the case of Fe^{3+} in tetrahedral surroundings (the information about the nature of the cubic crystal field is included in the parameter describing the strength of the field, provided the strong field levels are reassigned). At about this separation from the ground state $^4T_1$ and $^2T_2$ levels "cross" and calculations which start from states which are eigenstates of the crystal field, and only insert the influence of spin-orbit coupling as a perturbation will be quite inadequate in this region. New states must be formed from the $^4T_1$ and $^2T_2$ which are eigenstates

of the spin-orbit coupling operator. This has not yet been studied in detail. Perturbations involving second order wavefunctions produce a negligible g-shift of about -0.001, if only the $^4T_1$ level is considered. Normally, higher orders of perturbation are necessary to include doublet levels and if the separation is large between the doublets and the quartets, the effect as far as the g-value is concerned is small compared with the second order corrections. If the separation of the $^4T_1$ and $^2T_2$ levels is of the order of $\lambda \approx 400 cm^{-1}$ (the spin-orbit coupling constant), this approximation is no longer valid. All interactions with higher order $^4T_1$ levels can also be neglected in the first instance as the energy splitting of the next $^4T_1$ above the ground state (Figure 4.2) is more than double that of the $^4T_1$ (^4G) level (in second order the effect is squared, so that the result is a correction four times smaller).

So far, the most important difference between the tetrahedral and octahedral cubic symmetry has not been mentioned, namely the lack of inversion symmetry for tetrahedral coordination. This is unimportant for d electron states as they have even parity, if some 4p states are admixed, the tetrahedral and octahedral symmetries are no longer equivalent. While this can be important in a point charge calculation, Ballhausen (5) has pointed out that the effect is much smaller when a molecular orbital treatment is necessary. As the latter is the case here, ~~the ignoring~~ omission of the 4p states is probably justified; moreover if it was necessary to include 4p states, Geschwind's results would have shown a similar g-shift (see above).

A configurational calculation which considers an admixture of some ($Fe^{2+}Cl\ Cl_3^-$) into the ($Fe^{3+}Cl_4^-$) complex may reveal with more physical meaning the nature of the g-shift.

The discussion above has attempted to describe some of the interactions which could be important in explaining the g-shift of the $(FeCl_4)^-$ complex. The approximations which have been made are not ~~as~~ valid ~~when considering~~ for the cubic field splitting parameter (a) as the Γ_7 and Γ_8 levels of the $^4T_1$ state are only split by spin-orbit coupling when their interaction with other states (e.g. $^2T_2$) is taken into account. This is the reason for the inaccuracy of Watanabe's calculations (see section 4.4c).

It is appropriate at this point to indicate the methods which have been used to calculate wavefunctions and matrix elements. The correct spin-orbital states for the central ion have been set up using the methods described by Ballhausen (6). The free ion terms are first split according to the symmetry of the crystal field and then spin degeneracies are included by allowing them to "interact" with the orbital states. The transformation of the five-electron Slater Determinants in the T_d double group is examined and the final wavefunctions describe the effect of spin-orbit coupling on the crystal field states*. The wavefunctions of the ground state of Fe^{3+}

---

* Care should be taken in following Ballhausen's transformation procedures, as there appears to be some confusion in the use of active and passive transformations. Griffith (7) gives a good simple account of spin transformation..

are simply those which are obtained in the spin Hamiltonian treatment if the cubic "a" term is included.

The hybrids which are made up of ligand functions to form the independent bonding molecular orbitals are given in reference 1.

The perturbation Hamiltonian which has been employed is in the form

$$\mathcal{H}_1 = \sum_{i,n} [\zeta_i^n \underline{l}_i.\underline{s}_i + \beta \underline{H}.(\underline{l}_i + 2\underline{s}_i)] \qquad 8.1$$

where the summation over i implies that each one electron function is operated on in turn. The orbital operator $\underline{l}_i$ is transported from the central ion to each of the ligands in turn. This is the meaning of n, and ζ_i^n is the one electron spin-orbit coupling constant for the ion denoted by n.

The spin-orbit matrix elements for the important states of the central ion are given by Griffith (7), as is an alternative method for deriving the wavefunctions. The methods for the calculation of matrix elements involving ligand functions are to be found in reference 29 of Chapter IV. All the terms involving $\sum_{i,n} \underline{H}.\underline{l}_i$ and the ground state disappear as this is an S-state.

If it is possible to explain the large g-shift of the Fe^{3+} resonance in silver chloride, this should be directly applicable to the even larger deviation in AgBr, assuming the iron complex in AgBr has the same structure.

facing page 176

figure 8.2

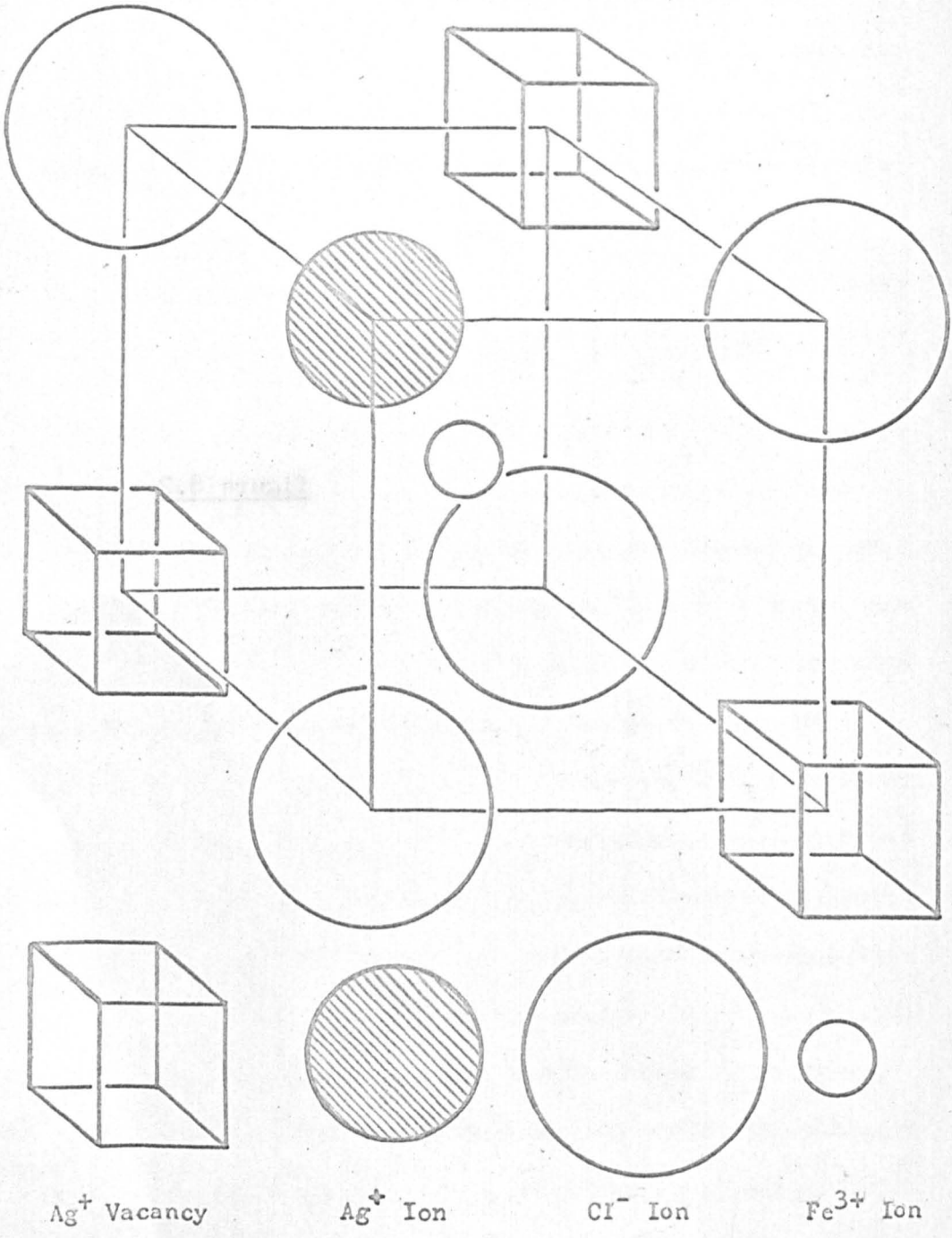

Figure 8.2

Model of Trigonal $(FeCl_4)^{-}$ Centre

8.2 The Trigonal $(FeCl_4)^-$ Centre

(a) The Model

There are two possible sites for the Fe^{3+} ion in the silver chloride lattice with an axial distortion along a crystallographic (111) axis. The Fe^{3+} ion could be at a substitutional site (i.e. occupying an Ag^+ site), but there is no reasonable ionic arrangement around the ion which could provide the trigonal distortion. (The Jahn-Teller effect is not operative as the S-state is an orbital singlet.) To obtain charge compensation, two silver ion sites should be vacant and if the Fe^{3+} ion is allowed to move into an interstitial site, there will be three Ag^+ ion vacancies. It is this model which is proposed for the spectrum B (see Figure 8.2), the three silver ion vacancies are all in the same simple cube. This is the same as the model for the $(FeCl_4)^-$ centre but one of the Ag^+ vacancies is occupied. This structure is in good agreement with the observations of ionic rearrangement which are discussed in 8.3.

The small value of the parameter D is of some interest. If the magnitude of D is a measure of the strength of the axial distortion on the complex, then the total distortion must be very small.

D can be much larger than the quanta usually used in e.s.r. experiments, in some cases, it might be greater than $5cm^{-1}$(7,8). Typically, D is rather larger than the $(-)81 \times 10^{-4}cm^{-1}$ measured for this complex. Geschwind (3) finds $D = -880 \times 10^{-4}cm^{-1}$ in the tetrahedral garnet complex. From an ionic point of view this effect

is probably rather surprising as the Ag^+ ion sites are only 2.40Å from the Fe^{3+} ion and it would be reasonable to expect the Ag^+ ion to ~~appreciably~~ appreciably distort the complex. If the bonding between the Fe^{3+} ion and the four halogen ligands is strong, the influence of the nearest neighbour Ag^+ ion will be much smaller. Electrostatic attraction will be towards the complex as a whole rather than to individual chlorine ions. Measurements of the bond length of the tetrachloroferrate ion indicate a length of 2.21Å (9), which will further reduce the interaction with the Ag^+ ion. Thus it is possible that the small D value is again a consequence of the covalency which has been discussed in 8.1.

The magnitude of the "a" parameter ((+) 187 x $10^{-4}cm^{-1}$) is not especially different from that for many Fe^{3+} arrangements and the positive sign is only nominally assigned for convenience. It may be worth noting that Geschwind determined the absolute signs of a and D for the tetrahedral centre in garnet with a positive and D negative (3), also Garth (reference 4 of Chapter VII) found a positive value for the a parameter in cubic $(FeCl_4)^-$. The g-value which is nominally quoted in section 7.1b is only of value as an approximate fitting parameter and does not necessarily have any special significance.

Taking into account the great similarity between this centre (i.e. that responsible for spectrum B) and the cubic $(FeCl_4)^-$ complex, as well as the very weak binding of the last neighbouring Ag^+ ion,

this complex is also referred to as an $(FeCl_4)^-$ complex. To distinguish it from A, it is called the trigonal or neutral $(FeCl_4)^-$ complex; it is understood that it is associated with an Ag^+ ion.

(b) Discrepancies in the Spin Hamiltonian

It is shown in section 7.1b that the spin Hamiltonian 7.2 is not adequate to describe spectrum B. On the other hand, it has not been possible to find any other combination of parameters which would explain spectrum B in any way or include spectrum C. It is interesting to study the nature of the deviations from the "least squares" fit in some detail.

The parameters a, D and F which have been used in section 7.1b are the best fit for the splittings $W_{1,5}$ and $W_{2,4}$ between the respective pairs of lines. These splittings depend to a first order on the zero-field splittings and only to a second order on the Zeeman term. The absolute fields at which the absorptions occur are to a first order a Zeeman splitting and to a second order a consequence of the crystalline zero-field splittings and the spin-orbit coupling.

The errors in the fitting of a, D and F to the measured values for various $W_{1,5}$, $W_{2,4}$ are small although they are outside the accuracy of measurement ~~errors~~. This could be a consequence of small misorientations, or in some cases, simply a result of the difficulties associated with separating nearly coincident lines. In a spin Hamiltonian (e.g.

equation 7.2), the terms of even order in spin operators are those which describe the zero-field or Stark splittings. This is a result of the requirement for the invariance under time reversal which also leads to Kramer's theorem. If attention is restricted to states with even parity (e.g. d states), only even components of the spin operators will occur (10). The spin Hamiltonian 7.2 is thus consistent with the effect of a cubic and an axial distortion on d levels. It fully describes the zero field splittings which can occur as the result of purely electrostatic effects. If states of odd parity are admixed with the d levels (e.g. 4p states), the requirement for overall even parity still holds, but individual components can occur with odd order. The consequence of this is that the zero-field terms in 7.2 are not now sufficient to describe the possible energy scheme of the ion. Such terms appear to be negligible for systems involving paramagnetic d electrons and moveover they would not explain the errors in the Zeeman splittings of spectrum B.

Generally, a spin Hamiltonian for an ion in an axial field requires two g values ($g_{||}$ and $g_{\perp}$) to describe the spectrum (the two values are indistinguishable in spectrum B). This does not fully take account of Zeeman terms in excited states which may be admixed by spin-orbit coupling. It is useful to give a simple example to demonstrate this effect.

Considering an S-state with a $^6A_1$ ground state (as in the previous section), and the cubic field excited state $^4T_1$, the only matrix elements connecting the two states are those involving the spin-orbit coupling (using the perturbation Hamiltonian 8.1). In a cubic field this does not lead to any zero field splitting of the $^6A_1$ level in second order as the matrix elements connecting Γ_7 and Γ_8 states are equal, (7, Table A34)

$$\langle \Gamma_{7j}^{g} | \sum_i \zeta_i \underline{l}_i \cdot \underline{s}_i | \Gamma_{7j}^{e} \rangle = \langle \Gamma_{8j}^{g} | \sum_i \zeta_i \underline{l}_i \cdot \underline{s}_i | \Gamma_{8j}^{e} \rangle = -\sqrt{2}\zeta$$

where $\Gamma_{7j}^{g,e}$ and $\Gamma_{8j}^{g,e}$ are eigenstates for the spin-orbit coupling, referred to the ground (g) and the excited (e) states. j is an individual component of the doubly degenerate Γ_7 or the quadruply degenerate Γ_8. If the S-state complex is distorted along a cubic axis (i.e. a tetragonal distortion) the Γ_8 levels are split into a Γ_6 and a Γ_7 of the D_4^* group so that the ground state is now made up of the three doublets $\Gamma_6 + 2\Gamma_7$. The matrix elements of each of these three doublets with corresponding states of the distorted $^4T_1$ (= $^4A_2 + {}^4E$) are different. Griffith considers the $^4A_2$ part of this in the D_4^* group and he gives the spin-orbit coupling matrix elements as (7,p.368)

$$\langle \Gamma_{6j}^{g} | \sum_i \zeta_i \underline{l}_i \cdot \underline{s}_i | \Gamma_{6j}^{e} \rangle = -\sqrt{\frac{6}{5}}\zeta ; \langle \Gamma_{7j}^{(1)g} | \sum_i \zeta_i \underline{l}_i \cdot \underline{s}_i | \Gamma_{7j}^{(1)e} \rangle = -\frac{2}{\sqrt{5}}\zeta$$

and $\langle \Gamma_{7j}^{(2)g} | \sum_i \zeta_i \underline{l}_i \cdot \underline{s}_i | \Gamma_{7j}^{(2)e} \rangle = 0$

where the ground spin-orbit states can be recognised as the usual spin states, $|\Gamma_{6j}g\rangle = |\pm\frac{1}{2}\rangle$, $|\Gamma_{7j}^{(1)}g\rangle = |\mp\frac{3}{2}\rangle$ and $|\Gamma_{7j}^{(2)}g\rangle = |\mp\frac{5}{2}\rangle$.

As at least second order wavefunctions must be used to examine effects with the excited state, all these matrix elements must be squared. If the immediate effect of these elements is taken into the spin Hamiltonian formula they contribute to the term $D(S_z^2 - 1/3\ S(S+1))$. If the Zeeman effect in the excited state is studied, these spin-orbit matrix elements will be different multiplying factors to each of the excited spin states. As far as a spin Hamiltonian is concerned, each pair of transitions $W_{1,5}$ and $W_{2,4}$ and also the $|-\frac{1}{2}\rangle \rightarrow |+\frac{1}{2}\rangle$ transition (H_3) will appear to have a different g-value.

Generally S-state ion g-shifts are small (section 8.1) and as these shifts occur because of Zeeman interactions in excited states, the departures from a simple spin Hamiltonian g-value will also be small but of comparable magnitude. The g-shift of the $(FeCl_4)^-$ complex is not small ($\approx$20 gauss at X band) and it is errors of the type described in the example, and of about 20 gauss in magnitude which must be explained. Such large errors would not appear for the cubic centre because of the equality of all matrix elements between the ground state and the $^4T_1$ excited state.

In conclusion, the new terms which would be required in a spin Hamiltonian are included in those occurring in the generalized

Hamiltonians (section 4.4b). They are field dependent terms which must be of odd order in the spin operator to retain time reversal invariance. The general form of such terms in fourth order will be fourth order tensors of the form $S_i S_j S_k H_l$ where i,j,k,l indicate components of the operators. Symmetry arguments will greatly reduce the possible combinationsof these components (this is the effect of the various generalized treatments mentioned in 4.4b), but unfortunately such arguments leave no suggestion of the relative importance of the various terms.

At this stage there are apparently two courses open: one is to attempt to fit the data to a generalized Hamiltonian consistent with the axial symmetry of the centre, the other is to study the coupling with excited state levels which are near enough to contribute substantially to the ground state to modify the spin Hamiltonian and to fit the data to the new Hamiltonian. According to the arguments which have been proposed, the latter is fundamentally the same problem as that of understanding the g-value of spectrum A. It is proposed that the same process is responsible for the g-shift in A as is necessary to explain the discrepancies in spectrum B.

8.3 Proposed Mechanism for the Formation of Fe^{3+} Centres in AgCl

The observations described in the last chapter indicate an explanation for the formation of the stable trivalent iron centre in the characteristically monovalent silver chloride lattice.

The explanation proposed by Hayes, Pilbrow and Slifkin (referred to in 2.4.5(b)) relied on the diffusion of silver interstitial ions or vacancies to or from the crystal surface during a high temperature anneal in chlorine. Adsorption of a chlorine molecule at the surface allows the formation of additional AgCl and of two holes which can diffuse through the crystals and be trapped by Fe^{2+} ions to form Fe^{3+}. They then propose that the trivalent ion stabilizes itself in the cubic tetrahedral configuration, either by capturing other silver vacancies or by the diffusion of ligand silver ions away through the crystal.

This mechanism is clearly not adequate to explain the formation of the cubic $(FeCl_4)^-$ complex following irradiation below room temperature. The source of halogen is not available, nor is such high mobility of silver vacancies and interstitials as is observed at high temperatures.

It is first of all assumed that when iron is dissolved in silver chloride and no resonance is observed, it is in the divalent state. The monovalent state (d^7 rather than $d^6 4s^1$) is not probable chemically and it is only known as a result of irradiation in salts (11). Moreover, it is a Kramers ion and should be quite easily detectable by e.s.r. It is very probable that Fe^{2+} ions dissolve substitutionally in AgCl and the tendency for Fe^{2+} e.s.r. spectra to be very susceptible to line broadening by lattice distortions has been mentioned in section 2.4.5(b).

An alternative explanation for the non-appearance of the Fe^{2+} spectrum, even at very low temperatures, is that the Fe^{2+} ions may be in a low spin (diamagnetic) configuration if the octahedral crystal field is sufficiently large.

The formation of spectrum B may be assisted by previously cooling the crystal slowly (7.2), which implies that a silver ion vacancy has been allowed to associate with the substitutional Fe^{2+} ion (2.4.2 and 5). It is normally assumed that a nearest neighbour Ag^{+} site is vacant, but this is probably not important. Irradiation creates electrons in the crystal conduction band and holes in the valence band (2.3) and it is presumably the trapping of an electron or a hole by the Fe^{2+} ion which initiates the formation of the complex. A process involving the trapping of an electron would not appear to be important as Fe^{+} would be formed and this would occur more easily after rapid cooling of the crystal, when the substitutional Fe^{2+} ions are not associated with Ag^{+} vacancies. While this process must be considered as possible, it must be realised that Fe^{+}, like Cu^{+} is probably a very efficient hole trap, so that this mechanism only allows the Fe^{2+} ion to act as a recombination centre. This would also appear to be true at sufficiently low temperatures (below $-110^{\circ}C$, say) when a hole is trapped first and Fe^{3+} is formed, as this ion is not detected following irradiation at these low temperatures. It is interesting to note that the possibility of hole trapping by a divalent ion at

a substitutional site is being suggested, usually divalent ions, such as Cu^{2+} and Ni^{2+} act as electron traps (2.4.5).

The important criterion, remembering the electrostatic effect of a possible associated vacancy, is that trapping should form an alternative, but chemically acceptable valency. It is also probably a general rule that trapping of one charge carrier is followed by a trapping of the other unless a more effective alternative trap is available (e.g. case of Cu^{+}), or else unless the centre formed by the first trapping can alter its form within the lifetime of this state. It is the latter mechanism which appears to stabilize the $Fe^{2+} + h^{+} \rightarrow Fe^{3+}$ trapping; the fate of the conduction electrons is ignored at this stage.

The observation of a threshold temperature for the formation of the trigonal $(FeCl_4)^{-}$ complex described in the last section implies that some ionic as well as electronic rearrangement is necessary. It is proposed that the strength of the binding of the tetrahedral $(FeCl_4)^{-}$ complex in AgCl is sufficiently high to "pull" the Fe^{3+} ion towards an interstitial site. This state shall be rather like the model in Figure 8.1, but two of the vacant Ag^{+} ion sites shall be occupied and the centre shall have an overall charge of (+e). Below $-105^{o}C$, this apparently acts as an electron trap, but above this temperature, there is a competing process, namely that one of the Ag^{+} ions in an occupied tetrahedral site can jump into one of its other neighbouring

facing page 186

figure 8.3

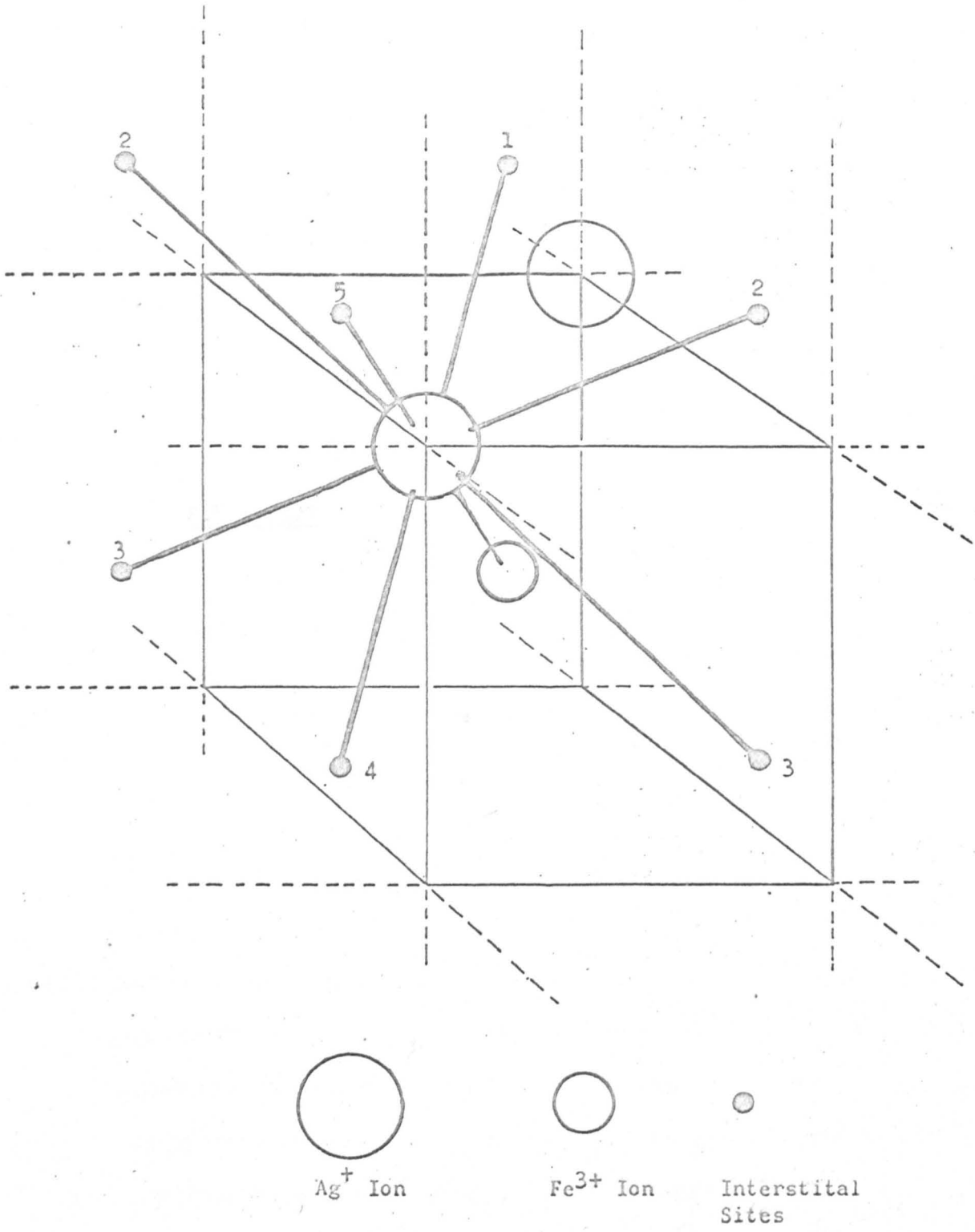

Figure 8.3

Model Indicating the Single Jumps of an Ag^+ Ion into Interstitial Sites, to leave the Model in Figure 8.2

interstitial sites (Figure 8.3). This is precisely the model which has been proposed to explain spectrum B (Figure 8.2) with the additional information that an interstitial site neighbouring the tetrahedron is occupied (i.e. 6 of the possibilities). The other possible interstitial site is not at the nearest but the next nearest interstitial site to the Fe^{3+} ion. Figure 8.3 indicates the possible single jumps for this ion by arrows, those carrying the same number being indistinguishable with respect to the orientation of the complex. The site 5 is the next nearest one.

It is possible to estimate the activation energy for the loss of this Ag^{+} ion from the complex if a value can be estimated for the lifetime of conduction electrons in this crystal. The electron mobility at this temperature is about $100cm^2$/volt sec (Figure 2.6) and the electron range is nominally assumed to be $10^{-4}cm^2$/volt (2.3.3 b), which implies a lifetime of about 10^{-6}secs. Assuming an atomic frequency factor (ν_0) of about $10^{13}sec^{-1}$, equation 2.8 gives an activation energy of 0.23e.v. As the activation energy for the diffusion of an interstitial ion is 0.10e.v. (2.4.2), the ion can be expected to diffuse away into the crystal as there is no electrostatic attraction between the ion and the neutral $(FeCl_4)^{-}Ag^{+}$ complex.

The equilibrium of the crystal shall be upset by the insertion of the additional interstitial Ag^{+} ions (2.4.2), but it may be expected that they would combine with the conduction electrons on

dislocations (2.6). This would imply substantial darkening of the crystals which is not detected, although the optical spectrum has not been examined in detail. There is definitely no darkening of the amount observed in AgCl:Cu^{+} crystals. Another possibility is that some of the interstitial ions will spend some time in the vicinity of the neutral $(FeCl_4)^{-}$ complex. If this occurs with sufficient probability, it could suggest an explanation of the spectrum C which occurs as a background to B. Figure 8.3 indicates all the possible nearest interstitial sites which an ion may occupy (four distinct sites). Also probable may be the next nearest sites, such as 5, and the sites along body diagonals from the Fe^{3+} ion through its Cl^{-} ligands. The binding energy associated with the various sites will vary, perhaps quite substantially, so that one or two of the possibilities may be preferred. If the spectrum C is a result of this type of centre, the principal axis (i.e. of the D and F terms) will be slightly altered and a rhombic E term will probably be necessary in the spin Hamiltonian.

Warming a crystal containing the sites B to -75^{o}C causes about half of them to decay in minutes. The last tetrahedral Ag^{+} ion is lost with an activation energy of 0.61 e.v. The stable $(FeCl_4)^{-}$ complex has now been formed.

It is not clear why rapid warming of the crystal should sometimes produce a distinct effect. It may be possible that the interstitial

silver ions which have been released during irradiation and have been trapped in shallow traps are all released in a short period. The thermal equilibrium of the crystal will be upset and the trivalent iron centres may trap the excess of ions forming a tetrahedral complex with two of the neighbouring Ag^+ ion sites occupied. It is precisely this type of model which Castner proposes for the iron complex in glass with a g-value of 4.3 (7.1 c). This may be acceptable as a tentative explanation of spectrum D. It would explain the difficulty which has been found in reproducing this result. This complex was involved in the description of the initial hole trapping by an Fe^{2+} ion, but it was suggested that it was an efficient electron trap to explain the threshold temperature of $-105^{o}C$. If this model for spectrum D is correct, irradiation at $77^{o}K$ should at least partially bleach the spectrum. Further support of this model is that the spectrum is normally seen at a very low level following irradiation to form the cubic spectrum. The E spectrum is connected with the decay of D and if this model can be substantiated, the complex responsible for E may be associated, for example, with the Fe^{3+} ion jumping to a substitutional (octahedral) site.

At this stage it is worth discussing briefly the fate of the conduction electrons and of the interstitial Ag^+ ions which must be formed during irradiation. The conditions would apparently be correct for the decoration of dislocations; although the darkening has not

been measured quantitatively, none of the crystals investigated exhibited obvious darkening. In the absence of detailed information on the subject, it must be assumed that this accounts for at least part of the electrons and Ag^+ ions. The subject is much more complicated than this as it is virtually certain that some iron will be deposited on crystal dislocations (2.5.2(b) and (12)), upsetting the simple model. As the experiments which have been described are only indirectly sensitive to these interactions, it is not possible to understand these effects. On the other hand, the dislocations are in principle assumed to be a useful "sink" for conduction electrons and excess interstitial Ag^+ ions.

The discussion above suggests a process for the formation of the cubic centre. It does not explain the first stage in the formation of this complex when the crystal is irradiated at higher temperatures (i.e. above -75^oC). That no spectra are observed when a crystal is irradiated at temperatures above -95^oC can be explained by assuming that it is at about this temperature that vacancies can dissociate from the substitutional Fe^{3+} ions. This will have two effects: firstly, an electrostatic repulsion from the now locally uncompensated Fe^{2+} ions will repel positive holes, secondly, the quantity of vacancies in the lattice will be greatly increased, reducing the number of interstitial ions which can exist (a consequence of the Law of Mass Action, equation 2.6).

As formation of a stable trivalent complex involves the production of three interstitial ions, it will only be possible if sufficient traps exist for interstitial Ag^+ ions. It would appear that this can only happen above -75^oC. Although the mechanism is not clear, it must be associated with dislocations. The exponential temperature dependence of the equilibrium constant in the Law of Mass Action may also have an important role. This argument suggests that holes are actually trapped by uncompensated Fe^{2+} ions. The probability of such a process would appear to be very low but could be important if sufficiently effective traps existed for electrons. Hole trapping would presumably occur when a vacancy was in the vicinity of an Fe^{2+} ion. After a hole has been trapped the formation of the cubic $(FeCl_4)^-$ complex will proceed as before.

This suggested process for the direct formation of the cubic centre implies a number of properties which should be observable experimentally. In particular, it is suggested that the efficiency of formation of $(FeCl_4)^-$ complex will be rather low (i.e. efficient hole traps do not exist above -95^oC). It should be possible to measure this at least to within an order of magnitude, by comparing the number of incident quanta with the magnitude of the spectrum which is produced. Also, as the thermodynamic arguments imply large changes in the ratio of silver vacancies to interstitials at different temperatures, some information could be obtained from

dark ionic conductivity measurements. More careful measurements of the importance of vacancy association with Fe^{2+} ions should be quite straightforward provided the cooling rate of the crystal can be carefully controlled. Data concerning the degree of vacancy association is likely to be of considerable value in elucidating the more doubtful stages in the formation of the cubic $(FeCl_4)^-$ centre.

In general, if some of the more tentative processes can be confirmed, it would be possible to extend the arguments given above to explain in more detail the complicated processes which are implicitly assumed to occur at or near to dislocations. If it appears that processes around dislocations are being used too extensively to explain the difficulties which have appeared in the discussion, it should be realised that it is essentially such complexities that make possible practical photographic processes in the silver halides.

To summarise the formation mechanism of the cubic iron centre, it appears that under specific conditions, an Fe^{2+} ion, whether or not it is associated with a silver ion vacancy, can trap a positive hole. Trivalent iron appears to be very stable and tends to prefer an interstitial site, forming tetrahedral bonds with four chlorine ions. A result of this is that the neighbouring Ag^+ ions are no longer adequately bound to their sites. The last tetrahedral Ag^+ ion requires an activation energy of 0.61e.v. which is considerably less than the energy required to remove a silver ion from a normal site

to an interstitial position (1.4e.v., section 2.4.1). This comparison is interesting as the difference is probably a result of the degree of covalent bonding in the iron complex, reducing the ionic and covalent strengths of the ligand chlorine-silver bonds. The relaxation of the lattice around the complex will also contribute to the reduction of the activation energy. The activation energy necessary for the second last tetrahedral Ag^{+} ion to leave its site is rather lower (0.23e.v.) owing to the excess local positive charge at the centre.

It appears that Fe^{2+} can act as electron-hole recombination centre below about 165°K. This is in agreement with low temperature electron mobility data (2.3.3; 2.4.5 b, reference 73 of Chapter II). Fe^{2+} does not have a very large effect on electron mobility, it will only limit the lifetime. Fe^{3+} severely reduces the electron mobility at low temperatures probably because the overall negative charge and the lattice distortion around the $(FeCl_4)^{-}$ centre scatters the conduction electrons.

8.4 Precipitation Effects

When the spectrum from the cubic $(FeCl_4)^{-}$ spectrum decays, it is apparently not possible to restore it by irradiation. The rate of decay is very dependent on the overall doping and on the crystal history. This implies a precipitation effect in the crystal. Spectrum F is typical of this type of effect, as spin-spin interactions between ions can no longer be neglected.

No spectra have been observed for a recombination of Ag^+ interstitial ions with the cubic centre and as it is stable in the crystal even at high temperatures, the precipitation must be associated with diffusion of the entire $(FeCl_4)^-$ complex. This type of process is quite possible as there is no doubt quite a high probability of finding neighbouring Ag^+ ions at the vacant Ag^+ sites at room temperature. If two such processes occur simultaneously, the complex may have a 50% probability of jumping into a neighbouring site. The electrical and mechanical atmospheres (2.5.2) around dislocations would provide sufficient local field to attract the diffusion of fairly close complexes. More distant complexes would suffer much less attraction, explaining greater stability in samples with fewer dislocations and lower doping (the doping will be particularly important if the overall solubility of Fe^{2+} ions in this temperature region has been exceeded and the excess ions have precipitated on dislocations). Also important in this process will be the quantity of interstitial Ag^+ ions which have been produced in the formation of the $(FeCl_4)^-$ complex. Charge compensation is provided by the conduction electrons for only half of those. The uncompensated Ag^+ ions may play a very important part in the field surrounding dislocations and during a precipitation, they would provide charge compensation for the $(FeCl_4)^-$ complexes.

If two $(FeCl_4)^-$ centres should interact during their diffusion forming another fairly stable complex, this larger defect will be

"locked" into the lattice. The temperature independence of the curious saturation of spectrum G and its anisotropy suggest that it may be due to coupled paramagnetic complexes. Spectrum G is quite stable once formed and the initial formation is intimately connected with the decay of A. Less resolved spectra would be associated with the interaction of more than two centres.

As was the case in the previous section, a limit exists to the understanding of the diffusion processes in the crystal. It is difficult to suggest mechanisms for precipitation, or for some of the stages in the formation of the complexes, taking account only of the lattice properties. Nevertheless it is not essential that the precipitation must occur in the vicinity of a dislocation, but there are a number of advantages in assuming that it does. Dislocations will provide a field to attract a diffusing $(FeCl_4)^-$ complex and if there are excess interstitial Ag^+ ions associated with dislocations, they will add to the dislocation "atmosphere". On the other hand, the spectrum F may be that of single Fe^{3+} ions in the very inhomogeneous crystal field around a dislocation. The "precipitation" model is perhaps to be preferred but the characteristics of the spectrum F have not been studied in detail.

In the arguments which have been put forward in this and in the previous sections, the thermodynamic equilibrium of the crystal has been taken into account as much as could be done with the information available. The quantitative application of the Law

of Mass Action is not straightforward owing to the uncertain role played by dislocations. An attempt has been made to restrict the qualitative discussion to arguments which would be thermodynamically allowable. There are at least 10^{20} iron centres per cm^3 and only about 10^{12} Frenkel defects at room temperature in a pure, perfect AgCl crystal, so that the iron centres must dominate the equilibrium of interstitial ions and vacant sites at all stages of their production and precipitation.

8.5 Conclusions

The work described in this thesis is essentially in two parts. One of these is perhaps more relevant to the theory of e.s.r. spectroscopy, while the other has attempted to study the trapping of charge carriers and the subsequent ionic reorganisation which takes place.

Problems have arisen in the spectral interpretation of the trigonal $(FeCl_4)^-$ spectrum are perhaps a result of inadequacies in the spin Hamiltonian which would usually be applicable for a complex of this type. The results suggest that this centre is only a slightly perturbed version of the cubic $(FeCl_4)^-$ complex. The cubic spectrum is also unusual in that its g-value deviates from the free spin value by about ten times the usual amount. It has not been possible to understand the detailed origin of this shift, but there is some indication that it may be a consequence of close mixing of the $^4T_1$ and $^2T_2$ levels in the excited state of the S-state Fe^{3+} ion.

The covalency is likely to play an important part in explaining the spectra fully, owing to the relatively large spin-orbit coupling constant of the halogen ligands. A measurement of the optical splittings associated with the complex will provide a sound basis for further study of this problem. It is probable that the discrepancies in the spin Hamiltonian of the trigonal centre are to be associated with the large g-shift of the cubic spectrum. If this suggestion is valid, it would imply that the "fit" which is usually obtained with a spin Hamiltonian for S-state ions is only obtained because of the typically small g-shifts.

There has been considerable experimental difficulty in reproducing some of the spectra which have been observed in iron doped silver chloride crystals. It has been possible to propose a mechanism for the process which occurs in an iron doped silver chloride crystal during irradiation and in the thermal treatment following this. The parts of this mechanism which are more difficult to understand are often under conditions where crystal dislocations could play an important part. There is insufficient information available to allow more than tentative suggestions regarding some details of the processes.

8.6 Suggestions for Future Work

(a) More data ~~is~~ are required to study further the fitting of the trigonal $(FeCl_4)^-$ complex to a spin Hamiltonian. Specifically, details of the angular variation of the spectrum would be useful

and the relationship of the spectrum C to this would also be of interest. It should be possible to separate C and fit a spin Hamiltonian to it. If it is necessary to use a generalized form of the spin Hamiltonian to explain the trigonal spectrum, measurements at a different frequency (e.g. 36Gc/s) would be invaluable since it is suggested that the additional terms would be field dependent.

(b) Measurement of the optical splitting (Δ) for the cubic $(FeCl_4)^-$ centre would be of great value in indicating the source of the large g-shift. This will probably also indicate the extra spin Hamiltonian terms necessary to explain the trigonal spectrum. The extension of this work to the study of iron in silver bromide would be very interesting as the measured g-shift is about three times that in silver chloride. In addition, the fine structure lines of this spectrum have not been identified. There are few publications of transition ion e.s.r. in silver bromide; there appear to be some difficulties regarding the resolution of spectra but it is not clear whether this is a consequence of crystal imperfections or of large ligand interactions broadening the spectral lines.

(c) Some experiments which could test and extend the tentative mechanisms proposed in section 8.3 are suggested at the end of that section. Useful e.s.r. experiments could examine the efficiency of processes during irradiation at different temperatures and for various periods of time. It may also be possible to define more carefully what has been rather vaguely called "crystal history"

together with the importance of dislocations. Optical measurements of volume darkening in the crystal will perhaps elucidate the electron trapping measurements.

(d) The suggestions above are restricted to the study of iron impurity in the silver halides. The preliminary experiments with gold doped samples indicate that some further work, particularly with relatively undamaged crystals, may reveal a fairly stable divalent gold state.

(e) The description given in Chapter V of the use of a helix instead of a cavity in an e.s.r. spectrometer indicates that it can be a realistic alternative. The matching conditions have not been examined in any detail and some care in design might improve the sensitivity.

CHAPTER VIII - REFERENCES

1. W. Hayes, J.R. Pilbrow and L.M. Slifkin, J. Phys. Chem. Solids, 25, 1417 (1964).

2. R. Nathans et al., Proc. Int. Conf. Mag. Nottingham, p.327, Inst. of Phys. (1965).

3. S. Geschwind, Phys. Rev., 121, 363 (1961).

4. H.L. Friedman, J. Am. Chem. Soc., 74, 5 (1952).

5. C.J. Ballhausen and H.D. Liehr, J. Mol. Spectroscopy, 2, 342, (1958): Errata 4, 190 (1960).

6. C.J. Ballhausen, "Introduction to Ligand Field Theory", McGraw-Hill (1962).

7. J.S. Griffith, "The Theory of Transition Metal Ions", Cambridge (1961).

8. J.F. Gibson, D.J.E. Ingram and D.S. Schonland, Disc. Farad. Soc., 26, 72 (1958).

9. N.S. Gill and R.S. Nyholm, J. Chem. Soc., 3997 (1959).

10. W. Low, "Paramagnetic Resonance in Solids", Solid State Physics, Suppl. 2, Academic (1960).

11. T.P.P. Hall, W. Hayes, R.W.H. Stevenson and J. Wilkens, J. Chem. Phys., 39, 35 (1963).

12. H. Layer, M.G. Miller and L.M. Slifkin, J. Appl. Phys., 33, 478 (1962).

APPENDIX I

The field equations for a helix containing a lossless dielectric ϵ_1 and enclosed by a dielectric ϵ_2. The coordinates are shown in Figure 5.2b and all equations should be multiplied by $[e^{\,j(\omega t - \beta z)}]$.

Inside the Helix:

$$H_z = H_1 I_o(\gamma r) \qquad \text{AI.1}$$

$$H_r = j H_1 \frac{\beta}{\gamma} I_1(\gamma r) \qquad \text{AI.2}$$

$$H_\phi = -H_1 \frac{\beta_o^2}{\gamma^2} \epsilon_1 \cot\psi \frac{I_1}{I_o} I_1(\gamma r) \qquad \text{AI.3}$$

$$E_z = jH_1 \frac{k\beta_o}{\gamma} \cot\psi \frac{I_1}{I_o} I_o(\gamma r) \qquad \text{AI.4}$$

$$E_r = -H_1 \frac{k\beta\beta_o}{\gamma^2} \cot\psi \frac{I_1}{I_o} I_1(\gamma r) \qquad \text{AI.5}$$

$$E_\phi = -jH_1 \frac{k\beta_o}{\gamma} I_1(\gamma r) \qquad \text{AI.6}$$

Outside the Helix:

$$H_z = -H_1 \frac{I_1}{K_1} K_o(\gamma r) \qquad \text{AI.7}$$

$$H_r = jH_1 \frac{\beta}{\gamma} \frac{I_1}{K_1} K_1(\gamma r) \qquad \text{AI.8}$$

$$H_\phi = H_1 \frac{\beta_o^2}{\gamma^2} \epsilon_2 \cot\psi \frac{I_1}{K_o} K_1(\gamma r) \qquad \text{AI.9}$$

$$E_z = jH_1 \frac{k\beta_o}{\gamma} \cot\psi \frac{I_1}{K_o} K_o(\gamma r) \qquad \text{AI.10}$$

$$E_r = H_1 \frac{k\beta\beta_o}{\gamma^2} \cot\psi \frac{I_1}{K_o} K_1(\gamma r) \qquad \text{AI.11}$$

$$E_\phi = -jH_1 \frac{k\beta_o}{\gamma} \frac{I_1}{K_1} K_1(\gamma r) \qquad \text{AI.12}$$

The relation between γ, a and $\cot\psi$ is given by

$$(\gamma a)^2 \frac{I_o K_o}{I_1 K_1} A = (\beta_o a \cot\psi)^2 \qquad \text{AI.13}$$

where $A = \dfrac{I_1 K_o + I_o K_1}{\epsilon_1 I_1 K_o + \epsilon_2 I_o K_1}$

The radial phase constant γ is given by $\gamma^2 = \beta^2 - \beta_o^2$;

$k = \sqrt{\mu_o/\epsilon_o} = 120\pi$ ohms, and $I_n(x)$, $K_n(x)$ are modified Bessel functions of order n and argument x. When $x = \gamma a$ these are abbreviated to I_n, K_n.

The power associated with the propagation is given by

$$P = \tfrac{1}{2} \mathcal{R}_e \int_\tau \underline{E} \times \underline{H}^* d\tau$$

and by taking this over a plane normal to the axis of propagation,

$$P = \pi \mathcal{R}_e \left[\int_o^a (E_r H_\phi^* - E_\phi H_r^*)\, r dr + \int_a^\infty (E_r H_\phi^* - E_\phi H_r^*) r dr\right] \qquad \text{AI.14}$$

Substituting for E and H inside and outside the helix and integrating gives

$$P = H_1^2 \frac{\pi k}{2} \frac{\beta\beta_0}{\gamma^4} (\gamma a) \frac{I_1}{K_1} \left\{ \left[\left(\frac{K_0}{K_1} - \frac{I_0}{I_1} \right) + A\left(\frac{I_1}{I_0} - \frac{K_1}{K_0}\right) + \frac{2(1+A)}{\gamma a} \right] + \gamma a \, I_1 K_0 (\epsilon_1 - 1) A \left[\frac{2}{\gamma a} - \left(\frac{I_0}{I_1} - \frac{I_1}{I_0}\right) \right] + \gamma a \, I_0 K_1 (\epsilon_2 - 1) A \left[\frac{2}{\gamma a} + \left(\frac{K_0}{K_1} - \frac{K_1}{K_0}\right) \right] \right\} \quad \text{AI.15}$$

$$= 600 H_1^2 \frac{\beta\beta_0}{\gamma^4} B^{-1}(\gamma a) \quad \text{AI.16}$$

where B (γa) is a function of γa, ϵ_1 and ϵ_2.

When $\epsilon_1 = \epsilon_2 = 1$, B($\gamma a$) is related to Pierce's F (γa) by the relation

$$B(\gamma a) = \frac{\pi}{2k} \frac{I_0 K_1}{I_1 K_0} [F(\gamma a)]^3 \quad \text{AI.17}$$

Pierce gives $F(\gamma a) = 7.154 \, e^{-0.6664 \gamma a}$ in the range of γa : 0.5 to 8.0.

APPENDIX II

Angular variation of spin Hamiltonian fine structure terms up to fourth order in even spin operators, specified relative to a fixed axis.

The spin Hamiltonian may be written as (1)

$$\mathcal{H} = g\beta\underline{H}.\underline{S} + D(S_1^2 - \tfrac{1}{3}S(S+1)) + E(S_2^2 - S_3^2)$$
$$+ \frac{a}{6}[S_\xi^4 + S_\eta^4 + S_\zeta^4 - \frac{1}{5}S(S+1)(3S^2+3S-1)]$$
$$+ \frac{F}{6}[\frac{7}{6}S_1^4 - S(S+1)S_1^2 + \frac{5}{6}S_1^2 - \frac{1}{5}S(S+1) + \frac{1}{10}S^2(S+1)^2] \quad \text{AII.1}$$

$$= g\beta\underline{H}.\underline{S} + D\mathcal{H}_D + E\mathcal{H}_E + \frac{a}{6}\mathcal{H}_a + \frac{F}{6}\mathcal{H}_F \quad \text{AII.2}$$

when $H \| z$ and this is taken as the principal axis of quantization of the spin operators, then the other terms are as given below. The basis is S_z, S_+, S_-, where $S_\pm = S_x \pm iS_y$.

θ is the angle between the z axis and $\underline{1}$, ψ is the angle between the z axis and one of ξ, η, or ζ, say ζ, with the condition that z lies in the (110) or $(\bar{1}10)$ plane specified by these axes. ϕ is the angle between the $\underline{2}$ axis in the E term and the z axis (see Figure 7.2).

$$\mathcal{H}_D = \alpha_D[S_z^2 - \tfrac{1}{3}S(S+1)] + b_D(S_+[S_z + \tfrac{1}{2}] + S_-[S_z - \tfrac{1}{2}])$$
$$+ \frac{1}{4}c_D[S_+^2 + S_-^2] \quad \text{AII.3}$$

$$\mathcal{H}_E = \frac{3}{2}\beta^2 \cos 2\phi\left[S_z^2 - \frac{1}{3}S(S+1)\right] + \beta\cos 2\phi\left[(\alpha + \frac{i}{2}\tan 2\phi)\right.$$

$$\left. S_+ (S_z + \tfrac{1}{2}) + (\alpha - \tfrac{i}{2}\tan 2\phi) S_- (S_z - \tfrac{1}{2})\right] + \tfrac{1}{4}\cos 2\phi$$

$$\left[(1+\alpha^2)(S_+^2 + S_-^2) + i\alpha \tan 2\phi (S_+^2 - S_-^2)\right] \qquad \text{AII.4}$$

$$\mathcal{H}_a = \alpha_a Z_o(S) + \tfrac{1}{8} b_a[Z_1(S) + Z_{-1}(S)] - \tfrac{1}{8} c_a[Z_2(S) + Z_{-2}(S)]$$

$$+ \tfrac{1}{4} d_a[Z_3(S) + Z_{-3}(S)] + \tfrac{1}{32} e_a[Z_4(S) + Z_{-4}(S)] \qquad \text{AII.5}$$

$$\mathcal{H}_F = \alpha_F Z_o(S) + \frac{7}{24} b_F[Z_1(S) + Z_{-1}(S)] - \frac{1}{24} c_F[Z_2(S) + Z_{-2}(S)]$$

$$+ \frac{7}{12} d_F[Z_3(S) + Z_{-3}(S)] + \frac{7}{96} e_F[Z_4(S) + Z_{-4}(S)] \qquad \text{AII.6}$$

where

$$Z_o(S) = \left[\frac{7}{6} S_z^4 - S(S+1) S_z^2 + \frac{5}{6} S_z^2 - \frac{1}{5} S(S+1) + \frac{1}{10} S^2(S+1)^2\right]$$

$$Z_{\pm 1}(S) = S_\pm\left[14 S_z^2 \pm 21 S_z^2 + 19 S_z - 6S(S+1) S_z \pm 3S(S+1)\right]$$

$$Z_{\pm 2}(S) = S_\pm^2\left[7 S_z^2 \pm 14 S_z + 9 - S(S+1)\right]$$

$$Z_{\pm 3}(S) = S_\pm^3\left[S_z \pm \frac{3}{2}\right]$$

$$Z_{\pm 4}(S) = S_\pm^4$$

and

$$\alpha_D = \tfrac{1}{2}(3\alpha^2 - 1); \quad b_D = \alpha\beta; \quad c_D = (1 - \alpha^2)$$

$$\alpha_a = \frac{3}{8}(15\gamma^4 - 10\gamma^2 + 1); \quad b_a = \gamma\omega(1 - 3\gamma^2); \quad c_a = (3\gamma^4 - 4\gamma^2 + 1);$$

$$d_a = \gamma\omega(3\gamma^2 - 5); \quad e_a = (3\gamma^4 - 10\gamma^2 + 3)$$

$$\alpha_F = \frac{3}{8}(15\alpha^4 - 10\alpha^2 + 1); \quad b_F = \alpha\beta(\alpha^2 - {}^3/28);$$

$$c_F = (7\alpha^4 - 8\alpha^2 + 1); \quad d_F = \alpha(1 - \alpha^2)$$

$$e_F = (\alpha^4 - 2\alpha^2 + 1)$$

where $\alpha = \text{Cos}\ \theta$, $\beta = \text{Sin}\ \theta$, $\gamma = \text{Cos}\ \psi$, $\omega = \text{Sin}.\psi$.

Matrix elements for many of the operators are given by Low (2).

The equations given below specify the magnetic fields at which various $\Delta S = +1$ transitions occur within the $S = 5/2$ manifold for trigonal or tetragonal symmetry (i.e. $E = 0$). $H_o = \frac{h\nu}{g\beta}$, and D, a and F are now understood to be the D, a and F above divided by $g\beta$, provided they are now measured in terms of magnetic field rather than energy units. The fields for the various absorption transitions are,

$$H_{1,5}: \left|\pm\tfrac{3}{2}\right> \rightleftarrows \left|\pm\tfrac{5}{2}\right>; \quad H_{2,4}: \left|\pm\tfrac{1}{2}\right> \rightleftarrows \left|\pm\tfrac{3}{2}\right>; \quad H_3: \left|-\tfrac{1}{2}\right> \rightarrow \left|+\tfrac{1}{2}\right>$$

$$H_{1,5} = H_o \mp 4D\alpha_D \mp \frac{4}{3}a\alpha - \frac{10(2Db_D + \frac{1}{2}ab)^2}{H_{1,5} \pm 4D\alpha_D \pm \frac{4}{3}a\alpha} - \frac{\frac{5}{4}(Dc_D - \frac{3}{4}ac)^2}{H_{1,5} \pm 3D\alpha_D \mp \frac{1}{6}a\alpha}$$

$$- \frac{\frac{5}{24}(ad)^2}{H_{1,5} \pm 2D\alpha_D \mp \frac{1}{9}a\alpha} + \frac{2(2Db_D - \frac{5}{8}ab)^2}{H_{1,5} \pm 2D\alpha_D \mp \frac{5}{3}a\alpha}$$

$$+ \frac{\frac{1}{4}(3Dc_D + \frac{5}{4}ac)^2}{H_{1'5} \pm D\alpha_D \mp \frac{5}{6}a\alpha}$$

$$H_{2,4} = H_o \mp 2D\alpha_D \pm \frac{5}{3} a\alpha - \frac{4(2Db_D - \frac{5}{8} ab)^2}{H_{2,4} \pm 2D\alpha_D \mp \frac{5}{3} a\alpha}$$

$$+ \frac{5(2Db_D + \frac{1}{2} ab)^2}{H_{2,4} \pm 4D\alpha_D \pm \frac{4}{3} a\alpha} - \frac{\frac{5}{256} (ae)^2}{H_{2,4} \mp D\alpha_D \mp \frac{1}{3} a\alpha}$$

$$+ \frac{\frac{5}{24} (ad)^2}{H_{2,4} \mp 2D\alpha_D \pm \frac{1}{9} a\alpha} - \frac{\frac{5}{4} (Dc_D - \frac{3}{4} ac)^2}{H_{2,4} \pm 3D\alpha_D \mp \frac{1}{6} a\alpha}$$

$$H_3 = H_o + \frac{\frac{5}{2} (Dc_D - \frac{3}{4} ac)^2}{H_3 - (3D\alpha_D - \frac{1}{6} a\alpha)^2/H_3} + \frac{4(2Db - \frac{5}{8} ab)^2}{H_3 - (2D\alpha_D - \frac{5}{3} a\alpha)^2/H_3}$$

$$- \frac{\frac{1}{2}(3Dc_D + \frac{5}{4} ac)^2}{H_3 - (D\alpha_D - \frac{5}{6} a\alpha)^2/H_3} - \frac{\frac{5}{12} (ad)^2}{H_3 - (2D\alpha_D - \frac{1}{9} a\alpha)^2/H_3} \qquad \text{AII.7}$$

where $a\alpha$ should be read as $(a\alpha_a + F\alpha_F)$;

ab $\quad (ab_a + \frac{7}{3} Fb_F)$;

ac $\quad (ac_a + \frac{1}{3} Fc_F)$;

ad $\quad (ad_a + \frac{7}{3} Fd_F)$;

ae $\quad (ae_a + \frac{7}{3} Fe_F)$.

The precision of these splittings is about 0.05% for $a \approx 10\%\ H_o$ $D \approx 5\%\ H_o$; the accuracy for high symmetry directions can easily be improved by carrying out additional calculations. In principle, the actual magnitudes of $H_{1,2,4,5}$ are sensitive to the absolute signs of the parameters a, D and F; a change in absolute sign will alter the magnitude of a splitting by about 0.2% for $a \approx 10\%\ H_o$ and $D \approx 5\%\ H_o$.

The equations AII.7 reduce to those given by a number of authors (2-5) by making suitable approximations; unfortunately none of these cases are sufficient ~~in~~ for the analysis of spectrum B.

APPENDIX II - REFERENCES

1. B. Bleaney and K.W.H. Stevens, Rep. Prog. Phys., 16, 108 (1953).
2. W. Low, Solid State Physics, Suppl. 2, Academic Press (1960).
3. B. Bleaney, Phil. Mag., 42, 441 (1951).
4. B. Bleaney and D.J.E. Ingram, Proc. Roy. Soc., A205, 336 (1951).
5. S. Geschwind, Phys. Rev., 121, 363 (1961).